Reliability and Processing of Ferroelectric Thin Film Capacitors with Emphasis on Fatigue and Etching

by

Dilip P. Vijay

Dissertation submitted to the Faculty of the

Virginia Polytechnic Institute and State University

in partial fulfillment of the requirements for the degree of

Doctor of Philosophy

in

Materials Engineering Science

APPROVED :

Dr. S.B. Desu, Chairman

Dr. R.W. Hendricks

Dr. R. Davis

Dr. W.T. Reynolds, Jr.

Dr. S.L. Kampe

July 11, 1995

Blacksburg, Virginia

Keywords : Ferroelectrics, Thin Films, Fatigue, Reactive Ion Etching, Lead Zirconate Titanate, Strontium Bismuth Tantalum Oxide, Laser Ablation

.2

Reliability and Processing of Ferroelectric Thin Film Capacitors with Emphasis on Fatigue and Etching

by

Dilip P. Vijay

S.B. Desu, Chairman

Materials Engineering Science

(ABSTRACT)

Ferroelectric materials are characterized by a reversible spontaneous polarization in the absence of an electric field. The characteristic polarization response of a ferroelectric material to an applied electric field enables a binary state device in the form of a thin film ferroelectric capacitor that can be used to store digital information. This provides opportunities for the development of high speed, low cost and low power, nonvolatile memory devices. The development of commercial ferroelectric memory devices has however been hampered by (a) several reliability issues including fatigue, leakage current, aging, time dependent dielectric breakdown, retention and imprint and (b) processing problems including the development of a low temperature thin film deposition process and the development of a patterning technology.

Lead zirconate titanate (PZT) is now widely considered as the most promising material for ferroelectric memory applications as a result of its excellent ferroelectric properties and wide operating temperature range. However, it is commonly found that metal electroded-PZT capacitors (e.g., Pt/PZT/Pt) show a loss of switchable polarization with cumulative switching cycles. This phenomenon is known as fatigue and is the one of the critical problems affecting the lifetime of ferroelectric memories.

This research is primarily focused on the problem of fatigue. On the basis of a quantitative model, various guidelines to minimize the degradation problem have been derived. The model attributes fatigue to domain pinning by space charge that is caused by defect (e.g. oxygen vacancy) entrapment at various interface sites such as electrode-ferroelectric interface, domain boundaries and grain boundaries. Two different approaches to minimize the problem have been outlined : (a) control of the defect density and (b) control of the interface state. The control of interface state was achieved by replacing the metal electrodes with conducting oxide electrodes such as RuO_2. The oxide electrode/PZT capacitors were characterized for their diffusion barrier properties, perovskite phase formation, interface nature and ferroelectric properties. The results indicate that these oxide electroded PZT films are good candidates for nonvolatile memory applications. However, the leakage current levels at the operating voltages are far higher than the metal counterparts. Simultaneous minimization of fatigue and leakage current in PZT films was achieved by using multilayer metal/conducting oxide electrodes (e.g., Pt/RuO_2).

The control of defect density was attained by (a) donor doping to compensate for the oxygen vacancies (e.g, Nb doping in PZT) and (b) utilizing ferroelectric materials that have a low intrinsic defect concentration. As a result of the latter approach, novel ferroelectric materials belonging to the layer-structure family of oxides have been identified as excellent candidates for fatigue free nonvolatile memory applications. Laser ablated $SrBi_2(Ta_xNb_{1-x})_2O_9$ ($0<x<1$) films showed very good hysteresis characteristics (remnant polarization value of 11 $\mu C/cm^2$, coercive field of 60 kV/cm), no fatigue was observed up to 10^9 switching cycles and very low leakage current densities. Furthermore, the formation and properties of these films were characterized. It was found grain size and

orientation played a major role in determining the properties of these films. C-axis oriented films were found to exhibit almost no polarization.

An additional objective of this research was to identify an etching technology (process integration issue) for patterning of the ferroelectric capacitors. The etching process should provide high etch rates, good etch anisotropy, high etch selectivity and minimal post etch residues. It has been shown that a reactive ion etch process with CCl_2F_2/O_2 as the etch gas mixture can meet these requirements. A detailed process study has been conducted to determine the mechanism of etching.

Dedication

To my parents

Geetha and Vijayan

and my sister

Devi Vijay

Acknowledgments

I wish to first thank Dr. S.B. Desu for not only providing me with inspiration and moral support through this dissertation but for also being my mentor, guide and a good friend. I respect him for his brilliance, hard work and exhaustive knowledge of this field. I am grateful to him for allowing me to pursue my own research interests while providing me with guidance when asked or needed. I also wish to thank him for all his support and suggestions in my career decision making processes.

I am grateful to Dr. R.W. Hendricks for serving on my committee and guiding me solely through the early part of my graduate study. He was mainly responsible for my admission to Virginia Tech and the financial support that followed. Without his enthusiastic support, I would not be here. I am forever indebted to him.

I am grateful to Professors Bill Reynolds (whose patience, quest for knowledge and willingness to help never ceases to amaze me), Steve Kampe and Rick Davis for including me in their already heavy loads of responsibility by serving on my committee and showing a great deal of interest in my dissertation. Most of the improvements in the final version of this dissertation are due to their expert and suggestions. Through useful discussions with them, I have been able to gain a wider perspective on my work.

My work was greatly expedited by Jan Doran, Suzette Sowers, Amy Hill, Cindy Klien, Tabatha Johnson, Amber Neilsen, Julie Bhatt and Lisa Mullins, who somehow remained patient and cheerful no matter how often I pestered them. In particular, I would like to thank Adele Hobday for providing me with a great deal of assistance and for being a very good friend.

There were always fellow lab workers, past and present, to whom I turned to gratefully for assistance. I greatly enjoyed working with Hemanshu Bhatt, Shanky Ramanathan, Greg Menk, Justin Gaynor, Steve Stowell, Carlos Suchicital, Ashraf Khan, Warren Hendricks, Xubai Zhang, Wei Pan , Jei Sie, Jhing Fang, Hollywood Chen, Chiencha Chiu, Gene Li, Chi Kwok, Jhin-Yi Tsai, Yoogjong Song, Calvin Doss, J.J. Lee,

Tingki Li, Yong-Fei Zhu, Brian Dickerson, Chai-Liang Thio, Z. Chen, May Nyman, Dr. Cho, Ryu, Nikhil, Jay Senkewich, Hwang (Golden Child), Paige, P.C. Joshi and, of course, Ramu (Suku) and Shamu (Vedula). Steve Macartney, Dr. Baoping He and Dr. Gang Chen greatly aided my work through their competent assistance with microscopy, composition analysis and x-ray diffraction analysis.

My sincere thanks go to very many friends, both in this department and in other departments, for all their support and encouragement. I consider myself fortunate that I have come to know fellow colleagues and great friends such as Christophe Vailhe, Srivatsan Srinivas (Watty), Anne Vilette, Liz Myers, Joy Longhenry, Mike Stawovy, Virginie Vaubert, Kermit Kwan, Mona Moret, Nikhil Verghese, Joel Lee, Ravi Verma, Dave Teter, Batsy and Tobeka with whom I have shared many a good time.

I wish to thank SHARP Microelectronics, Inc., Japan, CERAM, USA, ARPA, CIT-Va and Radiant Technologies for providing us with continued financial support through this dissertation work.

To Jen Elster I offer special thanks for all her support and her assistance in the preparation of this dissertation.

I dedicate this dissertation to my parents, Geetha and Vijayan, my sister Devi, my grandmother Ammini and all my other family without whose blessings I would not have been able to achieve this goal. I have no words to describe the guidance, support and encouragement that they have provided me with over the years.

Table of Contents

Chapter 1.	Introduction	1
1.1	Ferroelectric Memories	1
1.2	Basic Operation	3
1.3	Purpose of Research	8
1.4	Objectives of Research	11
1.5	Presentation of Results	12
1.6	References	13
Chapter 2.	Fatigue - Problem Definition and Modeling	16
2.1	Abstract	16
2.2	Introduction	16
2.3	Fatigue Model	19
2.4	Experimental Evidence	31
2.5	Guidelines for Minimization	37
2.6	Summary	38
2.8	References	38
Chapter 3.	Minimization of Fatigue I : Oxide Electrodes	42
3.1	Abstract	42
3.2	Introduction	42
3.3	Experimental Procedure	45
3.4	Results and Discussion	47
3.5	Conclusions	76
3.6	References	78
Chapter 4.	Minimization of Fatigue II : Multilayer Metal/Metal	

	Oxide Electrodes	80
4.1	Abstract	81
4.2	Introduction	81
4.3	Experimental Procedure	84
4.4	Results and Discussion	87
	4.4.1 Pt/RuO_2 Multilayer Electrodes	87
	4.4.2 $Pt\text{-}Rh/Rh_2O_3$ Multilayer Electrodes	94
4.4	Conclusions	104
4.5	References	105
Chapter 5.	Minimization of Fatigue III : Control of Defect Density	107
5.1	Abstract	108
5.2	Introduction	108
5.3	Dopant Additions	109
5.4	Alternate Materials	115
5.5	Summary	126
5.6	References	127
Chapter 6.	Formation and Properties of $SrBi_2Ta_2O_9$ Thin Films	129
6.1	Abstract	130
6.2	Introduction	130
6.3	Experimental Procedure	132
6.4	Results and Discussion	131
6.5	Conclusions	142
6.6	References	142

Chapter 7.	Oriented Growth of $SrBi_2Ta_2O_9$ Thin Films	143
7.1	Abstract	144
7.2	Introduction	145
7.3	Experimental Procedure	150
7.4	Results and Discussion	151
7.5	Conclusions	159
7.6	References	159
Chapter 8.	Reactive Ion Etching of Lead Zirconate Titanate Thin Film Capacitors	161
8.1	Abstract	162
8.2	Introduction	162
8.3	Experimental Procedure	164
8.4	Results and Discussion	166
8.5	Conclusions	181
8.6	References	181
Chapter 9.	Conclusions and Recommendations	183
Appendix A.	Sol-gel Processing of PZT Films	188
Appendix B.	Ferroelectric Property Measurements	190
Vita		192

List of Figures

Figure 1.1 ABO_3 perovskite unit cell

Figure 1.2 Hysteresis loop of a ferroelectric material

Figure 1.3 Proposed ferroelectric memory cell device configuration

Figure 2.1 Schematic of the read/write operation in a ferroelectric memory cell

Figure 2.2 Effect of fatigue on the properties (polarization and coercive field) of a thin film ferroelectric material [13]

Figure 2.3 Temperature dependence of the fatigue rate [13]

Figure 2.4 Schematic of the fatigue model for a ferroelectric capacitor

Figure 2.5 Fatigue curve fitting for Pt/PZT/Pt capacitors as a function of voltage ($t = 0.3\ \mu m$, size = $0.1 \times 0.1\ mm^2$) [20]

Figure 2.6 Voltage dependence of the decay constant. Calculated jump distance = 0.418 nm, measured lattice constants : a = 0.4113 nm and c = 0.4138 nm [20]

Figure 2.7 Auger microprobe data for fatigued PZT films with Pt and Au electrodes. Note that the oxygen concentration drops off near the electrodes [26]

Figure 2.8 The fatigue cycle and thickness dependence of 1/Cm for Pt/PZT/Pt capacitors. The increasing value of the intercepts shows that the width of the space charge layer increases with fatigue cycling

Figure 3.1 Comparison of relative Pb concentrations on the surface of RuO_2/PZT (x=.53) and ITO/PZT films as a function of annealing temperature

Figure 3.2 The Zr/Ti ratio and Pb/(Zr + Ti) ratio on the surface of RuO_2/PZT films of different compositions annealed at 650°C

Figure 3.3 RBS profile of the as-deposit, 500°C and 550°C annealed Si/ITO/PbO samples

Figure 3.4 RBS profile of the as-deposit, 500°C and 550°C annealed Si/ITO/PZT samples

Figure 3.5 RBS profile of the as-deposit, 500°C and 550°C annealed Si/RuO_2/PbO samples

Figure 3.6 RBS profile of the as-deposit, 550°C and 600°C annealed Si/RuO_2/PZT samples

Figure 3.7 XRD patterns of Si/RuO_2/PZT samples annealed at various temperatures between 400°C and 700°C

Figure 3.8 A typical hysteresis loop obtained from RuO_2/PZT/RuO_2 capacitors

Figure 3.9 Comparison of fatigue properties of PZT films on Pt and RuO_2 electrodes

Figure 3.10 Overview of Si/SiO_2/RuO_2/PZT thin film showing the interface structures and texture of the RuO_2 and PZT layers

Figure 3.11 Typical electron diffraction pattern of the Si/SiO_2/RuO_2/PZT thin film

Figure 3.12 Enlargement of Figure 3.10 showing lattice fringes within the RuO_2 grains. Note also the nanocrystalline pyrochlore layer

Figure 3.13 RuO_2/PZT interface showing curved interphase boundaries.

Figure 3.14 HRTEM image of the RuO_2/PZT interface showing [101] zone axis of PZT

Figure 3.15 Electrode effects on I/V characteristics of PZT films

Figure 3.16 Typical current-time behavior for a ferroelectric capacitor

Figure 3.17 Results of the unified fatigue/TDDB test on PZT capacitors

Figure 4.1 Schematic of the proposed multilayer metal/metal oxide electrode structure for PZT thin films

Figure 4.2 XRD pattern of PZT films deposited on Pt/RuO_2 electrodes with various thickness' of the oxide electrode. PZT films were annealed at 650 ^oC for 30 min.

Figure 4.3 Glancing angle XRD pattern of PZT films on Pt/RuO_2 multilayer electrodes.

Figure 4.4 XRD pattern of Pt/RuO_2 as a function of RuO_2 thickness : (a) 70 nm (b) 50 nm.

Figure 4.5 Hysteresis properties of PZT films on Pt/RuO_2 multilayer electrodes

Figure 4.6 Fatigue properties PZT films on Pt/RuO_2 multilayer electrodes

Figure 4.7 Current-Voltage characteristics of Pt/RuO_2 (50 nm)/PZT capacitors

Figure 4.8 RBS profile of Pt-Rh electrodes (3/19/3) multilayer electrodes deposited on Si/SiO_2 substrates by reactive sputtering in O_2 atmosphere at 450 ^oC

Figure 4.9 XRD pattern of PZT films deposited on Si/SiO_2/Rh_xO_y/Pt-Rh/Rh_xO_y substrates. The patterns are shown as a function of surface Rh_xO_y layer thickness. PZT films were annealed at 650 ^oC for 30 min

Figure 4.10 Typical hysteresis behavior of PZT films annealed at 650 °C for 30 min on 3/16/6 Pt-Rh multilayer electrodes

Figure 4.11 Fatigue behavior of PZT films annealed at 650 °C for 30 min on 3/16/6 Pt-Rh multilayer electrodes

Figure 4.12 TDDB characteristics PZT films annealed at 650 °C for 30 min on 3/16/6 Pt-Rh multilayer electrodes

Figure 5.1 (a) Fatigue and (b) leakage current properties of undoped Pt/PZT and RuO_2/PZT capacitors

Figure 5.2 (a) Fatigue and (b) leakage current properties of Nb-doped Pt/PZT and RuO_2/PZT capacitors

Figure 5.3 Schematic of the pulsed laser deposition chamber used for the growth of $SrBi_2(Ta_xNb_{1-x})_2O_9$ (SBTN) thin films

Figure 5.4 The plots of refractive index and extinction coefficient as a function of wavelength for SBTN films with a composition of x = 0.8.

Figure 5.5 XRD pattern of $SrBi_2(Ta_{0.4}\ Nb_{0.6})_2O_9$ films grown on $Si/SiO_2/Ti/Pt$ at 700 °C by laser ablation

Figure 5.6 Microstructure of SBTN films deposited using PLD at 700°C on Pt electrodes by laser ablation.

Figure 5.7 (a) Hysteresis properties of $SrBi_2(Ta_{0.4}\ Nb_{0.6})_2O_9$ films grown on $Si/SiO_2/Ti/Pt$ at 700 °C before fatigue cycling (b) the fatigue behavior of Pt/SBTN/Pt capacitors at 5V and 1 MHz (bipolar square wave) frequency (c) hysteresis characteristics of Pt/SBTN(x=0.8)/Pt films after fatigue cycling

Figure 6.1 XRD pattern of $SrBi_2Ta_2O_9$ films as a function of deposition temperature.

Figure 6.2 Bi concentration of $SrBi_2Ta_2O_9$ films as a function of deposition temperature.

Figure 6.3 (a) Grain size of $SrBi_2Ta_2O_9$ on $Pt/Ti/SiO_2/Si$ substrates. Results were taken from SEM photographs using the linear intercept method (b) the corresponding SEM micrographs of $SrBi_2Ta_2O_9$ film fabricated at deposition temperatures of 650 °C and 700 °C

Figure 6.4 Hysteresis properties measured at a frequency of 100 Hz and an applied voltage of 5V for 200 nm thick $SrBi_2Ta_2O_9$ films fabricated at various deposition temperature

Figure 7.1 (a) Schematic of the currently used capacitor structure for nonvolatile memory applications of SBT films. (b) Schematic of the device structure proposed in this paper.

Figure 7.2 Schematic of the unit cell of $ABi_2B_2O_9$ layered structure oxides; for $SrBi_2Ta_2O_9$, A = Sr and B= Ta

Figure 7.3 X-ray diffraction patterns of Pt films sputter deposited on single crystal MgO (100) substrates as a function of deposition temperature; (a) room temperature deposition, (b) 600 °C deposition and (c) 700 °C deposition

Figure 7.4 X-ray diffraction patterns of $SrBi_2Ta_2O_9$ thin films deposited on (a) MgO/Pt (RT), (b) MgO/Pt(600 °C) and (c) MgO/Pt(700 °C) substrates at a substrate temperature of 700 °C

Figure 7.5 Pole figures of $SrBi_2Ta_2O_9$ thin films deposited on (a) MgO/Pt (RT), (b) MgO/Pt(600 °C) and (c) MgO/Pt(700 °C) substrates at a substrate temperature of 700 °C

Figure 7.6 The hysteresis characteristics of $MgO/Pt/SrBi_2Ta_2O_9/Pt$ capacitors as a function of degree of c-axis orientation; (a) MgO/Pt (RT)/SBT, (b) MgO/Pt(600 °C)/SBT and (c) MgO/Pt(700 °C)/SBT. Ch1 and Ch2 denote the x-axis and y-axis divisions respectively.

Figure 7.7 The dielectric properties of $MgO/Pt/SrBi_2Ta_2O_9/Pt$ capacitors as a function of degree of c-axis orientation.

Figure 8.1 Schematic of the etch structures used in the etching of PZT and RuO_2 thin films

Figure 8.2 The etch rate of PZT thin films as a function of CCl_2F_2 gas flow rate.

Figure 8.3 The effect of RF power on the etch rate of PZT thin films at constant gas pressure

Figure 8.4 The etch rate of PZT films as a function of % O_2 in the etch gas.

Figure 8.5 SEM micrograph of PZT thin film sample showing the high etch anisotropy obtained under conditions of low gas pressure and low RF power

Figure 8.6 (a) The ESCA wide scan of the PZT film surface before and after the etch process (b) the ESCA wide scan of the PZT film surface after partial etching (4 min under the given conditions) and (c) the composition of the PZT film surface as a function of etch time determined from the ESCA narrow scans.

Figure 8.7 The etch rate of RuO_2 thin films as a function of flow rate of CCl_2F_2 gas (no oxygen added to the etch gas)

Figure 8.8 The etch rate of RuO_2 thin films as a function of gas pressure. 30% of the etch gas contained oxygen. The effect of O_2 addition can be seen by comparing this result to Figure 8.7

Figure 8.9 The etch rate of RuO_2 thin films as a function of $\%O_2$ in the etch gas at various gas pressures.

Figure 8.10 The effect of RF power on the etch rate of RuO_2 thin films.

List of Tables

Table 2.1 Role of oxygen vacancies on the ferroelectric and fatigue properties of the films [27]. Fatigue properties of Pt/PZT capacitors as a function of partial pressure of oxygen is presented.

Table 3.1 EPMA results on the PZT samples of different compositions, all annealed at 650^0C on sapphire substrates.

Table 4.1 Summary of the electrical properties (hysteresis, fatigue and leakage current) of PZT films on the various Pt-Rh electrodes.

Chapter 1 : Introduction

In this chapter, the reader is introduced to the current status of digital memories and how ferroelectric materials can radically impact this technology. The basic operation of a ferroelectric memory device is then discussed. Following this, the processing and reliability problems involved in the development of commercial ferroelectric memories is assessed to lay the foundation for the purpose of this research. The specific objectives of this dissertation is outlined subsequent to this section and finally a brief description of the contents of this dissertation is provided.

1.1 FERROELECTRIC MEMORIES

There are fourteen generically different kinds of digital memories in use today. These memories range from the slow, inexpensive tapes or disks used for archival storage to fast but expensive static random access memories (SRAMs) and the slightly slower dynamic random access memories (DRAMs) [1]. Some of the more expensive devices including the plated wire, complementary metal oxide semiconductor (CMOS) with battery backup, electrically erasable read-only memories (EEPROMs) and core memories generally have a combination of attributes required for specific applications, particularly nonvolatility and radiation hardness. Among all these devices, the DRAMs are the most popular and widely used memories in the computer industry today. These memories are now available up to 1 Mbit and dominate the $8 billion per year computer memory market today.

Typically, the memory cell in a DRAM consists of a single transistor and a single capacitor in which the information is stored in the form of charge in the capacitor and the

switching transistor is used to isolate the capacitor [2]. To satisfy the compelling need to increase the density of DRAMs above 1 Mbit (4 to 256 Mbit), more capacitor cells need to be packed in the same die size. This makes the use of the current candidate SiO_2 as the dielectric layer impractical. The dielectric layer has to be so thin that process control becomes extremely difficult and electron tunneling becomes a major concern. One of the ways to overcome this problem is to change the design of the capacitors from the presently used planar structure to either a 'trench' or a 'stack' structure [3]. These geometries provide greater capacitative area, so the capacitor can store the total required charge even though it occupies less real estate on the die. However, these designs will make the processing undoubtedly complex and thus not be able to satisfy the 256 Mbit requirements. The other alternative is to look for dielectric materials that have substantially higher dielectric constants and therefore higher charge storage capacities. It is this search that has resulted in a closer examination of ferroelectric materials for memory applications.

Some of the more commonly used ferroelectrics have dielectric constants at least two orders of magnitude higher than that of SiO_2. More importantly, the characteristic polarization response of a ferroelectric to an electric field make them perfect candidates for use as nonvolatile memory devices. The information in current DRAMs is stored in the form of charge in a linear capacitor (SiO_2 dielectric). To maintain the charge, a constant voltage is always required on the capacitor and therefore the information is lost when the power is turned off (volatile). In contrast, the information in ferroelectric memories is stored in the polarization state of the ferroelectric material itself [1-3]. The ferroelectric capacitor has a highly nonlinear dielectric with permanent charge retention capabilities after application of a voltage by an external circuit [4]. Additionally, ferroelectric materials are also extremely radiation hard; for example, a typical ferroelectric can withstand 5

Mrad of high energy x-rays per square centimeter and an intensity of 10^{11} rad/cm/sec [1]. The intrinsic nonvolatility and radiation hardness of ferroelectric RAMs may greatly simplify the existing collection of computer memories. In principle, the FRAM could replace the SRAM in cache memory, DRAM in the main system memory and EEPROM in the lookup tables. The distinct advantages of FRAMs over other nonvolatile memories include fast write and erase access times on the order of nanoseconds, low operating voltages (5V or less), long write/erase lifetime, wide operating temperature range (-180 ^{o}C to 350 ^{o}C) and high radiation hardness necessary in military and space applications. If the cost of FRAMs can be reduced to the level comparable to magnetic storage, it could also replace the hard disk as the mass storage device because of its faster access speeds and due to the lack of any mechanical wear problems. Finally, in addition to computer memories, ferroelectric memories can be used for a wide variety of other applications ranging from automobiles and mobile phones to kitchen and household appliances.

1.2 BASIC OPERATION

Ferroelectric materials are characterized by a reversible spontaneous polarization in the absence of an electric field [4--7]. Spontaneous polarization in a ferroelectric arises from a noncentrosymmetric arrangement of ions in its unit cells which produces an electric dipole moment associated with the unit cell. Adjacent unit cells tend to polarize in the same direction and form a region called a ferroelectric domain. The most common ferroelectrics have the ABO_3 perovskite structure as shown in Fig.1.1. Above the Curie temperature, these materials have a centrosymmetric structure and therefore lose all spontaneous polarization. In this state, the material is termed paraelectric. As the temperature is lowered through the Curie point, a phase transformation takes place from

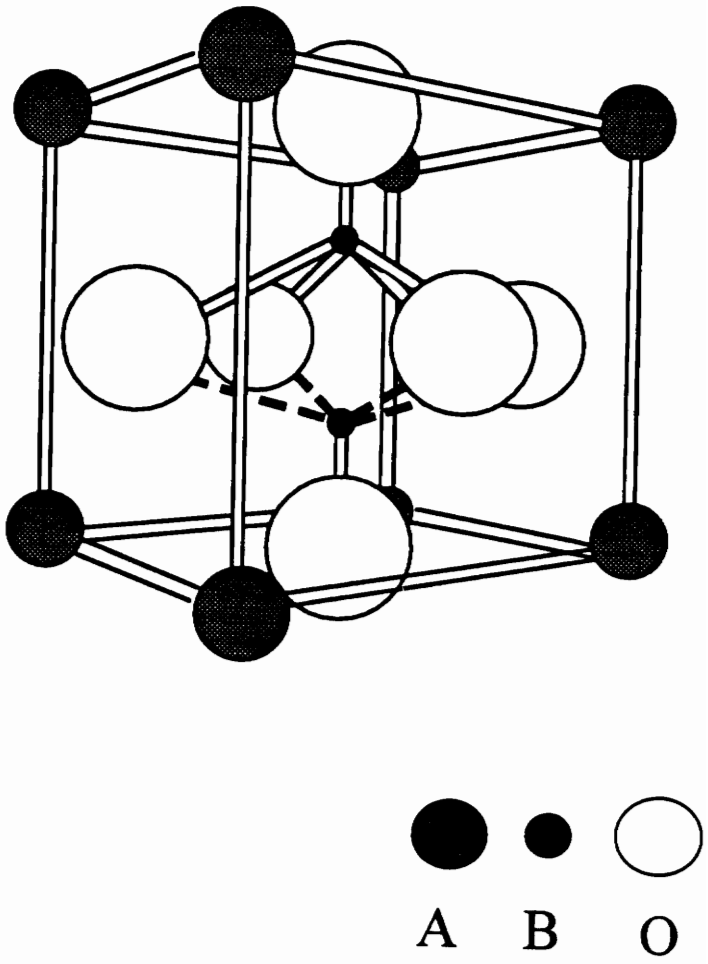

Figure 1.1 ABO_3 perovskite unit cell

the paraelectric state to the ferroelectric state. The center ion is displaced from its body-centered position and the cubic unit cell deforms to assume one of the noncentrosymmetric structures such as tetragonal, rhombohedral or monoclinic structures. When an increasingly strong electric field is applied to a ferroelectric, the polarization shows a hysteresis behavior with the applied field (Fig. 1.2). In the initial stages, the ferroelectric domains that are oriented favorably with respect to the applied field direction grow at the expense of other domains. This continues until total domain growth and reorientation have occurred. At this stage, the material has reached its saturation polarization P_{sat}. If the electric field is then removed, some of the domains do not return to their random configurations and orientations. The polarization at this stage is called the remnant polarization P_r. The strength of the electric field required to return the polarization to zero is the coercive field, E_c.

Although it is possible to utilize these ferroelectric properties for a wide variety of applications, the primary impetus of recent research activity in this field is directed towards the development of nonvolatile random access memories [4]. In principle, the memory application is based on the hysteresis behavior of polarization with electric field as shown in Fig. 1.2. When an external voltage is applied to a ferroelectric capacitor, there is a net ionic displacement in the unit cells of the ferroelectric material. The individual unit cells interact constructively with their neighbors to produce domains within the material. As the voltage is removed, the majority of the domains will remain poled in the direction of the applied field, requiring compensating charge to remain on the plates of the capacitor. It is this compensating charge that causes the hysteresis in the polarization with applied external voltage [8]. At zero applied field, there are two states of polarization, $\pm P_r$. Furthermore, these two states of polarization are equally stable. Either of these two states could be encoded as a '1' or a '0' and since no external field (power) is required to

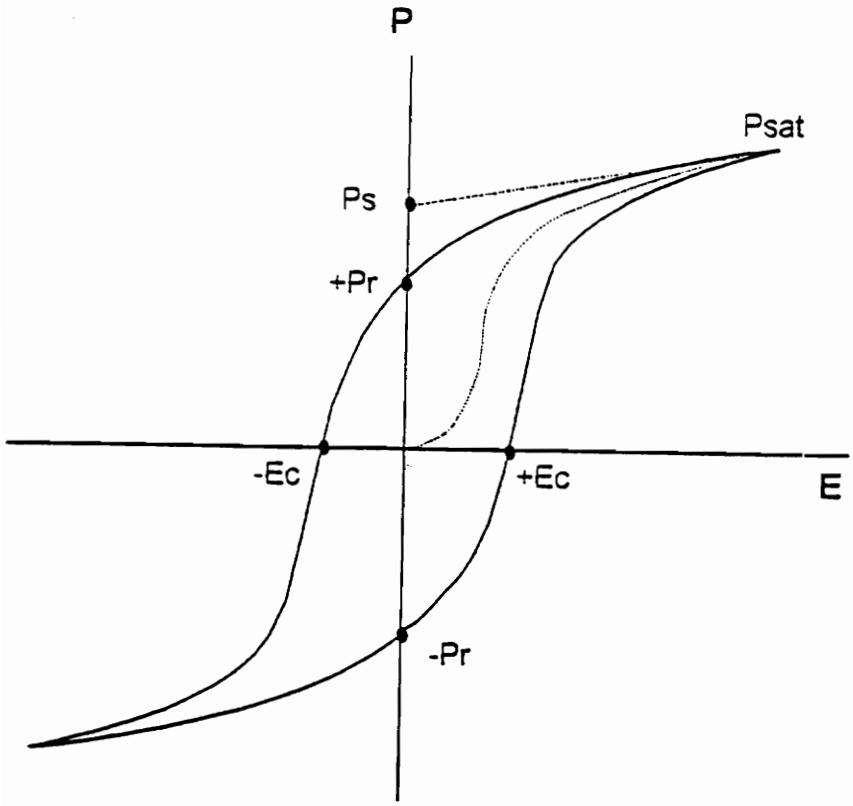

Figure 1.2 Hysteresis loop of a ferroelectric material

maintain these states, the memory device is nonvolatile. Clearly, to switch the state of the device, a threshold field greater than $\pm E_c$ is required. Additionally, in order to reduce the required applied voltage (to within 5V) for a given E_c, the ferroelectric materials need to be processed in the form of thin films.

From a digital point of view, if a voltage is applied to a ferroelectric capacitor in a direction opposite of the previous voltage, the remnant domains will switch, requiring compensating charge to flow onto the capacitor plates [8]. If the field is applied in the direction of the previously applied field, no switching takes place, no change occurs in the compensating charge, and a reduced amount of charge flows to the capacitor. This property can be used to read the state or write a desired state into the capacitor. In most ferroelectric memories, the memory cell is read destructively by sensing the current transient that is delivered to a small load resistor when an external voltage is applied to the cell. For example, if a memory cell is in a negative state ($-P_r$) and a positive switching voltage is applied to it, there will be a switching of charge given by [4-5]:

$$Q = A\varepsilon E_a + A(dP/dt) \qquad (1.1)$$

where A is area of the cell, ε is the dielectric constant of the ferroelectric material, E_a is the applied field and P is the polarization of the ferroelectric. Equation 1.1 indicates that this current transient, known as the "switching current", consists of a linear dielectric response ($A\varepsilon E_a$) and a displacement current. A "nonswitching current" transient, for example, is the response of a memory cell in a positive state ($+P_r$) to a positive applied voltage. In this case,

$$Q = A\varepsilon E_a \qquad (1.2)$$

A sense amplifier and other associated circuitry is used in a FRAM device to determine these current transients and thereby read the state of the device.

The basic operation discussed so far described the working of a typical destructive readout (DRO) single transistor-single capacitor ferroelectric memory device. It may noted that ferroelectric materials are also being considered for other memory device versions such as single transistor metal-ferroelectric-semiconductor (MFST) nonswitching memory applications and low voltage nondestructive readout applications [2-3]. However, throughout this dissertation, our focus will be on the DRO single transistor-single capacitor ferroelectric memories.

1.3 PURPOSE OF RESEARCH

One of the proposed memory cell configurations for a FRAM consists of a single ferroelectric capacitor on top of a single CMOS (complementary metal oxide semiconductor) transistor in each memory cell [1-2]. A schematic of this structure is shown in Fig. 1.3. The capacitor stores the charge (i.e., the information) and the CMOS transistor is used to access the device. From the standpoint of VLSI (Very Large Scale Integrated circuit) production, the insertion of the ferroelectric capacitor into the existing CMOS devices is far less complicated than developing an entirely new processing scheme. However, there are several technological issues involved in the integration process that are strongly dependent on the ferroelectric and electrode materials; therefore, the choice of materials is a critical factor in determining the performance of the device. The materials chosen must not only have excellent figures of merit, but also have to satisfy the very stringent VLSI fabrication requirements. In general, for FRAM applications, the ferroelectric material should show a high P_r, low E_c, low dielectric constant, low dielectric

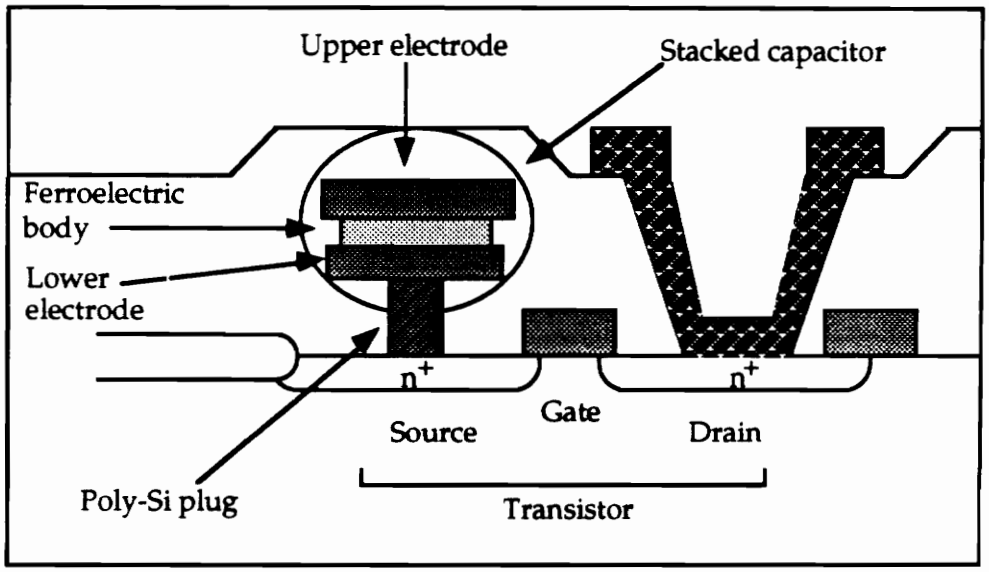

Figure 1.3 Proposed ferroelectric memory cell device configuration

loss, high Curie temperature and good thermal stability in a wide range of ambient conditions[1-3, 9]. Although several candidate ferroelectrics such as triglycerine sulphate (TGS), KNO_3, $BaTiO_3$, $PbTiO_3$ and other members of the perovskite titanate and niobate families have been proposed, it is now widely acknowledged that the solid solution of $PbTiO_3$ and $PbZrO_3$ i.e., $PbZr_xTi_{1-x}O_3$ (PZT) with a composition close to x = 0.5 is highly suitable for memory applications [1-3, 9]. The popularity of PZT (x =0.5) is due to a combination of excellent ferroelectric properties, a wide operating temperature range, stability in a wide range of operating conditions and the availability of a large knowledge base on this material in the bulk form [5]. The electrode material requires compatibility with VLSI processing, high conductivity, minimal interaction (interdiffusion barrier) with ferroelectric and substrate materials at the processing temperatures and amenability to dry etching. Currently, Pt is the most commonly used electrode material for PZT thin film applications because of its high conductivity and high chemical and thermal stability.

Although Pt/PZT/Pt capacitors are currently the most popular candidates for FRAM applications, there are still several technological issues that continue to hinder the commercial development of these memories. These problems can be broadly classified as : (a) development of a low temperature thin film deposition process for the ferroelectric and electrode materials; (b) reliability issues that include degradation problems such as fatigue (loss of polarization on repeated switching), aging (polarization decay with time), high leakage currents (conduction in the dielectrics), time dependent dielectric breakdown and imprint (locking in a preferred polarization state) in the ferroelectric films; and (c) process integration issues including the development of an etching technology for patterning the ferroelectric capacitors.

For ferroelectric thin films, the preferred deposition process is the one that can provide the required ferroelectric phase at fairly low growth temperatures. High growth

temperatures can cause interdiffusion problems between the ferroelectric, electrode and the substrate materials and thereby degrade the properties of the device. The deposition process should also provide stoichiometric control, smooth morphology and high packing density in the films. Significant progress has been made in identifying processes that can meet these requirements [10-15]. However, the reliability of the deposited films is still a major concern and a principal topic of research in this field. Reliability issues have been studied in detail for several years and yet no satisfactory explanation has been found. However, it is now widely believed that most of the degradation phenomena arise from a common source and therefore a thorough fundamental understanding of one of these issues may provide insight into the other issues as well.

Some of the suggested requirements for ferroelectric capacitors for DRO FRAM applications are [1-3]:

(1) The lower limit of charge capacity should be from 5-10 $\mu C/cm^2$.

(2) The coercive field should not be greater than 50-60 kV/cm.

(3) The desirable dielectric constant is in the range of 200-300.

(4) Fatigue lifetime up to 10^{12} cycles, the ideal lifetime being 10^{15} cycles.

(5) Wide operating temperature range (determined mainly by Curie point) : -55 ^oC to 120 ^oC. (6) Leakage current density smaller than 10^{-8} A/cm^2.

(7) Compatibility to VLSI fabrication.

(8) Etch rates of at least 20 nm/min.

1.4 OBJECTIVES OF THIS RESEARCH

This research is primarily focused on the problem of fatigue. One of the objectives is to devise and demonstrate means to minimize the problem of fatigue (reliability issue)

on the basis of currently available understanding on this phenomena. An additional objective is to identify an etching technology (process integration issue) for patterning of the ferroelectric capacitors. The etching process should provide high etch rates, good etch anisotropy, high etch selectivity and minimal post etch residues. Additionally, the damage to the ferroelectric properties of the capacitors due to radiation should be minimal. Although the primary focus is on these objectives, it will become clear through the course of this dissertation that these problems are not always addressed individually but rather in conjunction with the other listed requirements. In other words, the scientific efforts described here are also geared towards reaching the ultimate objective of producing a reliable ferroelectric memory device and not just solving these problems alone.

1.5 PRESENTATION OF RESULTS

Each chapter is a journal article and contains its own abstract, introduction, experimental procedure, results and discussion, conclusions and references. In chapter 2, the problem of fatigue is discussed along with some of the earlier models that have been used to describe the phenomenon. A quantitative fatigue model is then presented and experimental evidence to support the model is provided. Fatigue has been attributed to domain pinning by space charge due to oxygen vacancy entrapment at the electrode-ferroelectric interface in the capacitors. Based on this model, guidelines required to minimize the problem have been derived. These include (a) control of the interface state and (b) the control of defect density. Chapters 3 presents the results on fatigue minimization by using oxide electrodes (control of the interface state) for PZT thin films. However, it was found that the leakage current of oxide electrode/PZT capacitors are higher than their metal counterparts. Simultaneous reduction of fatigue and leakage

current has been achieved by using multilayer metal/metal oxide electrodes as shown in Chapter 4. Chapter 5 is devoted to the discussion on minimization of fatigue by controlling the defect density through : (a) addition of donor dopants (e.g., Nb in PZT) and (b) utilizing alternate ferroelectric materials with low intrinsic defect concentration. As a result of the latter approach, layered structure $SrBi_2Ta_2O_9$ thin films were identified as good candidates for fatigue free ferroelectric memory applications. The formation of these films and the effect of orientation on the ferroelectric properties of these highly anisotropic materials are discussed in Chapter 6 and Chapter 7, respectively. Chapter 8 addresses the process integration issue of etching and describes the results of a novel etch chemistry for patterning of PZT thin film capacitors. A mechanism for the etching process is also suggested. In chapter 9, the complete study is summarized and the overall conclusions are presented.

1.6 REFERENCES

1. J. F. Scott and C.A. Paz de Araujo, "Ferroelectric Memories', *Science*, 246, (1989), p.1400.

2. L.H. Parker and A.F. Tasch, "Ferroelectric Materials For 64 Mbit and 256 Mbit DRAMs", *IEEE Circuits and Devices*, Jan. 1990, pp.17.

3. A.F. Tasch and L.H. Parker, "Memory Cell and Technology Issues for 64- and 256-Mbit One Transistor MOS DRAMs", *Proc. IEEE*, 77(3), (1989), 374-378.

4. M.E. Lines and A.M. Glass, *Principles and Applications of Ferroelectrics and Related Materials*, Clanrendon Press, Oxford (1977).

5. B. Jaffe, W.R. Cook, and H. Jaffe, *Piezoelectric Ceramics*, London:Academic, (1971).

6. J.C. Burfoot and G.W. Taylor, *Polar Dielectrics and Their Applications*, Berkely: Univ. of Calif. Press, (1979).

7. J.M. Herbert, *Ceramic Dielectrics and Capacitors*, New York: Gordon and Breach, (1985).

8. J.T. Evans and R. Womack, "An Experimental 512-bit Nonvolatile Memory with Ferroelectric Storage Cell", *IEEE J. Solid. State. Circuits.*, 23(5), (1988), p.1171.

9. Anonymous, "Application Note: Nonvolatile Ferroelectronics", *Microprocessors and Microsystems*, 13(4), (1989), 291-296.

10. M. Okuyama, Y. Matsui, H. Nakano, T. Nagakawa and Y. Hamakawa, "Preparation of $PbTiO_3$ Ferroelectric Thin Films by RF Sputtering", *Jpn. J. Appl. Phys.*, 18(8), (1979), 1633-1634.

11. T. Nakagawa, J. Yamaguchi, M. Okuyama and Y. Hamakawa, "Preparation of $PbTiO_3$ Ferroelectric Thin Films by Chemical Vapor Deposition", *Jpn. J. Appl. Phys.*, 21(10), (1982), L655-L656.

12. S. Dey and R. Zuleeg, "Integrated Sol-gel PZT Thin Films on Pt, Si, and GaAs for Nonvolatile Memory Applications", *Ferroelectrics*, 108, (1990), 37-46.

13. K. Saenger, R.Roy, K. Etzold and J. Cuomo, "PZT Thin Films Produced By Pulsed Laser Ablation", *Mat. Res. Soc. Symp. Proc.*, 200, (1991), 115-120.

14. C. Peng and S.B. Desu, "Low Temperature MOCVD of Perovskite PZT Thin Films", *Appl. Phys. Lett.*, 61(1), (1992), p. 273.

15. R. Castellano, "Deposition of Thin Films of PZT by a Focused Ion Beam Sputtering Techniques", *Ferroelectrics*, 28, (1980), 387-389.

This paper titled

"Fatigue in Ferroelectric Thin Films"

has been submitted to

Physica Status Solidi, (1995)

The co-authors in this paper are Dr.S.B. Desu (first author) and Dr. I.K. Yoo. Most of the theoretical modeling described in this chapter have been conducted by Dr. S.B. Desu and Dr. I.K. Yoo. My contribution to this work was in experimental verification of the model and in providing the guidelines to overcome the fatigue problem.

Chapter 2 : Fatigue-Problem Definition and Modeling

2.1 ABSTRACT

Several of the previous models proposed for fatigue, pertaining to both bulk and thin film materials, are reviewed. A quantitative model is proposed that attributes fatigue to domain pinning by space charge at various interfaces in the ferroelectric capacitors. The origin of the space charge has been ascribed to oxygen vacancy movement and entrapment at the interfaces (e.g., electrode-ferroelectric, domain boundaries etc.) under a high alternating electric field. A quantitative expression for fatigue has been derived in accordance with this model. Experimental evidences that confirm the presence of the space charge layers at the electrode-ferroelectric interface are also presented. Based on this model, it is suggested that fatigue can be minimized by : (a) by replacing the conventional metal electrodes by conductive oxides to prevent space charge formation at the interfaces; (b) by addition of donor dopants (e.g., Nb, La in $Pb(Zr_xTi_{1-x})O_3$) to reduce the oxygen vacancy concentration and (c) by utilizing ferroelectric materials that have a low intrinsic defect concentration.

2.2 INTRODUCTION

Over the last few decades, there has been an increasing interest in ferroelectric materials for nonvolatile ferroelectric memory (FRAM) applications [1-3]. In principle, the memory application of these materials is based on the hysteresis behavior of polarization with applied electric field as shown in Fig. 2.1. At zero applied field, there are two equally stable states of polarization, $\pm P_r$ (remnant polarization). Integration of submicron thin film

ferroelectric capacitors, for e.g., lead zirconate titanate (PZT), into the existing silicon based transistor technology can provide a transistor-capacitor based ferroelectric memory cell. Either of the two states of polarization could be encoded as a '1' or a '0' in the memory device and since no external field is required to maintain these states, the memory device is nonvolatile.

Ferroelectric memories are most often designed with destructive electrical read out. To read the stored information, an electric field greater than the threshold field (E_c, see Fig. 2.1) is applied to each memory cell. In memory elements where the polarization is opposite to the applied field direction (for e.g., state '1' for a positive applied field in Fig. 2.1), there is a large displacement current accompanying the polarization reversal while only a displacement current occurs in elements having a polarization assisting the field (e.g., state '0' for a positive field). The state of each memory element is therefore read by measuring the displacement current corresponding to each voltage pulse. The difference between the two displacements currents corresponds to the net amount of switched charge for each polarization reversal [4]. Evidently, this kind of an electrical read out involves several polarization reversals in the ferroelectric films over the device lifetime.

In some of the more popular metal-ferroelectric-metal capacitor systems such as Pt/PZT/Pt, a progressive decrease in the amount of switched charge is commonly observed with increasing polarization reversals [1-4]. Eventually, after a large number of read/erase/write operations, the switchable polarization decreases to a value that is too low to distinguish between the states, thereby rendering the memory cells ineffective. Additionally, the threshold field required to switch the state of the device also increases with increasing polarization reversals. This degradation phenomenon is known as fatigue and is one of the more profound problems hampering the development of commercial FRAM devices. Fatigue in these memories can limit the number of read/erase/write

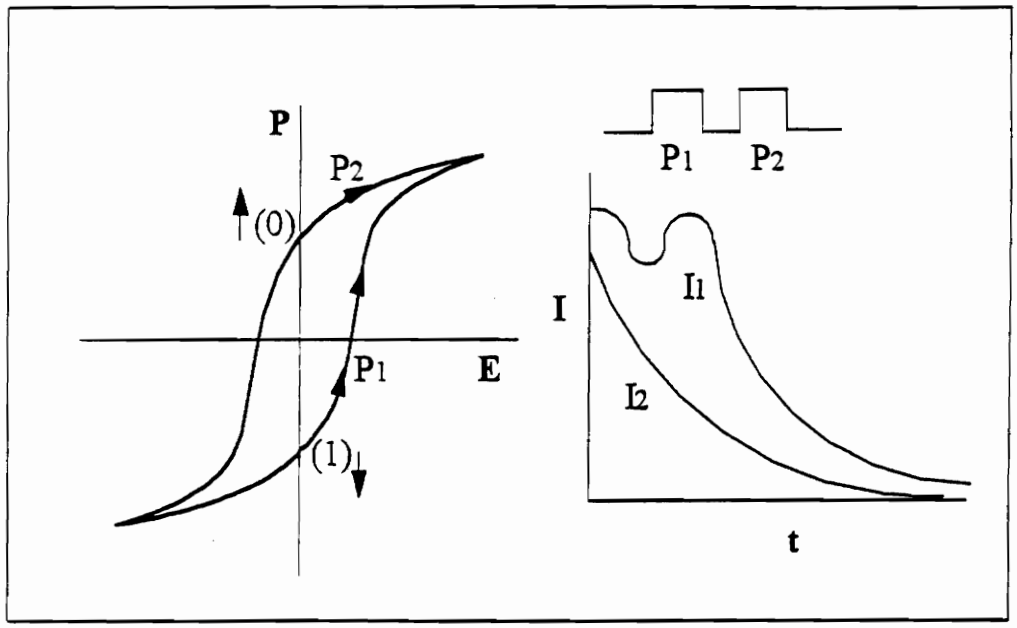

Figure 2.1 Schematic of the read/write operation in a ferroelectric memory cell

operations to less than 10^6 cycles [1]. For ferroelectric memories to become competitive with existing nonvolatile memories such as EEPROMs, they must either be improved to withstand at least 10^{12} erase/write operations or they must have qualitatively different nondestructive operations.

2.3 FATIGUE MODEL

Fatigue in ferroelectric devices has been studied for several years and several mechanisms have been proposed to explain this degradation phenomena [5-6]. For ferroelectric oxides, such as the commonly used perovskite titanates, fatigue is believed to occur form three different microscopic causes:

(1) The earlier mechanisms proposed for bulk ceramics were based on stress relaxation of 90^o domains in pseudocubic crystals [7-10]. The stresses originate when the ferroelectric material is cooled from high temperatures through its Curie point. As the internal mechanical stresses are released at low temperatures, the orthogonal domains relax back to their 180^o configurations and in doing so reorient and reduce the net polarization. Pelssener [7] has postulated that under the influence of a stress field, the domain walls are in a metastable position and therefore the material exhibits a larger value of polarization. With relaxation of the internal stresses, the domain walls move towards their equilibrium positions accompanied by a decrease in polarization. In the same light, the pinning of 180^o domains by stress or charge has also been proposed as a possible fatigue mechanism [10]. However, the stress relaxation model is more pertinent to bulk ferroelectrics. Additionally, the models have been proposed based on conventional low field measurements. In thin film ferroelectrics (~ 200 nm) used for memory applications, the electric fields are orders of magnitude larger (~ 1 MV/cm) than in bulk ceramics.

(2) Earlier models for fatigue in thin film ferroelectrics were based on 'poling' of charged defect pairs such as acceptor centers and oxygen vacancy neighbors (lead vacancies and oxygen vacancies form similar pairs) [11-13]. Repeated application of large electric fields can align these dipoles. However, these defect pairs take a longer time to undergo reversal in the alternating field, providing opposing dipoles that compensate much of lattice polarization and reduce the amount of switched charge in the film. The acceptor centers in PZT arises from an excess of acceptor impurities induced during the growth of the material. These acceptors are compensated by the oxygen vacancies causing the material to be a p-type wide-band-gap semiconductor. In an oxidizing atmosphere, a small percentage of the oxygen vacancies are filled, creating two holes for every filled vacancy. Under the high switching field employed in thin films, the trapped holes can hop through the unoccupied acceptor levels to redistribute the charge. This model provided the electrochemical basis for future models on fatigue.

(3) In many of the recent models, accumulation of space charge at or near the electrode-ferroelectric interface has been proposed as the source of fatigue [14-19]. A theoretical expression for polarization decrease was developed by Karan [18] based on space charge entrapment inside the ferroelectric that results in an increase in the interfacial resistance and decrease in the interfacial capacitance. Zheludev [19] proposed a planar model based on the formation of an inactive surface by space charge at the electrode-ferroelectric interfaces to produce a smaller amount of switched charge. Kudzin et al [15] ascribed fatigue to the accumulation and resorption of space charge at the domain boundaries. The domain wall loses its capacity to move and the resultant value of the switching charge diminishes. Duiker et al [13] simulated fatigue by assuming dendritic growth of oxygen-deficient filaments. They proposed a theoretical model based on impact ionization (e.g., Ti^{4+} to Ti^{3+} conversion in PZT) of the ferroelectric material near the electrodes. This is

followed by O^- diffusion away from the ion with the altered valance (Ti^{3+}) resulting in oxygen deficient regions near the electrode-ferroelectric interface. The spontaneous polarization was assumed to be proportional to the effective films thickness (distance between the dendritic filaments of growing from opposite electrodes) and with decreasing thickness the value goes down. Notwithstanding the popularity of this model, no experimental evidence is available to show this dendritic growth at the interfaces in thin film materials. However, such dendrites have been observed around micropores in bulk ferroelectrics after fatigue.

In this paper, the problem of fatigue is discussed on the basis of a recent quantitative model that has been developed by the authors [20-23]. A few characteristics of fatigue in thin film ferroelectric memories is presented before this discussion. Fatigue in ferroelectric capacitors is not only manifest as a loss of switchable polarization but also an increase in coercive field with increasing number of polarization reversals as shown in Fig. 2.2 . Additionally, the fatigue rate is much slower at higher temperatures as evident from the data for sputtered PZT in Fig. 2.3. Furthermore, it is commonly observed that the polarization loss in ferroelectrics such as PZT and KNO_3 can be recovered partly or fully either by applying a voltage pulse higher than the nominal switching voltage [1] or by thermally annealing the ferroelectric material above its Curie temperature. In other words, the capacitors can be "rejuvenated" after fatigue. Finally, although not often considered, the switching time decreases linearly with polarization during fatigue [13]. Considering these effects, a quantitative fatigue model for Pt/PZT/Pt capacitors is proposed in which defect movement under alternating pulses and defect entrapment at trapping sites such as electrode-ferroelectric interfaces, domain boundaries and grain boundaries has been cited as the source for fatigue. These point defects could either be extrinsic or intrinsic. Extrinsic defects are impurities (e.g., acceptor atoms in PZT) that are incorporated in the

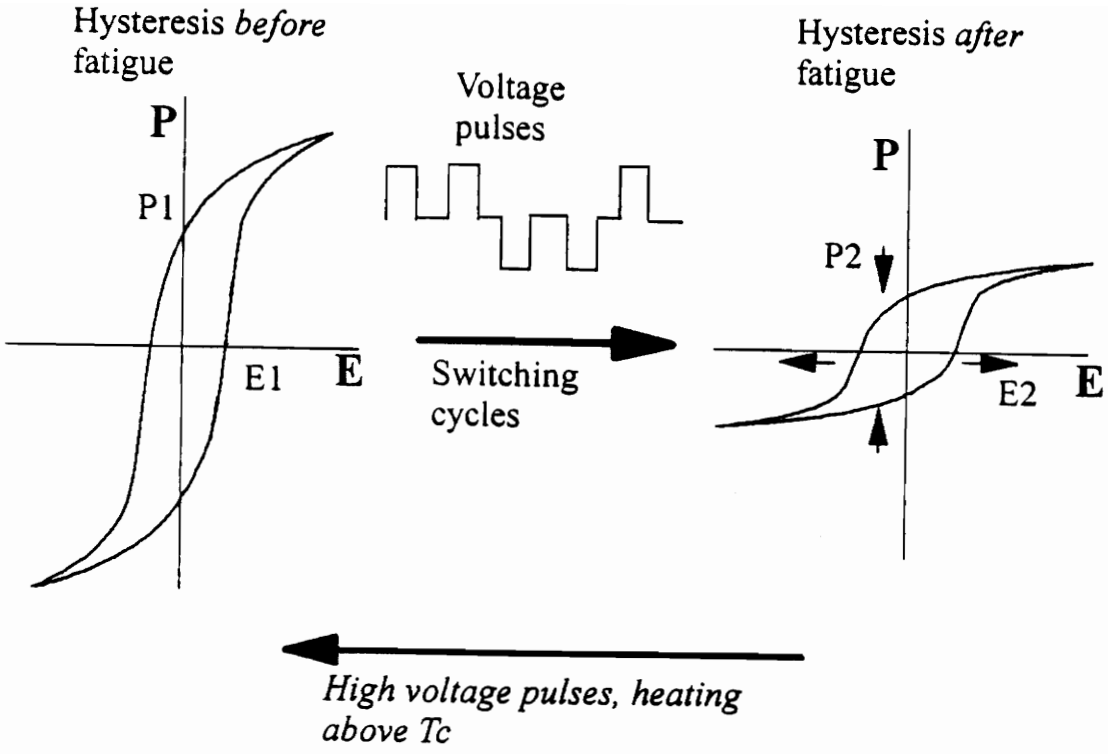

Figure 2.2 **Effect of fatigue on the properties (polarization and coercive field) of a thin film ferroelectric material [13]**

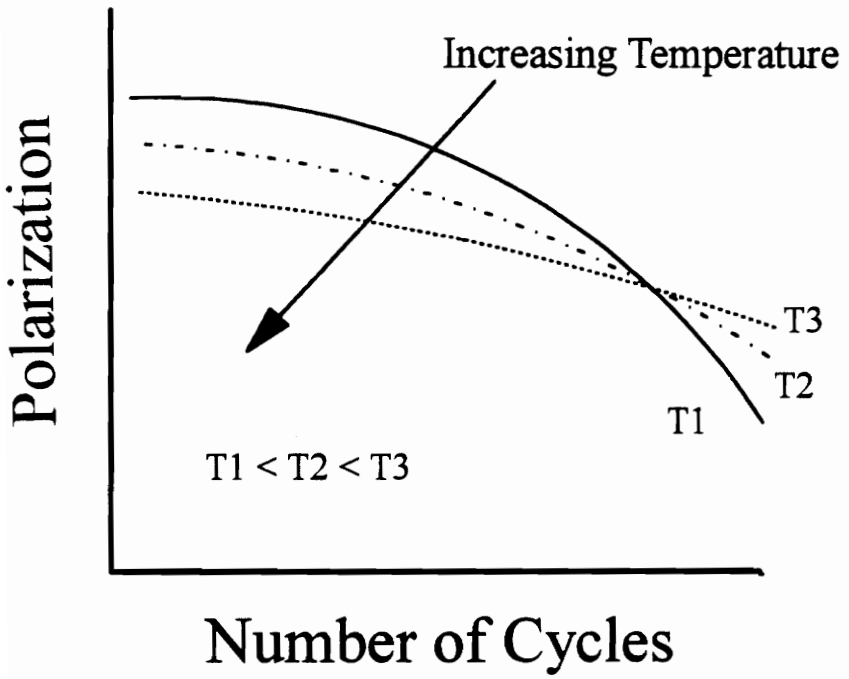

Figure 2.3 Temperature dependence of the fatigue rate [13]

films during processing and can be controlled by controlling the processing environment. Intrinsic defects may include both defects that maintain the stoichiometry (Schottky) and defects that alter the stoichiometry in the materials.

Schottky defects in perovskite (ABO_3) ferroelectrics may be represented by a quasi-chemical reaction (in Kroger-Vink notation) as :

$$A_A + B_B + 3O_O \rightarrow V_A'' + V_B'' + 3V_O^{\infty} + A_s + B_s + 3O_s \qquad (2.1)$$

where A_A, B_B, $3O_O$ represent respectively occupied A, B and O sites; V_A'',V_B'', V_O^{∞} represent vacancies of A, B and O atoms; and A_s, B_s, $3O_s$ are the respective Schottky defects. A typical example of defects that alter the stoichiometry are vacancies that are formed due to the vaporization of one or more volatile components in the multicomponent oxide materials. In the case of PZT, for example, a processing temperature of at least 600 °C is required to form the ferroelectric phase. However, the PbO component begins volatilizing at temperatures as low as 550 °C, resulting in the formation of oxygen and lead vacancies as shown below :

$$Pb_{Pb} + Ti_{Ti} + Zr_{Zr} + 3O_O \rightarrow xPbO + xV_{Pb}'' + xV_O^{\infty} + (1-x)\,Pb_{Pb} + Ti_{Ti} + Zr_{Zr} + (1-x)\,O_O \qquad (2.2)$$

When an a.c. field is applied to a ferroelectric capacitor shown schematically in Fig. 2.4, the ferroelectric material is polarized and an internal field is created by this polarization. The net local field is then expressed as [20-23] :

$$E_L = E_A - E_i \qquad (2.3)$$

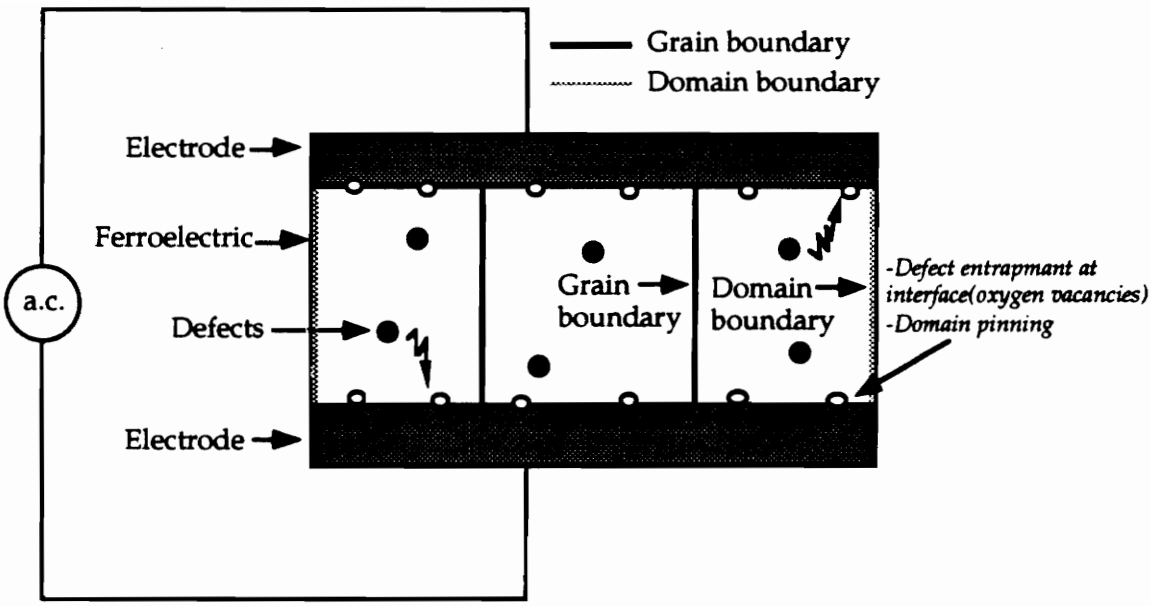

Figure 2.4 Schematic of the fatigue model for a ferroelectric capacitor

where E_A is the applied field and E_i is the internal field. Although the externally applied field is symmetric, the net local field is asymmetric as a result of the internal field contribution. Under this asymmetric local field, there is an effective one-directional movement of the mobile defects (mainly oxygen vacancies as shown in eqns. (1) and (2)) towards the electrode-ferroelectric interfaces. Additionally, the defect segregation to the interfaces with increasing polarization reversals could also be induced by the domain sweeping phenomena. In general, in polycrystalline thin films, the grain growth is usually continuous form the bottom interface to the top surface of the films. In ferroelectric thin films, each of these grains commonly constitutes a single domain. In other words, the grain boundaries and the domain boundaries are usually coincident with the electorde-ferroelectric interfaces. The large interfacial energy at these boundaries/interfaces provides low potential energy sites for the defects and as a result causes their entrapment. Defect entrapment at the interfaces results in the development of space charge in these regions which in turn causes the domains to be pinned. Clearly, for a given applied field, pinning of the domains results in a reduced polarization. Additionally, a greater field is required to cause the switching of the domains. This explains the increase in coercive field with fatigue. By applying a high voltage pulse or by thermal cycling, the domains can be "depined" from the space charge and thus the polarization values can be restored. At high temperatures, thermal effects cause a constant redistribution of the space charge and prevent their segregation at the interfaces. This explains the observation that fatigue rate is lower at higher temperatures.

To derive a quantitative fatigue expression, the number of defects trapped at the interface at a certain test cycling n was described by [20-23]:

$$dN/dn = \Delta j \, \Delta t \qquad (2.4)$$

where N is the total defect number trapped at the interface at n, Δj is the net defect flux density between n and n + 1 test cycles, and Δt is the applied pulse width. The polarization loss due to defect entrapment at the interfaces was then assumed to follow the relationship:

$$dP/dN = -\nu P \qquad (2.5)$$

where P is the polarization with defect entrapment N, and ν is the polarization loss constant related to lattice structures. The polarization at a certain test cycle will be different from the one following that as a result of the loss of polarization at the interface. This polarization difference itself will decrease as the defect entrapment continues and the polarization at both the polarities eventually goes to zero. The polarization is related to the domain size and the domain size to the domain wall velocity. The domain wall velocity is related to the domain mobility (μ) in the following way :

$$\Delta v_w = \mu \, \Delta E_i \qquad (2.6)$$

As the interface loses polarization, the internal field decreases resulting in an increase in the local field [Eqn. 2.3]. The domain wall velocity difference will therefore decrease as the number of trapped defects increases. The larger incoming defect flux will cause a higher decreasing rate of velocity difference of domain walls :

$$d\Delta v_w /dN = -\gamma \Delta j \Delta t \qquad (2.7)$$

where γ is a constant. The net flux density can be approximated as :

$$\Delta j = \lambda e^{-Q/kT} (zqb/2kT)(e^{zqbE_A/2kT})\Delta E_i \qquad (2.8)$$

where, $\lambda = \nu\rho e^{\Delta S/k}$, ν is the defect migration velocity, ρ is the defect concentration, ΔS is the entropy for defect movement, Q is the activation energy for defect movement, z is the valence number, q is the electronic charge and b is the jump distance. Equation 2.7 can therefore be expressed as:

$$d\Delta E_i/dN = (\gamma/\mu)(\Delta j \Delta t) = -\xi \Delta E_i \qquad (2.9)$$

where,

$$\xi = (\gamma/\mu)\,(\lambda e^{-Q/kT})\,(zqb/2kT)\,(e^{zqbE_A/2kT})\,\Delta t \qquad (2.10)$$

From equations (2.4), (2.5) and (2.9), a fatigue equation is derived as :

$$\mathbf{P = P_o[(\xi^2 \mu \Delta E_{io} n/\gamma) + 1]^{-\nu/\xi} = P_o(An + 1)^{-m}} \qquad (2.11)$$

where Po is the initial polarization, ΔE_{io} is the initial internal field difference, A is termed as the piling constant and m is the decay constant. A and m are voltage and temperature dependent constants related to the dielectric viscosity, defect velocity, defect concentration, activation energy for defect movement (Q), jump distance, polarization loss constant, domain wall mobility and activation energy for domain wall movement. The validity of the above fatigue equation was verified by measuring the fatigue of PZT thin film capacitors on Pt electrodes at various voltages [20-23]. Figure 2.5 illustrates the fatigue at room temperature in these samples at various voltages. The voltage dependence

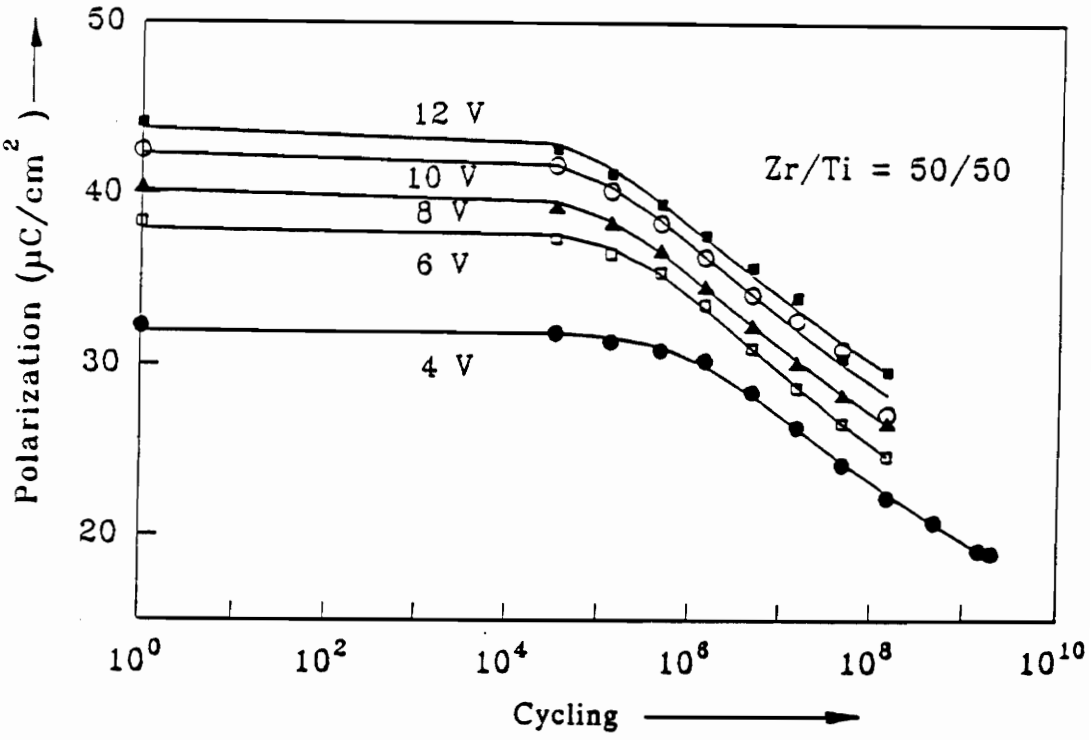

Figure 2.5 **Fatigue curve fitting for Pt/PZT/Pt capacitors as a function of voltage (t = 0.3 μm, size = 0.1x 0.1 mm^2) [20]**

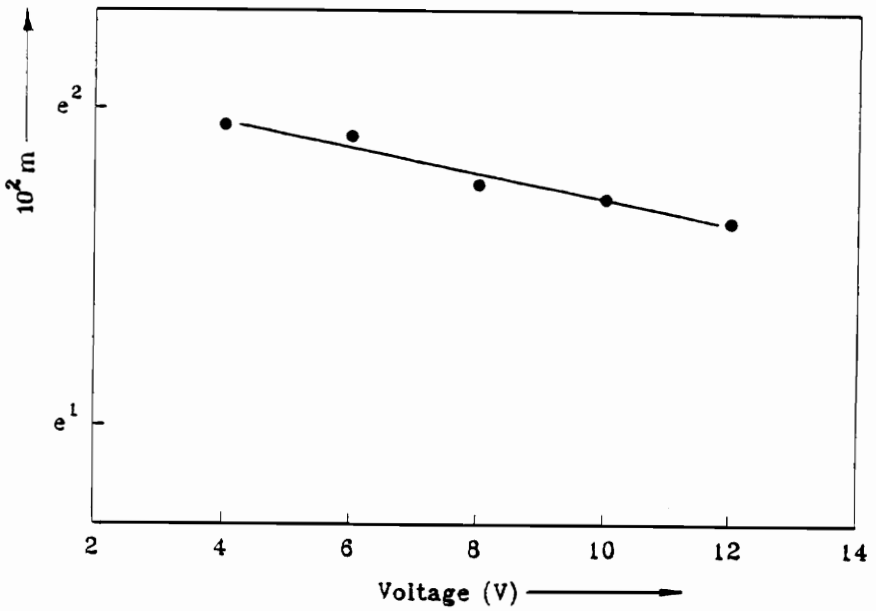

Figure 2.6 **Voltage dependence of the decay constant. Calculated jump distance = 0.418 nm, measured lattice constants : a = 0.4113 nm and c = 0.4138 nm [20]**

of the decay constant is then plotted based on these curves in Figure 2.6. Assuming migration of defects towards the interface with constant flux density, the dependence can be expressed as :

$$\ln (\nu/\xi) = \text{const} - (zqb/2kTd)\, V_A \qquad (2.12)$$

where V_A is the applied voltage and d is the thickness of the film. Using a valance (z) of 2 for oxygen or lead vacancies the jump distance b was calculated from the slope of this curve to be 0.418 nm which is very close to the lattice parameter c of PZT films (0.4138 nm). This result indicates oxygen and/or lead vacancies migrate to the parallel or antiparallel to the polarization direction depending on the sign of the vacancy charge.

2.5 EXPERIMENTAL EVIDENCE

There is sufficient experimental evidence to indicate that accumulation of oxygen vacancies at the electrode-ferroelectric interfaces has a direct effect on the fatigue properties of the ferroelectric films. The role of oxygen vacancies, at the surfaces of ferroelectric perovskites was first discussed by Kanzig [24]. Experimental evidence for the presence of surface space charge layers in very small semiconducting ferroelectric $BaTiO_3$ particles was provided by conducting x-ray and electron diffraction experiments. A discrepancy in symmetry was noticed between a surface layer of about 10 nm thick and the bulk; a tetragonal surface layer was observed above the Curie point while the bulk structure was cubic. The production of Schottky barriers due to this space charge at the electrode-ferroelectric interface (in bulk materials) was first examined by Triebwasser [25]. The relevance of this work is discussed in a later paper.

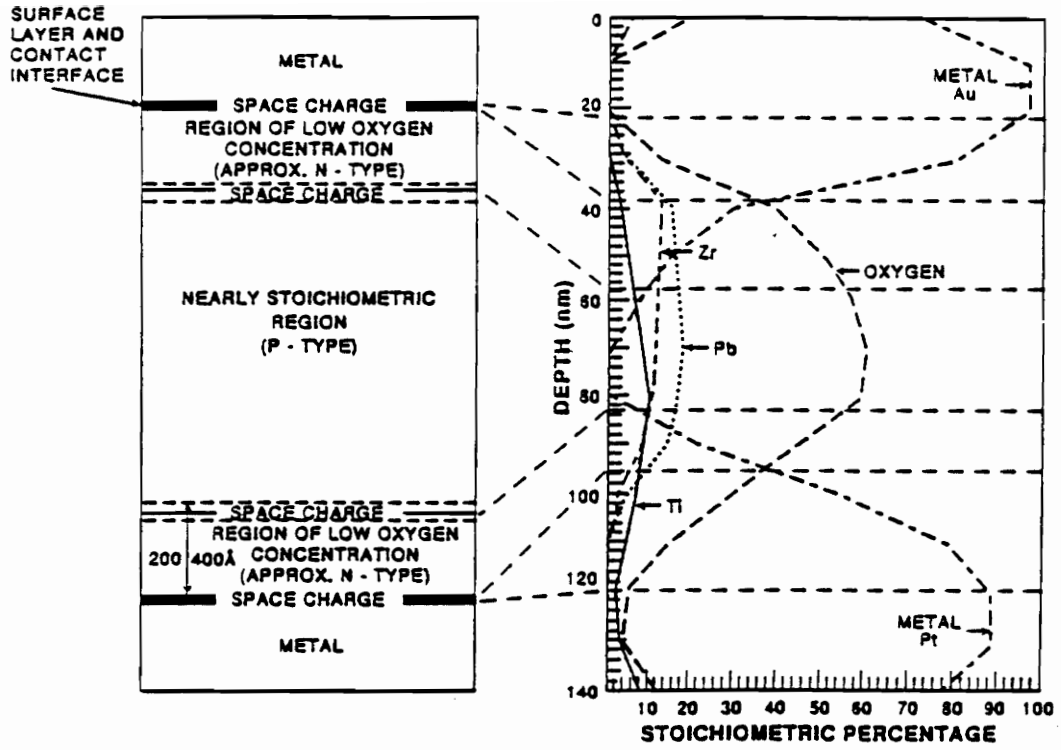

Figure 2.7 Auger microprobe data for fatigued PZT films with Pt and Au electrodes. Note that the oxygen concentration drops off near the electrodes [26]

For the case of thin film capacitors, Scott et al [26] have measured the oxygen concentration through the ferroelectric Pt/PZT/Au capacitors before and after fatigue by using Auger electron spectroscopy (AES). Using this technique they have probed through the depth of the capacitors to determine the composition profile. Fig. 2.7 is a typical AES plot that they obtained. It can be noticed that the oxygen concentration drops off to nearly 50 % of its value in the center (after fatigue) while still 20 nm from the Pt surface indicating the presence of oxygen vacancies in this region. The diffusion of the Pt and Au electrode materials into the PZT bulk was due to the annealing procedure. Since the data is symmetric at the top and bottom of the film, knock-in and related artifacts due to the sputtering process in AES did not seem to affect the obtained data. It is assumed that most of these oxygen vacancies are compensated for by the Pb vacancies in the material and only a few oxygen vacancies trap electrons and create space charge regions.

Kwok and Desu [27] created near-surface oxygen depletion regions of different thickness in PZT films by processing the films under different partial pressures of oxygen and studied the role of oxygen vacancies on the ferroelectric and fatigue properties of the films. Their results are summarized in Table 2.1. The films processed under a low partial pressure of oxygen in the processing ambient (i.e., higher oxygen vacancy concentration on the surface of the films) showed a lower P_r and a higher E_c. Additionally, these films showed a relatively higher rate of fatigue for a given number of cycles ($\Delta P/P$ for a given N) as can be observed from Table 2.1.

Lee and Desu [28] have noted the development of interface space charge layers through capacitance measurements in Pt/PZT/Pt structures. The measured capacitance (C_m) was composed of three capacitors in series: a capacitor representing the bulk of the ferroelectric thin film material (C_B) and two representing the interfaces (C_i) [see insert of Fig. 2.8]. The capacitance of the sample was therefore formulated as :

Table 2.1 Role of oxygen vacancies on the ferroelectric and fatigue properties of the films [27]. Fatigue properties of Pt/PZT capacitors as a function of partial pressure of oxygen is presented.

P_{O_2} (atm.)	P_r ($\mu C/cm^2$)	E_c (kV/cm)	$\triangle P/P$ % (after 10^6 cycles)
10^{-2}	22.5	80	34
2×10^{-1}	30	80	22
1	30	60	21

$$1/C_m = 1/C_B + 2/C_i \qquad (2.13)$$

$$d_m/\varepsilon_r\varepsilon_o A = d_B/\varepsilon_B\varepsilon_o A + 2d_i/\varepsilon_i\varepsilon_o A \qquad (2.14)$$

where d_m and ε_r represent the total sample thickness and dielectric constant respectively; d_B and ε_B are the bulk thickness and dielectric constant respectively; d_i and ε_i are the interfacial layer thickness and dielectric constant respectively; ε_o is the permittivity of free space and A is the sample area. Since d_i is very small in comparison to d_B, $d_B \sim d_m$ and eqn 2.14 can be approximated as :

$$1/C_m = d_m/\varepsilon_B\varepsilon_o A + 2/C_i \qquad (2.15)$$

Thus, a plot of $1/C_m$ versus d_m yields $1/C_i$ from the y-axis intercept and bulk thin film permittivity, ε_B, from the slope. By measuring the capacitance of the samples as a function of thickness and number of fatigue cycles for Pt/PZT/Pt capacitors, Lee and Desu [28] have determined the interfacial capacitance and the bulk permittivity after each period of cycling. The plot is show in Fig. 2.8. The almost parallel line indicate that the bulk dielectric permittivity remains constant while the interfacial capacitance increases with increasing fatigue. This is attributed to the development of a wider depletion width due to space charge accumulation at the interface with progressive fatigue. The space charge concentration due to the oxygen vacancy at the surface for PZT thin films has been estimated to be around 5×10^{20} cm^{-3} [26].

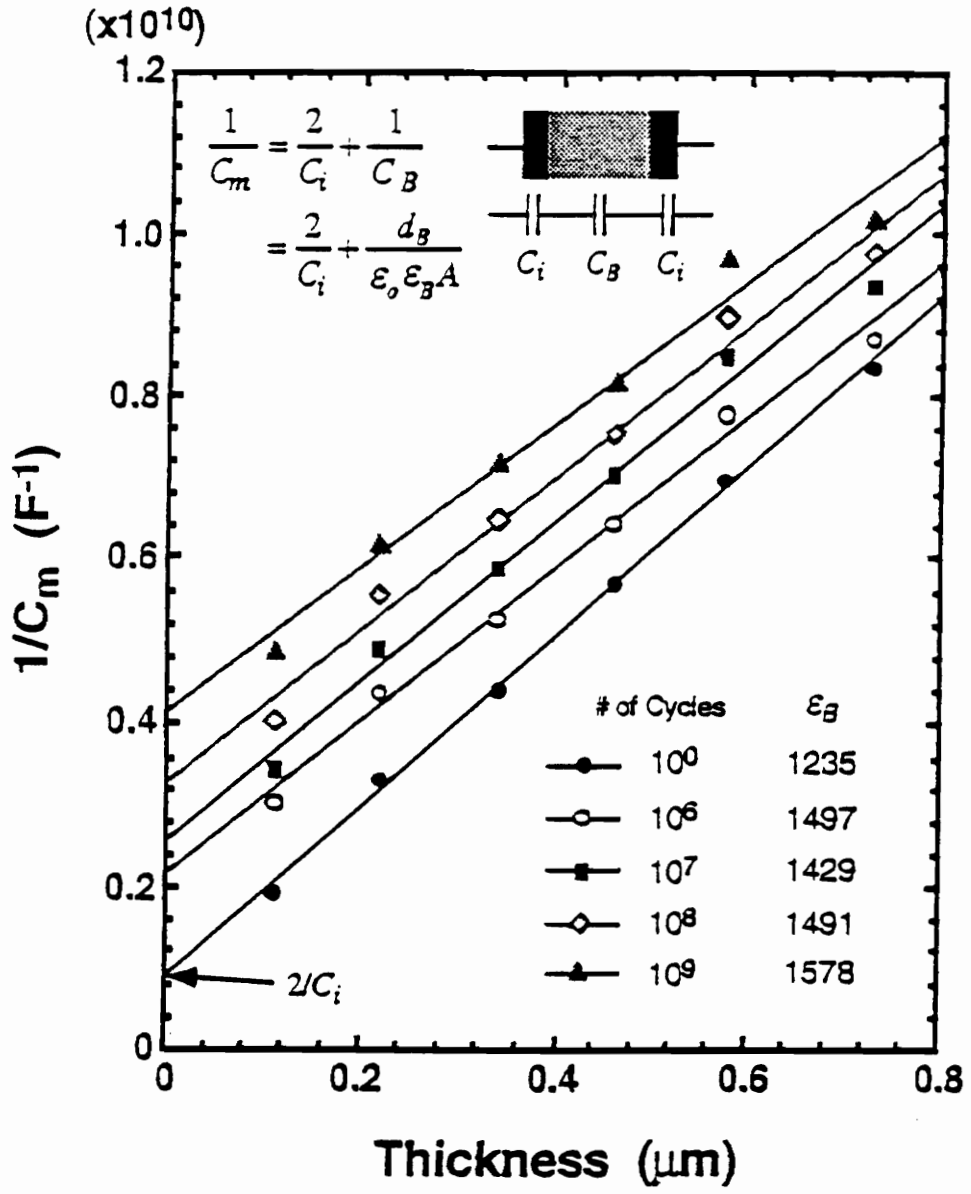

Figure 2.8 The fatigue cycle and thickness dependence of 1/Cm for Pt/PZT/Pt capacitors. The parallel lines indicates that the bulk dielectric constant does not change with fatigue cycling.

2.6 GUIDELINES FOR MINIMIZATION

The fatigue model discussed above provides some clear guidelines to minimize the degradation problem. If the relative movement of oxygen vacancies and their entrapment at the electrode-ferroelectric interface and/or at the domain boundaries and grain boundaries are the factors contributing to fatigue, then there are two possible solutions to overcome this problem : (1) reducing the tendency for defect entrapment by controlling the interface state and (2) controlling the defect density. To reduce the defect entrapment, the interfaces have to be made more stable or be minimized. To reduce the effect of grain boundaries, the thin films can be grown in the form of single crystals. However, processing of the single crystal thin films is not viable for large scale memory applications due to time and cost factors. In the case of Pt/PZT/Pt capacitors, the electrode-ferroelectric interface is highly unstable mainly because Pt is a metal that has very little affinity for oxygen and PZT is an oxide ceramic. A plausible way to increase the stability of the electrode-ferroelectric interface would therefore be to use an oxide electrode for the ferroelectric capacitor. Transition metal oxides such as RuO_2, IrO_2, OsO_2, Rh_2O_3 etc. are known to exhibit high electronic conductivity at room temperature and good thermal stability up to high temperatures. Therefore, one of the methods to minimize fatigue would be replace the current candidate Pt electrodes with these oxide electrodes. There are essentially two methods to minimize the defect density : (a) donor doping of the oxide ferroelectric films to compensate for the vacancies and (b) to use a ferroelectric material that a low intrinsic defect concentration. La and Nb are some of the more common donor dopants that can be used for PZT thin film materials. Replacing PZT with another ferroelectric material for memory applications is a difficult task. The replacement material will have to compete against other factors favoring PZT such as excellent ferroelectric properties, high Curie

temperature, wide operating temperature, well established low temperature (~ 600 ^{o}C) techniques and a wide knowledge base on this material.

2.7 SUMMARY

Fatigue in ferroelectric films has been attributed to domain pinning by space charge at the electrode-ferroelectric interfaces. The role of oxygen vacancies in the development of the space charge at the interfaces has been discussed. A quantitative expression for fatigue has been derived in accordance with this model. Various experimental evidences to support this model have also been presented. Based on this model, it has been suggested that fatigue can be minimized by : (1) controlling the interface state by using conductive oxide electrodes such as RuO_2 (for PZT films) which can consume the oxygen vacancies at the electrode and ferroelectric interface and thus eliminate the space charge development and (2) controlling the defect (mainly oxygen vacancies) density using donor dopants such as Nb in PZT that reduces the oxygen vacancy concentration or by utilizing ferroelectric films such which have inherently low defect concentration.

2.8 REFERENCES

1. J. F. Scott and C.A. Paz de Araujo, *Science*, 246, (1989), 1400-1405.
2. R. Ramesh, A. Inam, W.K. Chan, B. Wilkens, K. Myers, K. Remschang, D.L. Hart, J.M. Tarascon, *Science*, 252, (1991), 944-946.
3. L. Parker and A. Tasch, *IEEE Circuits and Devices*, pp.17, January 1990.
4. Anonymous, *Microprocessors and Microsystems*, 13, 291, (1989).
5. R.C. Pohanka and P.L. Smith, *Electronic Ceramics*, edited by L.M. Levinson, Dekker, New York, (1988).

6. Manfred Kahn, *Electronic Ceramics*, edited by L.M. Levinson, Dekker, New York, (1988).

7. K.W. Plessner, *Proc. Phys. Soc.*, B69, (1956), p.1261.

8. V.V. Prisedsky, V.I. Shishkovsky and V.V. Klimov, *Ferroelectrics*, 17, (1978), p.465.

9. K. Carl and K.H. Hardtl, *Ferroelectrics*, 17, (1978), p. 473.

10. G. Arlt, *Ferroelectrics*, 104, (1990), p. 217.

11. D.M. Symth, *Ferroelectrics*, *106*, (1990), p. 378.

12. G. Arlt and U. Robels, *Integ. Ferroelect.*, 3, (1993), 247-254.

13. H.M. Duiker, P.D. Beale, J.F. Scott, C.A. Paz de Araujo, B.M. Melnick, J.D. Cuchlaro and L.D. McMillan, *J.Appl. Phys.*, 68(11), (1990), 5783.

14. V.S. Postnikov, S. Palov, S.A. Gridnev and S.K. Turkov, *Sov. Phys. Solid St.*, 10, (1968), 1267-1270.

15. A.Y. Kudzin, T.V. Panchenko and S.P. Yudin, *Sov. Phys. Solid St.*, 16, (1975), 1589-1591.

16. W.C. Stewart and L.S. Cosentino, *Ferroelectrics*,1 , (1970), 149-153.

17. R. Lohkamper, H. Neumann and G. Arlt, *J. Appl. Phys.*, 68, (1990), 4220-4227.

18. C. Karan, *IBM Tech Report*, (1955).

19. I.S. Zheludev, *Physics of Crystalline Dielectrics, Electrical Properties*, Plenum, New York, Vol. 2, (1971), pp. 474-490.

20. I.K. Yoo and S.B. Desu, Mat. Sci. and Eng., B13, (1992), 319.

21. I.K. Yoo and S.B. Desu, Phys. Stat. Sol., a133, (1992), 565.

22. I.K. Yoo and S.B. Desu, J. Int. Mat. Sys., 4, (1993), 490.

23. S.B. Desu and I.K. Yoo, J. Electrochem. Soc., 140, (1993), L133.

24. W. Kanzig, *Phys. Rev.*, 98, (1955), p. 549.

25. S. Triebwasser, *Phys. Rev.*, 118, (1960), p.100.

26. J.F. Scott, C.A. Araujo, B.M. Melnick, L.D. McMillan, R. Zuleeg, *J. Appl. Phys.* 70 (1), (1991), 382.

27. C.K. Kwok and S.B. Desu, *Mat. Res. Soc. Symp. Proc.*, 243, 393, (1992).

28. J.J. Lee and S.B. Desu, *Mat. Res. Soc. Symp. Proc.*, Fall Meeting, (1994).

This paper titled

"Electrodes For Ferroelectric Thin Films"

was published in

Journal of The Electrochemical Society
Vol. 140, (1993), p. 2640

This paper is co-authored by Dr. S.B. Desu. My contribution included conducting almost all of the experimental work, analysis of the results and drawing of the conclusions. Dr. N.R. Parikh, University of North Carolina, Chapel Hill, NC, assisted us in the Rutherford backscattering study and Dr. Les Bursill, University of Melbourne, Australia in the interface study.

Chapter 3 : Minimization of Fatigue in Ferroelectric Thin Films I : Oxide Electrodes

3.1 ABSTRACT

Interface related degradation problems in $PbZr_xTi_{1-x}O_3$ thin film nonvolatile memories have led to the search for alternate electrode materials to replace the conventional metal electrodes. In this work, the suitability of ceramic electronic conductors [e.g. ruthenium oxide (RuO_2) and indium-tin-oxide (ITO)] as contact metallization for ferroelectric $PbZr_xTi_{1-x}O_3$ thin films has been investigated using techniques such as Rutherford backscattering spectrometry, x-ray diffraction, transmission electron microscopy and electron spectroscopy for chemical analysis. Thin films of RuO_2 and ITO were deposited onto Si substrates by reactive sputtering. Sol-gel derived PZT thin films were then deposited onto the conducting oxides and the samples were annealed at various temperatures between 400°C and 700°C. Less intermixing was observed in Si/RuO_2/PZT films when compared to Si/ITO/PZT under similar processing conditions. The ferroelectric properties of PZT films (hysteresis, fatigue and low voltage breakdown) on RuO_2 electrodes were compared to those on Pt electrodes. PZT films show improved fatigue properties on RuO_2 electrodes. However, the films on RuO_2 electrodes also showed higher leakage current densities.

3.2 INTRODUCTION

Lead zirconate titanate (PZT) thin films have been investigated as possible candidates for nonvolatile memory applications for more than a decade[1-4]. Combination

of good ferroelectric properties and stability in a wide range of operating conditions has lead to the increasing amount of study done on this material for nonvolatile memory applications[5]. However, there still remain many problems that need to be overcome before a viable commercial memory product can be produced. It is well known that electrical degradation problems in ferroelectrics, in general, is one of the main reasons for the continued setback towards the formation of reliable memory devices [6-7]. In addition, compatibility considerations impose stringent constraints on the nature of ferroelectric and electrode materials in the integration of the ferroelectric devices (ferroelectric capacitors) into the Si or GaAs VLSI. High temperature processing of the capacitors on the underlying semiconductor material could lead to interdiffusion of various elements in the semiconductor, electrode and ferroelectric materials. Therefore, the choice of the electrode and ferroelectric materials is an important consideration.

For PZT thin film applications, metal electrodes such as Au, Pt and Ag are being used widely. However, there are several disadvantages in using metal electrodes. In general, PZT films are known to suffer from fatigue (loss of switchable polarization on repeated polarization reversal) on metal electrodes [8]. Although several models have been proposed in the literature for fatigue in ferroelectrics thin films [9-12], no satisfactory explanation has yet been found. A recent model developed by Yoo and Desu [13] suggests that the fatigue and other degradation problems in oxide ferroelectrics are related to the nature of the electrode-ferroelectric interface. Intrinsic defect movement and entrapment at various trapping sites such as grain/domain boundaries and electrode-ferroelectric interface lead to the loss of polarization in the ferroelectric material under an AC field. Defect entrapment (e.g., oxygen vacancies) at the interfaces leads to space charge development at these sites which can 'pin' the ferroelectric domains. There is a large Schottky barrier at the electrode-ferroelectric interface that arises due to the lattice

mismatch and work function difference between the metal electrode and the ceramic ferroelectric. Another distinct disadvantage in using platinum electrodes is the difficulty involved in etching the material which is an important consideration in VLSI applications.

These considerations have lead to the search for alternate electrode materials for PZT thin films applications. To reduce the Schottky barrier height at the interface, it is necessary to use an electrode material whose work function and lattice parameter are similar to those of the PZT thin films. In a previous study, Parikh et al [14] investigated the use of ceramic nitride and oxide diffusion barriers such as ZrN_x, TiN_x, ZrO_x and TiO_x for PZT thin film applications. Their results indicate intermixing at low temperatures using these compounds. Ceramic conductors such as ruthenium oxide (RuO_2), Indium Tin Oxide (ITO) and other transition metal oxides (IrO_2, RhO_2, ReO_2 etc.) are some of the other choices. The metallic oxides of these transition metals tend to crystallize in the tetragonal rutile structure and are promising candidates for various metallization schemes primarily because of their low resistivity and high thermal stability [15]. Dioxides of these materials have bulk resistivities of the order of 30-100 μohm-cm and some of these oxides such as RuO_2 are known to have excellent diffusion barrier properties [15-16]. The use of these materials as electrodes in VLSI therefore obviates the need for an additional barrier layer film. Recently, it has also been shown that these films can be etched using the conventional dry etching techniques [17].

In this study, we have investigated the effectiveness of two different conducting oxide electrodes - RuO_2 and ITO - for PZT thin film applications and compared the ferroelectric properties and degradation of PZT films on ceramic and metal electrodes. The electrodes were sputter deposited onto Si substrates and spin coated with sol-gel derived PZT thin films. The samples were annealed at various temperatures between 400^0C-700^0C and characterized thereafter using Rutherford backscattering spectrometry,

x-ray diffraction (XRD) and electron spectroscopy for chemical analysis (ESCA). Top electrodes were once again deposited by sputtering to determine the electrical properties of PZT films. The results have been compared to PZT films processed on Pt electrodes under similar conditions.

3.3 EXPERIMENTAL PROCEDURE

Thin films of RuO_2 and ITO were reactively sputtered in oxygen atmosphere at a pressure of $2x10^{-4}$ Torr onto Si substrates. The substrates were maintained at a temperature of 200°C during deposition and the electrodes were deposited to a thickness of 500 nm. Sol-gel derived PZT films were then deposited onto these substrates. The PZT precursor was prepared from a metallorganic solution (0.4M) of lead acetate, zirconium n-propoxide and titanium iso-propoxide dissolved in acetic acid and n-propanol. The solution was hydrolyzed (R=10) to form the precursor. The method of preparing the precursor is similar to that suggested by Yi et al [18]; more specific details can be obtained from this reference. Ten percent excess lead was added to the solutions to compensate for the loss of lead during high temperature processing. Films were spin coated at 1500 rpm for 20 sec and subsequently dried at 150°C for 5 min. The cycle was repeated once or twice (spin-bake cycle) to obtain the desired thickness (300-450 nm). The films were coated to various compositions (Zr/Ti) of 30/70, 40/60, 53/47, 65/35 and 75/25. In a similar study, PbO films were deposited on the electrodes by the vacuum evaporation technique under a vacuum of 10^{-6} Torr to a thickness of 150 nm. The coated films were annealed at various temperatures between 400°C and 700°C in intervals of 50°C for 30 min in a quartz tube furnace under a controlled oxygen atmosphere.

The bulk compositions of the films (coated and annealed on sapphire substrates) were measured using electron probe microanalysis (EPMA). Quantitative analysis of Pb, Zr and Ti ions was performed using a 7 kV, 50 mA source. Ten measurements were made at different areas on the sample and averaged to obtain each data point. The surface composition of the films were determined by electron spectroscopy for surface analysis (ESCA) using a Kratos XSAM 800 photoelectron spectrometer. The specimens were excited using a 13 kV Mg K_a x-ray source and the standard-less ratio method was used for quantitative analysis. A background pressure of 10^{-8} Torr was used in the chamber and the specimen tilt angle was maintained at the normal 90^0. Pb4f, Zr3d and Ti2p integrated areas and the sensitivity factors calibrated specifically for the in instrument in use, were used to calculate the surface composition.

The presence of thin film phases and a qualitative estimate of the degree of intermixing as a function of annealing temperature were determined from thin film x-ray diffraction studies. RBS analysis of the samples were performed to determine the extent of intermixing using a 2 MeV He^{2+} beam reference. The sample sizes were typically 1 cm^2 in area. Sample normal tilts of -6^0 and 50^0 from the incident beam direction were used in the analysis with the detector placed at a backscattering angle of 165^0. A Win-spec (R) simulation program was used to obtain the concentration vs depth profile of the elemental distribution. Theoretical spectra were generated by varying the compositions of thin layers of the sample and compared to the experimental spectrum until a close match was obtained.

For the TEM study, four pieces (each 3 mm^2) were cleaved from the two PZT/electrode specimens crystallized at 650 ^oC. These were glued together using an epoxy resin as a stack with two pairs of PZT surfaces facing inward. These sandwiches were ground mechanically using fine-grade silicon carbide paper in such a way as to

produce transverse cross sections 30 μm deep. A 2.3 mm copper specimen support ring was glued to one surface and the sample ion thinned from both sides at an angle of incidence of 15^{o}. This is a modification of a technique developed by Reaney and Barber [19]. The thin specimens were examined using a Philips EM430 300 keV HRTEM instrument at Institut Interderdepartmentale de microscopic Electronique (I2M), EPFL. Observations were made close to room temperature using a $\pm$ 10^{o} double-tilt goniometer. The instrumental resolution was significantly better than 0.2 nm although the interpretable structure resolution was limited to 0.2 nm, since the spherical aberration coefficient was 1.2 mm. Selected area diffraction patterns were recorded suing the smallest projector lens aperture, when the effective beam diameter at the specimen plane was about 100 nm. Some energy dispersive x-ray spectroscopy (EDX) analysis was made using a Hitachi 2000-HF field emission analytical electron microscope at 200 keV.

Ruthenium oxide top electrodes were sputtered on the samples to a thickness of 500 nm under the same deposition conditions as the bottom electrode. The ferroelectric properties were measured using a standardized RT66A tester operating in virtual ground mode (see appendix). The capacitor cell size was 2.1×10^{-4} cm^2. An external pulse generator was used to obtain the desired input signal during the test. DC leakage current measurements were performed using a Keithley 617 electrometer.

3.4 RESULTS AND DISCUSSION

The results of the EPMA on the samples of different compositions, all annealed at $650^{o}C$ on sapphire substrates are provided in Table 3.1. The films were characterized on sapphire substrates to separate the effects of interdiffusion from the discrepancies in composition due to the precursor-making process itself. The elements of the substrates

Table 3.1 EPMA results on the PZT samples of different compositions, all annealed at 650^{0}C on sapphire substrates.

	Pb (at. concn.)		Zr (at. concn.)		Ti (at. concn.)	
Compn.	Expected	Measured	Expected	Measured	Expected	Measured
30/70	20	20.250	6.0	6.355	14.0	13.255
40/60	20	20.325	8.0	8.021	12.0	11.654
53/47	20	19.379	10.6	10.487	9.4	10.132
65/35	20	20.239	13.0	12.541	7.0	7.219
75/25	20	18.853	15.0	15.773	5.0	5.377

were not detected in the analysis showing that the analysis depth was restricted solely to the PZT film thickness. The measured values of Pb concentration and Zr/Ti ratios for all compositions are close to the desired stoichiometry. This indicates that the excess lead was not incorporated into the films. Measurements were made on different areas in the samples and compositional uniformity within one percent was obtained. In this work, ESCA was used to study the surface composition of the annealed PZT films.

Although bulk film compositions measured by microprobe analysis are close to the stoichiometric compositions, the surface composition can play an important role in determining the electrical properties of the PZT films. The spontaneous polarization, depolarizing field and domain distributions are critically controlled by the surface electronic states, which in turn is related to the chemical composition and structure of the surface [20]. Fig. 3.1 compares the Pb concentration of PZT films on RuO_2 and ITO electrodes. The loss of lead from the surface of PZT films can occur either through volatilization of PbO during high processing temperatures or due to diffusion towards the substrate. Since the processing and annealing conditions for PZT films deposited on both the electrodes are the same, the difference in surface lead concentration can be attributed to the Pb diffusion through the different barrier layers. At annealing temperatures up to 550 ^{0}C, there is very little difference in the relative Pb concentration in PZT films on both of these electrodes. However, above 550^{0}C, the relative Pb concentration in the RuO_2/PZT films remains almost constant, while in the ITO/PZT samples the Pb concentration shows a decreasing trend. Fig. 3.2 shows the variations of Pb surface concentrations and Zr/Ti ratios of PZT films deposited on RuO_2 as a function of composition. These films were annealed at 650^{0}C for 30 min. As the Zr/Ti ratio in the bulk of the PZT films increases (verified by EPMA), the Zr/Ti ratio on the film surface increases correspondingly. However, the Zr/Ti ratio is consistently higher on the surface

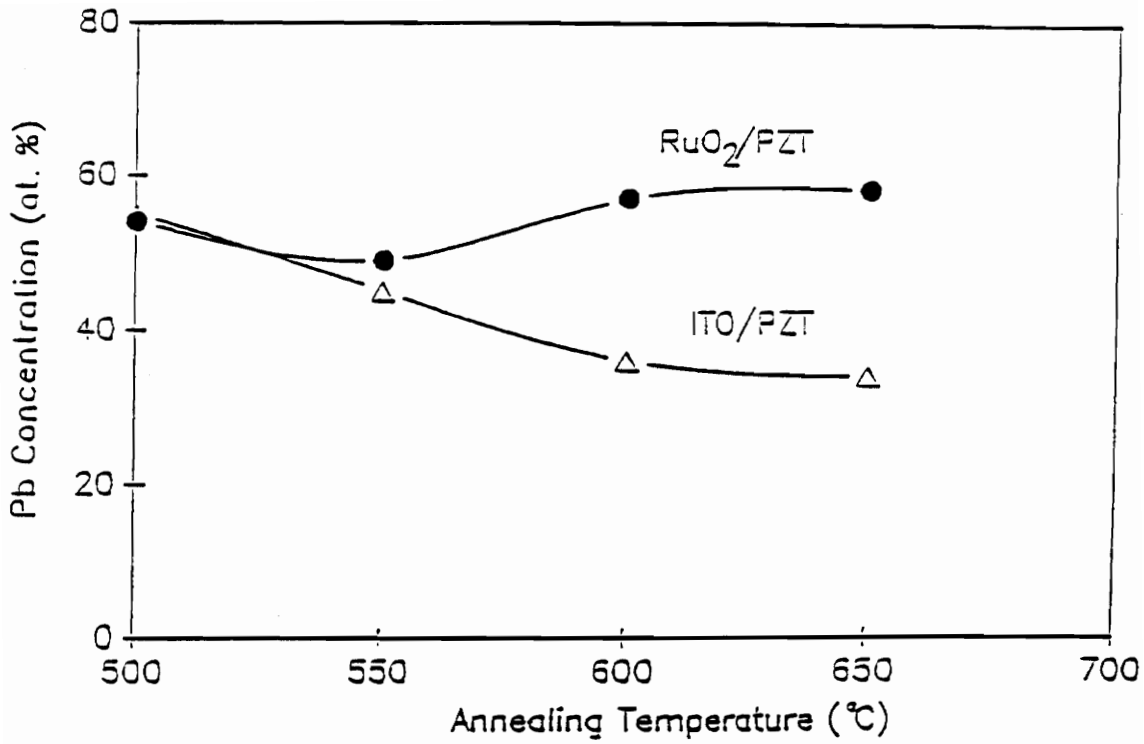

Figure 3.1 **Comparison of relative Pb concentrations on the surface of RuO_2/PZT (x=.53) and ITO/PZT films as a function of annealing temperature.**

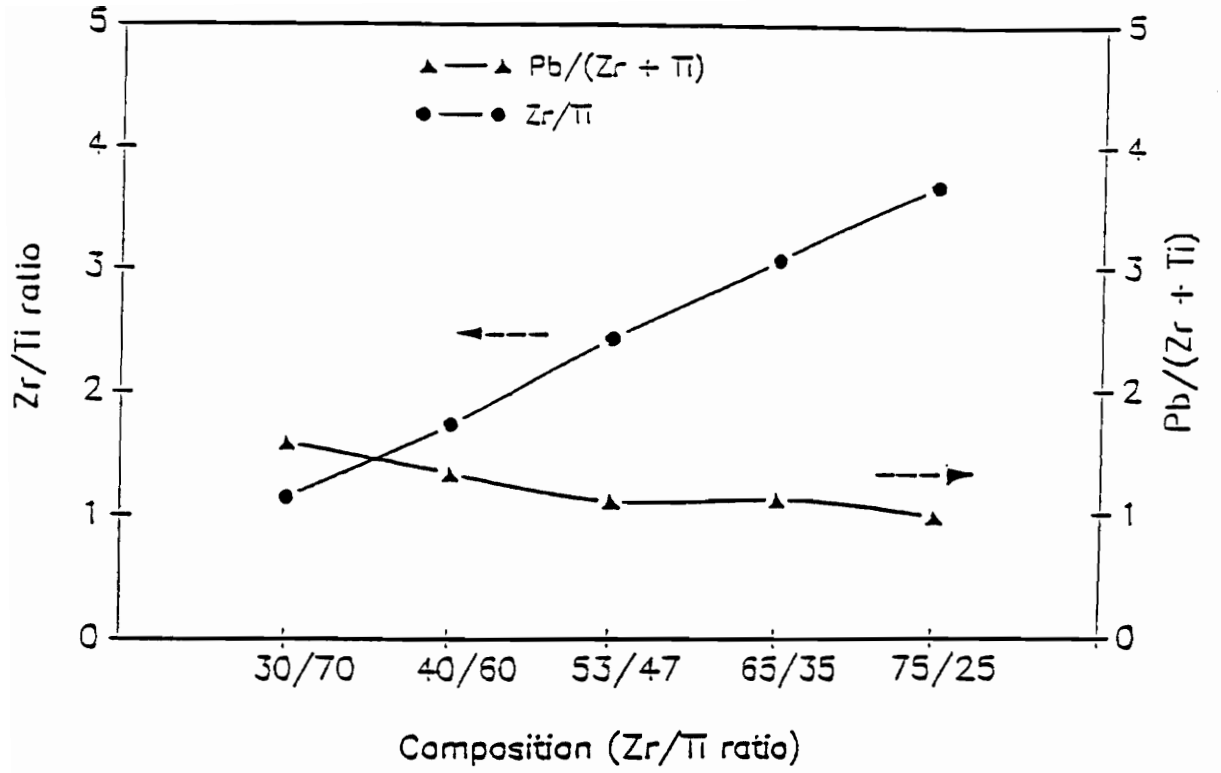

Figure 3.2 The Zr/Ti ratio and Pb/(Zr + Ti) ratio on the surface of RuO_2/PZT films of different compositions annealed at 650°C.

of the films indicating that preferential segregation of Zr could be occurring at the surface. Similar effects have also been observed by Desu and Kwok [20] in a previous study. Surface Pb concentrations remain relatively constant and close to the stoichiometric values in the films of different compositions.

Fig. 3.3 shows the RBS spectra obtained on the Si/ITO/PbO samples. The spectra of the samples annealed up to 450°C are essentially similar to that of the as-deposited sample. However, it can be seen that the Pb yield has decreased considerably, indicating a loss of Pb atoms from PbO. The drastic decrease in the low energy edge of Pb peak indicates that Pb diffuses into the ITO layer. In and Sn diffuse towards the surface and reacts with PbO to form a Pb-In-Sn compound. RBS spectra for the Si/ITO/PZT samples is shown in Fig. 3.4. As in the case of PbO, the intermixing occurs at or above 500°C. Comparison of the Si/ITO/PbO and Si/ITO/PZT spectra clearly indicates that the diffusion of Pb towards the substrate and the diffusion of In and Sn towards the surface are the main causes for intermixing in these samples.

In the case of Si/RuO_2/PbO samples, the RBS spectra show lead diffusion towards the electrode at and above 550°C as shown in Fig. 3.5. There is a tail in the Pb peak that extends towards the lower energies. At higher annealing temperatures, this low energy tail is more prominent. Fig. 3.6 shows the RBS spectra for the as-deposited and annealed Si/RuO_2/PZT samples. There is no noticeable intermixing between Pb and RuO_2 at or below 550°C. Increased intermixing is observed in the samples that were annealed at 600°C or higher temperatures. The depletion of Ru from the Ru edge indicates a possible reaction taking place between Pb and Ru around 600°C. Also, there is no significant change in the Si edge even at 600°C indicating that the diffusion of Si into the RuO_2 is minimal up to this temperature. Green et al [16] have investigated the effectiveness of RuO_2 as a diffusion barrier between Si and Al at high temperatures. Our results confirm

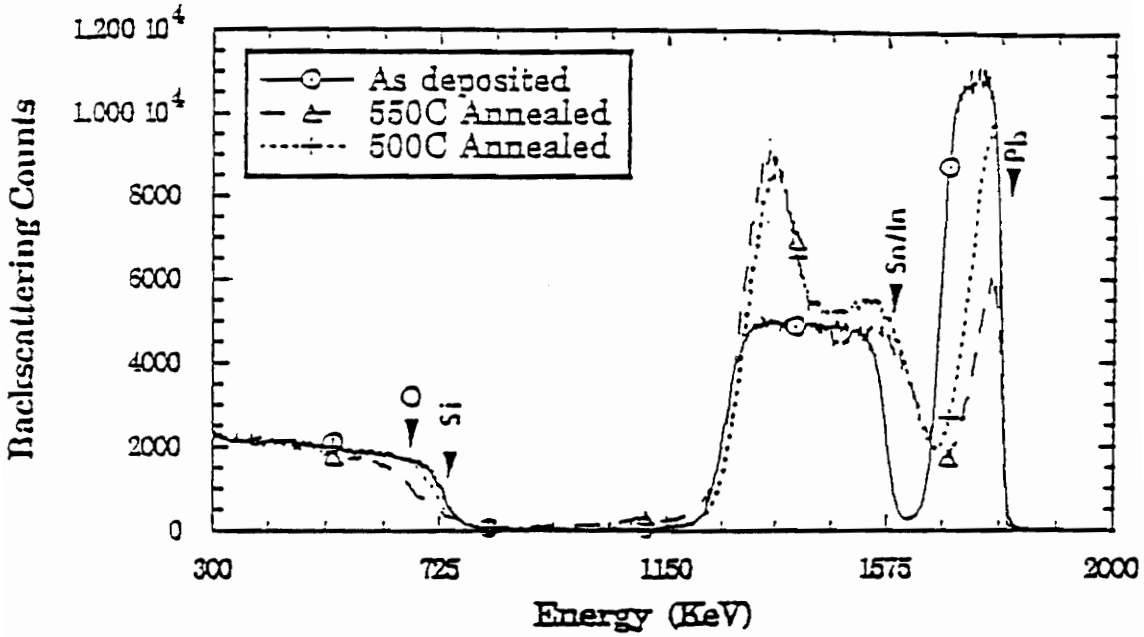

Figure 3.3 **RBS profile of the as-deposit, 500°C and 550°C annealed Si/ITO/PbO samples.**

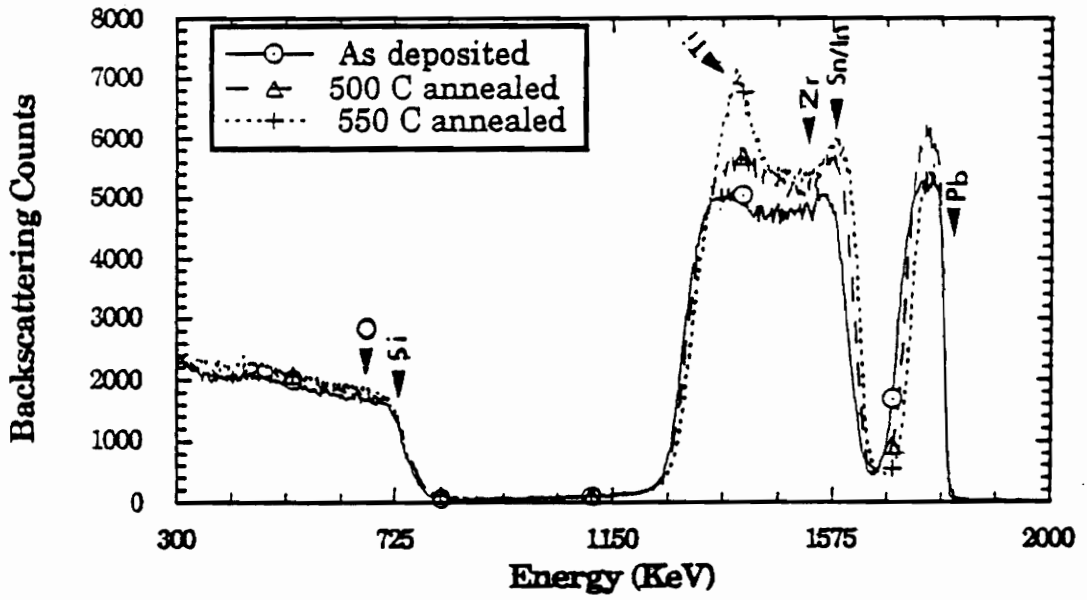

Figure 3.4 RBS profile of the as-deposit, 500°C and 550°C annealed Si/ITO/PZT samples.

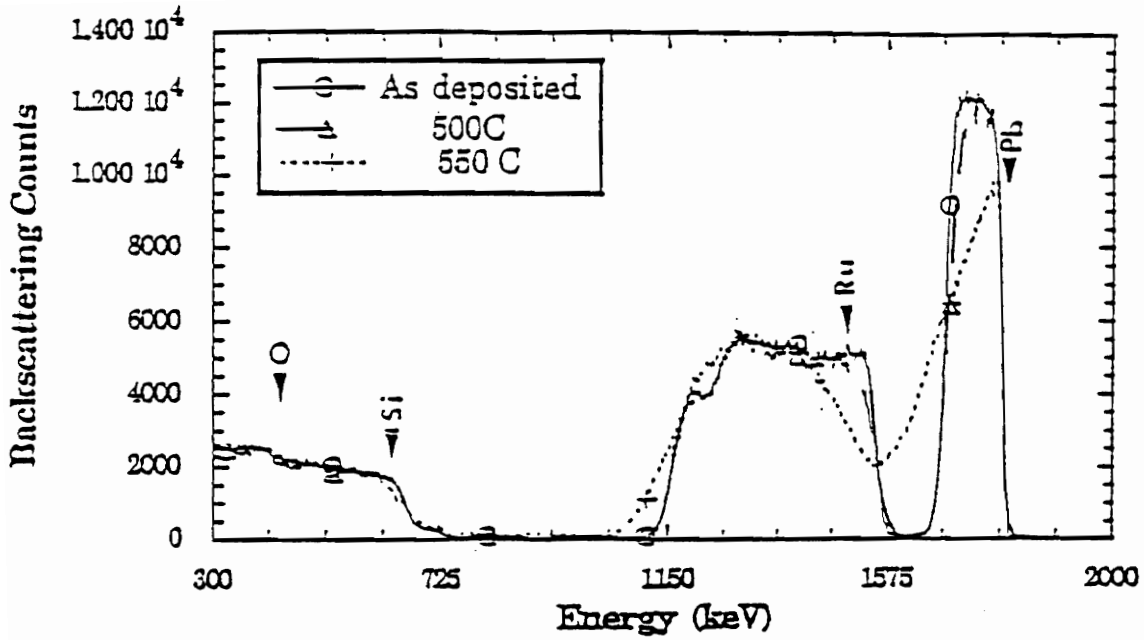

Figure 3.5 RBS profile of the as-deposit, 500°C and 550°C annealed Si/RuO_2/PZT samples.

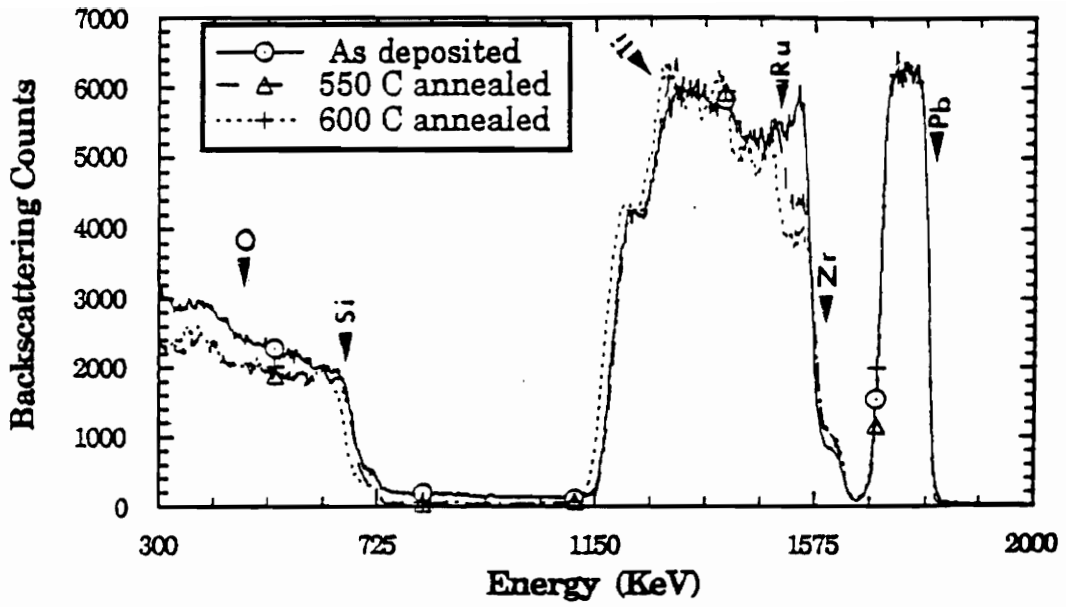

Figure 3.6 RBS profile of the as-deposit, 550°C and 600°C annealed Si/RuO_2/PZT samples.

their observations that RuO_2 is an effective barrier to Si diffusion up to an annealing temperature of 600°C.

The x-ray analysis was conducted on all samples as a function of annealing temperature to determine the formation temperature of the perovskite phase and detect the presence of any crystalline phase due to intermixing. The XRD results show that the as-deposited films are amorphous on these substrates. The PZT perovskite formation is initiated at 550°C and completed at 600°C on the Si/RuO_2 substrates as shown in Fig. 3.7. In addition to the PZT and RuO_2 peaks, there are other peaks that we believe are formed due to the intermixing. The XRD patterns from 600°C and above show small peaks of increasing intensity at 30.5° that we initially identified as the result of diffraction from the lead ruthenate ($Pb_2Ru_2O_{7-x}$) compound. It is known that the reaction between PbO and RuO_2 at these temperatures can lead to the formation of Pb-ruthenate [22]. Since the RBS results indicate that around 600°C, Pb diffuses towards the electrode and Ru towards the PZT surface, it is possible that this compound forms at the interface between the electrode and the ferroelectric. The formation of this compound at the interface has two important effects : (a) reduction in compositional gradient between the electrode and the ferroelectric materials (b) reduction in the actual ferroelectric film thickness. In the case of Si/ITO/PZT films, the high intensity peaks of PZT overlap with the peaks of ITO and therefore the identification of the formation temperature of the perovskite phase was difficult. However, the patterns did show a number of spurious peaks even at low temperatures that we believe are from the compounds formed due to intermixing.

Based on these results, it is appropriate to conclude that as far as diffusion barrier properties, PZT perovskite formation temperature and the surface composition of the films are concerned, RuO_2 is a better choice as an electrode for PZT thin film applications. Most significantly, we have seen that the PZT perovskite phase forms on

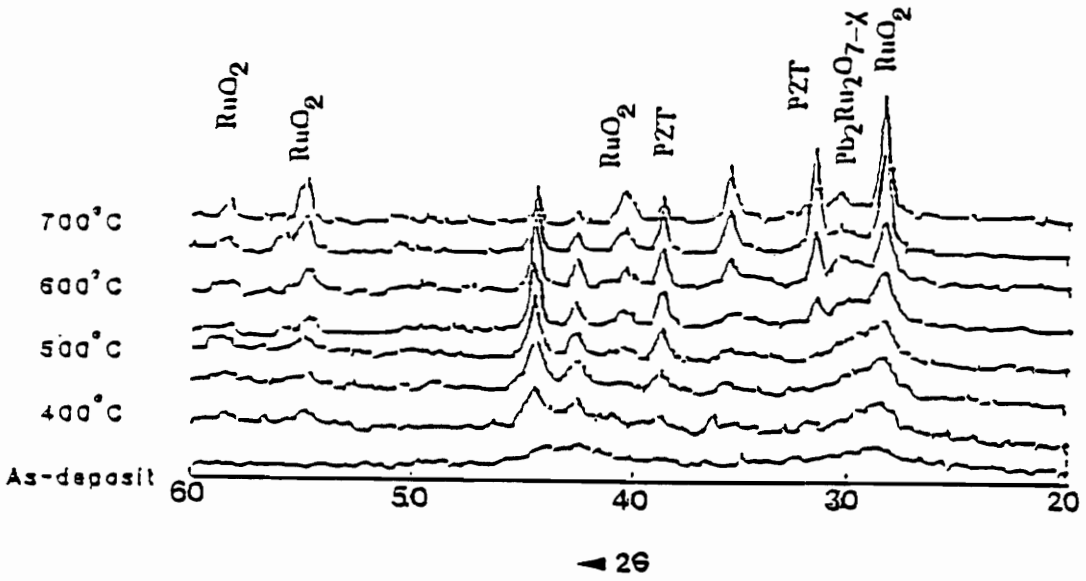

Figure 3.7 XRD patterns of Si/RuO_2/PZT samples annealed at various temperatures between 400°C and 700°C.

RuO_2 electrodes before any serious interdiffusion begins and therefore we are not limited by this factor in processing of the device. However, it is electrical properties of PZT films on these electrodes that determines the ultimate application of these electrodes for ferroelectric thin film capacitors.

The electrical properties of PZT films were investigated on both RuO_2 and ITO electrodes. PZT films (450 nm) annealed in the range of 400°C -700°C for 30 min on ITO electrodes did not show any well saturated hysteresis loops which is probably a result of insufficient perovskite formation or intermixing of the constituent elements of the electrode and the ferroelectric at high temperatures as observed from RBS and XRD studies. Therefore, further studies were focused on the electrical properties of PZT films on RuO_2 electrodes. Also, the degradation properties of these films were compared to that of Pt electrodes.

The hysteresis properties of PZT films of different compositions (all annealed at 650°C for 30 min in air) on RuO_2 electrodes were measured using the RT66A standardized tester. The PZT films were coated to a thickness of 450 nm. The films with compositions close to the morphotropic phase boundary (MPB) showed higher remnant polarization and lower coercive field values. A typical hysteresis loop obtained from the 53/47 sample is shown in Fig. 3.8. At compositions close to the MPB, both tetragonal and rhombohedral phases co-exist leading to a large number of polarization directions that can be used for domain switching. Therefore, the higher P_r and lower E_c values in the 53/47 films is to be expected. These values of P_r (~ 20 $\mu C/cm^2$) and E_c (~30 kV/cm) are well within the requirements for nonvolatile memory applications [23].

The significant difference in properties of PZT films on metal and ceramic electrodes was evident from the fatigue test (Fig. 3.9). Fatigue is the loss of polarization in a ferroelectric material that has been switched repeatedly. The fatigue test was performed

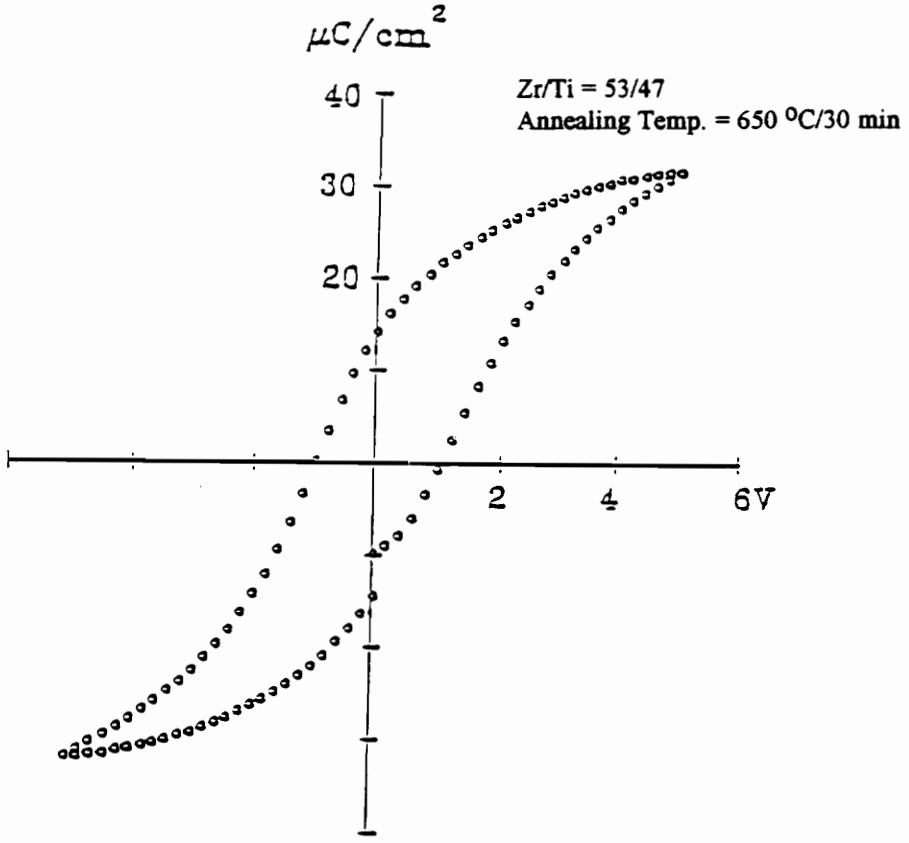

Figure 3.8 A typical hysteresis loop obtained from RuO_2/PZT/RuO_2 capacitors

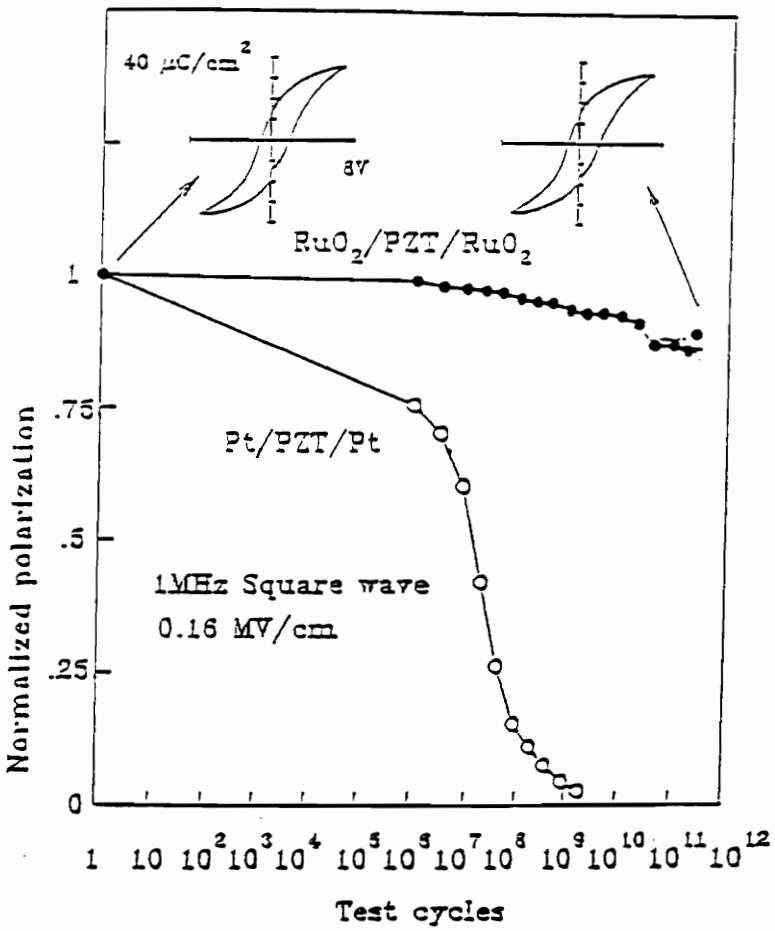

Figure 3.9 Comparison of fatigue properties of PZT films on Pt and RuO_2 electrodes.

under accelerated conditions using a 1 MHz square wave and an electric field of 0.16 MV/cm. The PZT films on Pt electrodes showed early loss of polarization, while no fatigue was observed up to 2 x 10^{11} cycles on RuO_2 electrodes. It is evident from Fig. 3.9 that there is no significant difference in the hysteresis properties of the films before and after the fatigue cycling. The difference in fatigue properties on metal and ceramic electrodes can be explained on the basis of the model developed by Yoo and Desu [13] for fatigue in oxide ferroelectrics. According to the model, defects such as oxygen vacancies, lead vacancies and other mobile impurity ions can migrate towards the electrode-ferroelectric interface under an AC field. Since the interface is chemically unstable, these defects tend to become entrapped there eventually. The experimental evidence for the increase in the number of oxygen vacancies at the interface as a result of fatigue has been shown by Scott et al [23] through Auger Spectroscopy studies on Pt/PZT samples . Such an entrapment can lead to structural damage at the interface leading to subsequent loss of polarization. To reduce the entrapment of defects at the interface, the interface stability needs to be increased. For PZT thin films on metal electrodes, there is a large lattice mismatch at the interface, resulting in a relatively unstable interface. Also, the large work function difference between the metal and the ceramic results in a large Schottky barrier at the interface. In contrast, when RuO_2 is used as the electrode (ceramic), the interface is more stable on account of the reduced lattice mismatch and work function difference. Additionally, it is highly possible that the oxide electrodes consume the oxygen vacancies that migrate to the interface to increase their nonstoichiometry. Thus the accumulation of oxygen vacancies and the related development of space charge at the interface is prevented at the electrode-ferroelectric interfaces.

One factor that needs additional confirmation in this study is the formation of the Pb-ruthenate layer at the interface indicated by XRD. If this layer forms at the interface, it

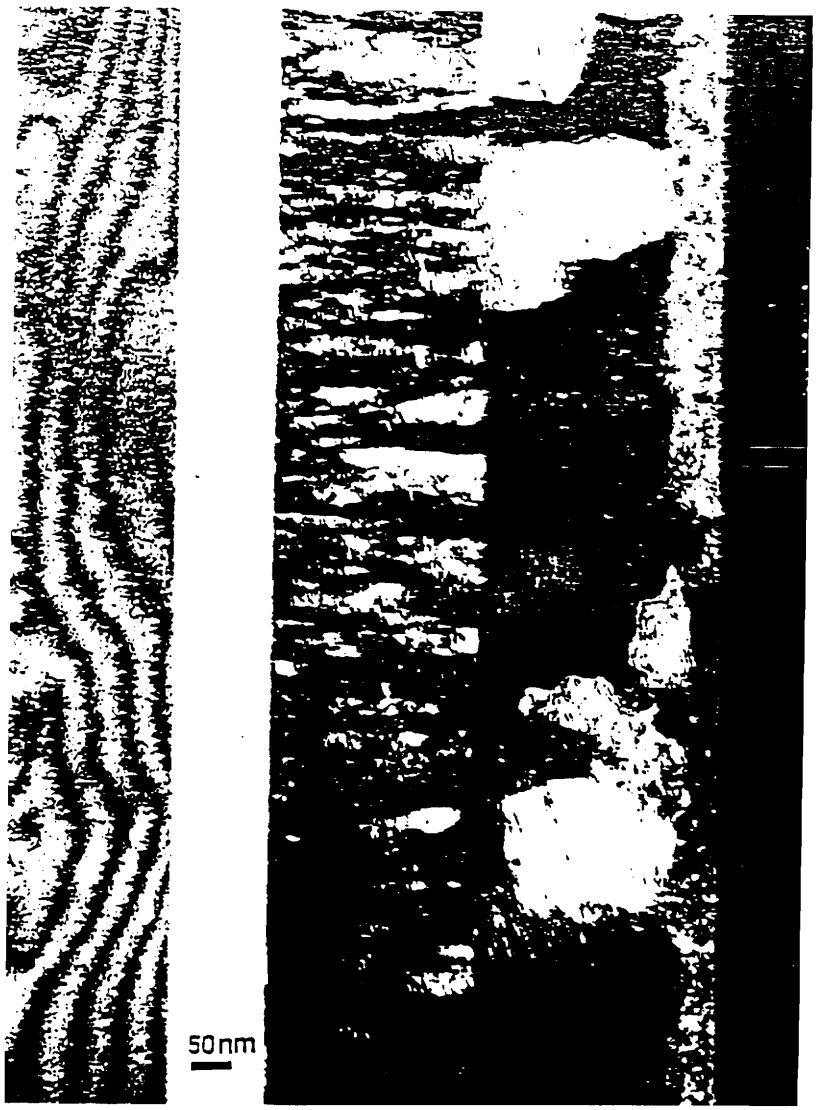

Figure 3.10 Overview of $Si/SiO_2/RuO_2/PZT$ thin film showing the interface structures and texture of the RuO_2 and PZT layers

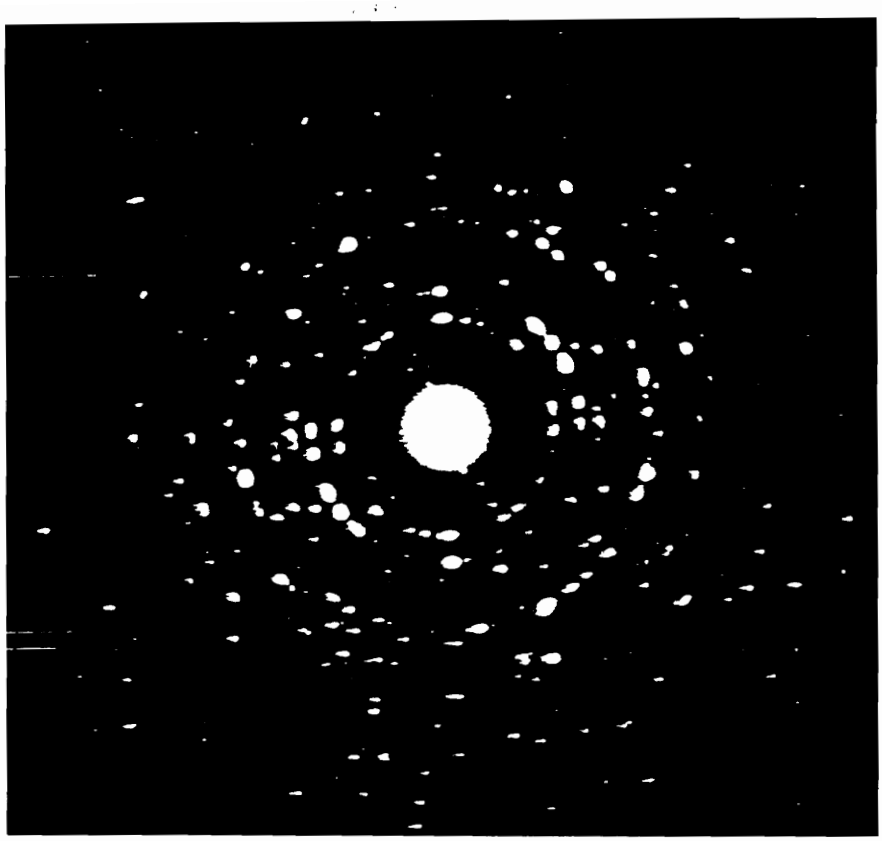

Figure 3.11 Typical electron diffraction pattern of the $Si/SiO_2/RuO_2/PZT$ thin film capacitors.

can reduce the compositional gradient between the electrode and the ferroelectric. The tendency for defect migration can therefore be reduced. The TEM studies were conducted to examine the nature of the interface in the RuO_2/PZT samples. For this study, well crystallized PZT films annealed at 650 ^oC were chosen. Fig. 3.10 is an overall view of one Si/SiO_2/RuO_2/PZT thin film cross section; from left to right may be seen crystalline Si/amorphous SiO_2/columnar crystallites of RuO_2/crystallized PZT /and amorphous epoxy. This is a dark field image with objective aperture centered over the polycrystalline electron diffraction ring pattern shown in Fig. 3.11. The PZT portion consists of grains some 25 nm in diameter. The RuO_2 is well crystallized, indicated by extensive array of lattice fringes; shown in the enlargement of Fig. 3.10 given as Fig. 3.12. It has a pronounced columnar texture (typical of sputtered films), where each grain (about 5 nm wide) extends throughout the thickness of the RuO_2 layer (about 250 nm thick). Further enlargement of the RuO_2/PZT interface (Fig. 3.13) indicates that this interface is not flat; it consists of a series of roughly periodic curved boundaries reflecting the shape of the outer of the columnar grains of RuO_2. Fig. 3.14 is a HRTEM image showing the atomic resolution detail of two such curved segments. The PZT appears well crystallized at this interface and is oriented with the (100) lattice planes parallel to the original substrate. Clearly, there is no evidence of an intermediate phase; in particular there is no pyrochlore type phase or Pb-ruthenate phase at this part of the RuO_2/PZT interface. However, at the surface, the PZT layer is incompletely crystallized as perovskite phase: a layer approximately 50 nm thick has been stranded as a nanocrystalline region as indicated by the bright contrast regions in the dark-field images shown in Fig. 3.10 and Fig. 3.12. A 10 nm dia probe was used to obtain EDX spectra from a series of points tracing a line perpendicular to the series of interfaces; there was no evidence for interdiffusion of RuO_2 into silica or of RuO_2 into PZT, and the Pb:Zr:Ti showed no systematic changes as a

Figure 3.12 Enlargement of Figure 3.10 showing lattice fringes within the RuO_2 grains. Note also the nanocrystalline pyrochlore layer.

Figure 3.13 RuO_2/PZT interface showing curved interphase boundaries.

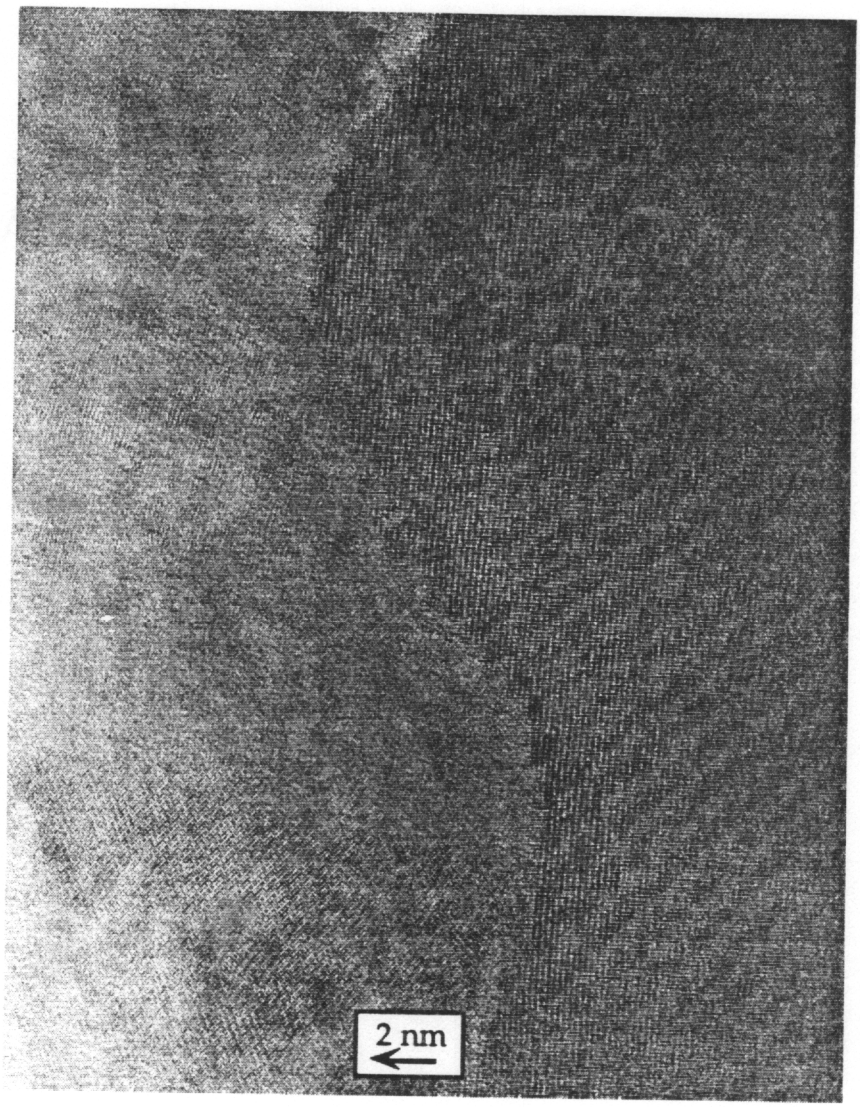

Figure 3.14 HRTEM image of the RuO_2/PZT interface showing [101] zone axis of PZT.

function of distance throughout the PZT layer, even up to the outer surface. This result indicates that the cation stoichiometry of the observed surface layer is essentially Pb_2ZrTiO_{7-x} ($0<x<1$) which is close to that expected for a pyrochlore phase.

The formation of surface pyrochlore phase often happens with sol-gel thin films if there is insufficient excess Pb added to the sol-gel precursor [24]. It is also well known that a nanocrystalline pyrochlore phase occurs as an intermediate step during the crystallization of the PZT thin films [25]. If the partial pressure of oxygen is too high or too low during annealing, then the nonstoichiometric pyrochlore phase is stabilized, rather than the stoichiometric perovskite structure. Perovskite is usually stochiometric within very narrow limits for all components. RBS results indicated Ru diffusion into PZT at an annealing temperature of 650 ^{o}C. However, no Ru was detected at all throughout the PZT film using EDX. In order to explain the RBS results, we note simply that the curvature of the grains forming the PZT/RuO_2 interface extends approximately 5-6 nm normal to the original substrate. This was most clearly seen for Fig. 3.13, where the interface appears to have curved character with amplitude about 3 nm (10 time d_{110} = 0.28 nm). This may be a pseudoperiodic minimal surface required to minimize elastic energy. Note that as this cusplike interface is eroded during a RBS experiment, starting from the PZT side, there will be an apparent diminution of Ru at the PZT/RuO_2 interface.

Although XRD and RBS indicated possible formation of the cubic pyrochlore Pb-ruthenate phase, the TEM results did not indicate such layer at the interface. However, these results do not absolutely rule out some chemical Ru/PZT intermixing at the atomic level; for example, the presence of a very thin layer of Pb-ruthenate would be difficult to detect in the HRTEM. Use of a nanoprobe (1 nm dia), rather than the 10 nm probe used for EDX analysis in this study would provide more sensitivity. These results clearly suggest that the assignment of the XRD peak at 30.5^{o} to Pb-ruthenate phase is incorrect.

If this compound is thick enough to be detected by XRD, it should be possible to observe it by TEM. It is not clear how the present results may be interpreted with respect to degradation properties. It appears necessary to examine films before and after fatigue experiments to search for nanostructural changes which may be expected to occur if oxygen diffusion and trapping plays a significant role in fatigue. So far, there have been no definitive studies on this point primarily because of the difficulty in ensuring that switching occurs in the large area electroded sample required for the analytical studies.

The results of the DC leakage current measurements on RuO_2/PZT/RuO_2 and Pt/PZT/Pt samples are shown in Fig. 3.15. For comparison purposes, only the results of the current flow in one direction (from the bottom electrode to the top) is plotted in the figure. The films on RuO_2 electrodes show a higher current level at any particular electric field. In particular, the measured current density at a field of 100 kV/cm (typical operating field for nonvolatile memories), the leakage current in RuO_2 based capacitors were at least three orders of magnitude higher than that for Pt electroded films. The leakage current measurements (I-V characteristic) were conducted by applying voltages of opposite polarity in steps of 0.5V and measuring the current level as it reached a stable value. In general, when a DC voltage (below the breakdown voltage) is applied to a ferroelectric capacitor, the current response follows the behavior shown in Fig. 3.16. The time taken for the current to reach the stable value (i.e., the true leakage current value) is called the soaking time. In our experiments, we noticed that while the soaking time for Pt electroded samples is very large (sometimes as large as an hour), RuO_2 electroded samples reach the stable value in a very short time (few minutes). Additionally, by measuring the instant breakdown characteristics (i.e., the minimum electric field at which devices breakdown as soon as it is applied to the sample), it was observed that the breakdown in Pt/PZT capacitors was dominated by the "fuse effect" as reflected by the smaller difference in the

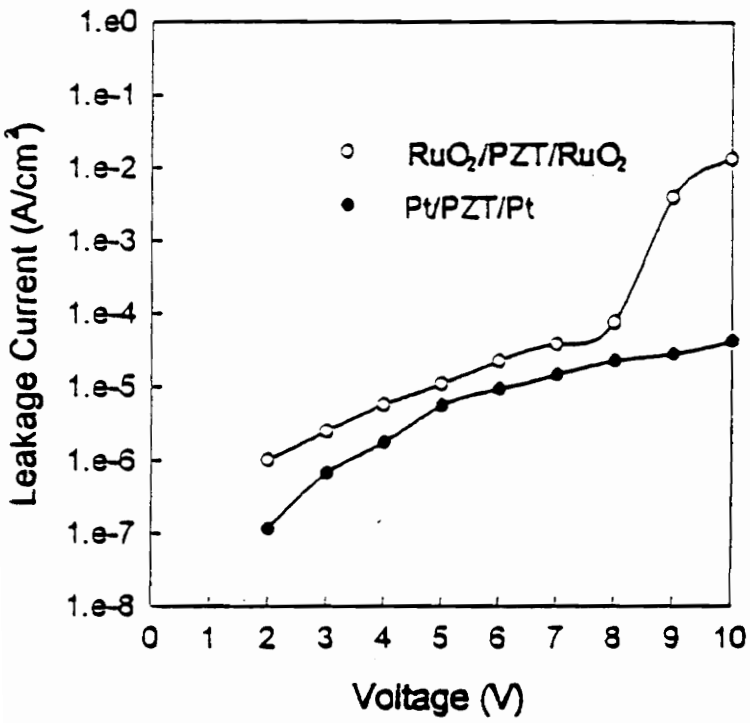

Figure 3.15 Electrode effects on I/V characteristics of PZT films.

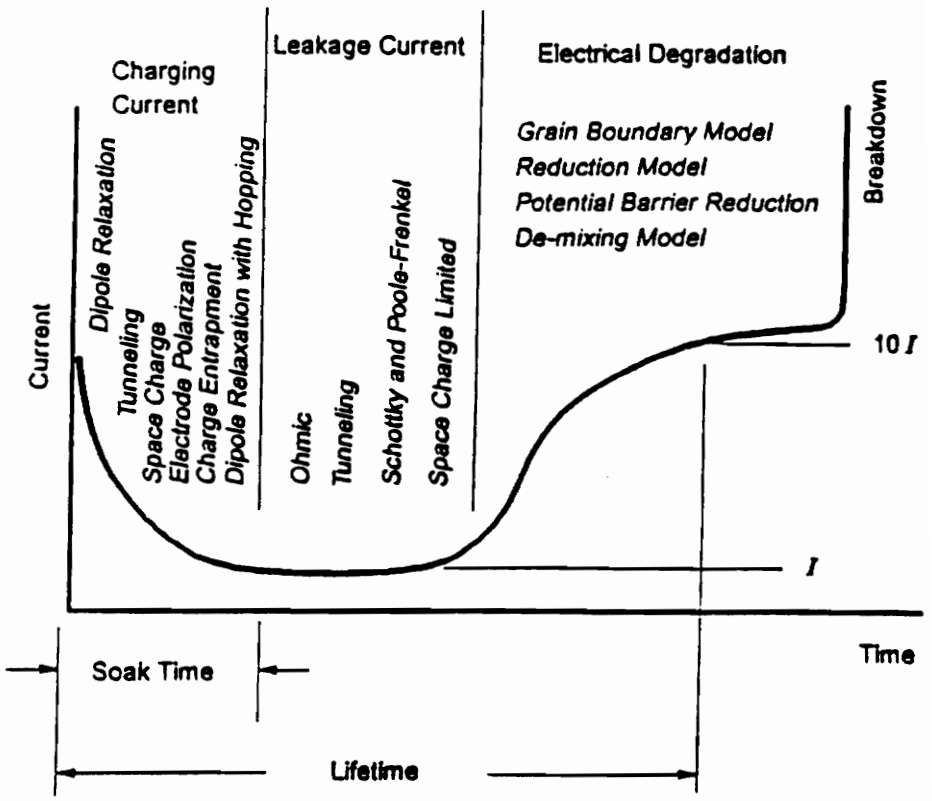

Figure 3.16 Typical current-time behavior for a ferroelectric capacitor

actual breakdown voltage and the instant breakdown voltage. In contrast, in RuO_2/PZT capacitors, electrical degradation occurs earlier and lasts longer before breakdown.

In general, there are several different types of leakage current mechanisms for insulators with metal contacts. Ohmic behavior is observed at low electric fields [26]. Under high electric fields, where devices exhibit non-ohmic current, electrical behavior is governed by oxygen vacancy diffusion, space charge limited current (SCLC) injection, grain boundary potential barrier, tunneling, Schottky emission, or Poole-Frenkel emission. SCLC injection occurs under fields of 1-10 kV/cm, and Schottky emission under fields of 0.1 MV/cm. Tunneling is observed under fields on the order of 100 MV/cm. Grain boundary potential barrier is a possible mechanism only when the film thickness' are of the order of 100 nm. As indicated in Fig. 3.15, the electric fields in our measurements were of the order of 100 kV/cm and the thickness of the PZT films 300 nm. Therefore, the likely leakage current mechanism may be Schottky emission or Poole-Frenkel emission. Schottky emission is a barrier limited phenomenon occurring at the electrode-insulator contact while Poole-Frenkel emission is a bulk limited mechanism. By simply noting that the I-V characteristic of PZT thin films on both RuO_2 and Pt electrodes is asymmetric when opposite polarities are tested, it may be concluded that the dominant mechanism for leakage current is Schottky emission. The nature of top and bottom electrode-insulator contacts are different for both the cases. While the bottom electrodes undergo annealing with the ferroelectric film on it, the top electrode merely provides an ohmic contact to the insulating film. As long as emission occurs in the bulk (Poole-Frenkel), the I-V curve should be symmetric. By measuring the temperature dependence of leakage current, it has been found that the behavior fits the Schottky emission equation given by [27]:

$$J = AT^2 \exp[(-\phi_B + a\sqrt{E})/kT] \qquad (3.1)$$

where J is the current density, A is the effective Richardson constant, ϕ_B is the effective Schottky barrier height, a is a constant, and E is the electric field. Additionally, it has been found that the Richardson constant values for RuO_2/PZT are higher than that for Pt/PZT capacitors. If Schottky emission is the dominant leakage current mechanism for PZT films, then the difference in leakage current observed for RuO_2 and Pt electroded films can be explained on the basis of the Schottky barrier height. The barrier height for Pt/PZT capacitors are higher because of the large difference in work function between the *metallic* Pt and the *ceramic* PZT. On the other hand, it is reasonable to expect that this barrier height is lower for the *ceramic* RuO_2/*ceramic* capacitors (the actual work function values for these materials are not listed in the literature and therefore we are unable to present them here). It is evident from Eqn. (3.1), that the leakage current is lower when the Schottky barrier is high.

Although DC leakage current measurements are useful in qualifying the device, it is the time dependent dielectric breakdown characteristics (TDDB) that determines the performance of the device under real service conditions. An accelerated unified test was used to evaluate the TDDB/fatigue phenomena in PZT films on Pt and RuO_2 electrodes. This test combines the effect of temperature, voltage and cycling frequency to accelerate the test conditions and can measure the fatigue and breakdown properties of the films simultaneously. The measured value of the polarization is a combination of the true polarization and the charge arising from leakage current effects under an AC field. The test was conducted at a temperature of 225^{0}C, a frequency of 1 MHz (square wave) and an electric field of 0.16 MV/cm. While the films showed early fatigue and breakdown on Pt electrodes, no breakdown was observed on RuO_2 electrodes (Figure 3.17). Also, the

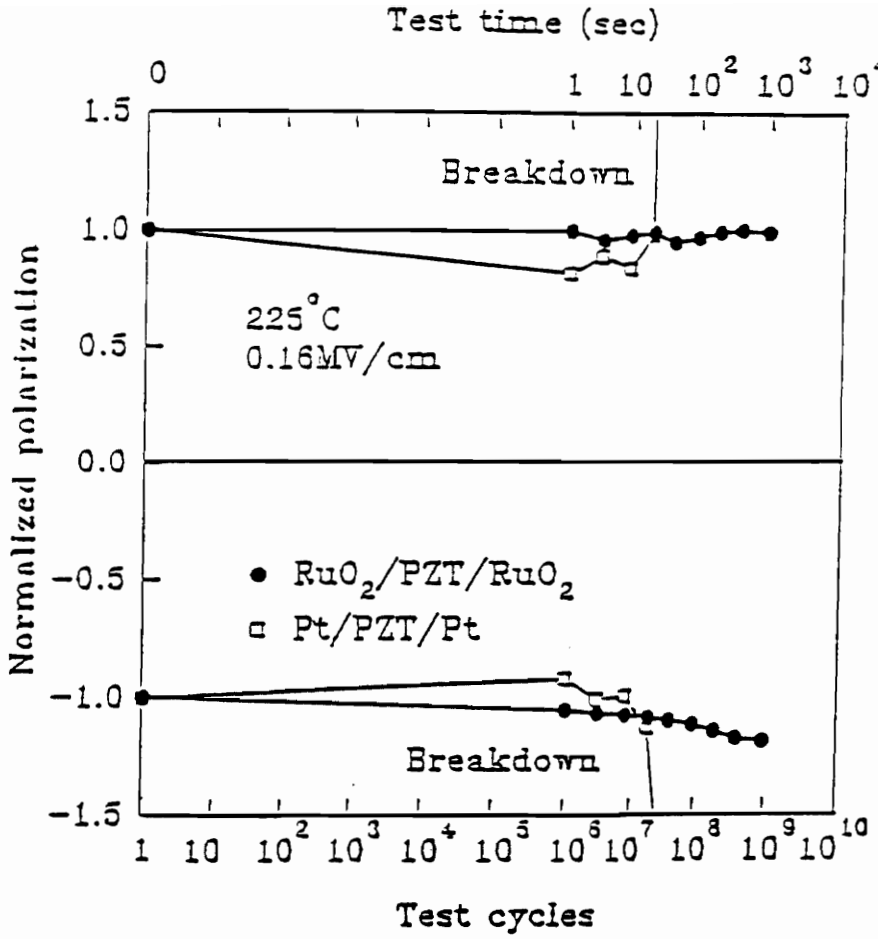

Figure 3.17 **Results of the unified fatigue/TDDB test on PZT capacitors.**

breakdown on Pt electrodes was an abrupt phenomenon. However, the films on RuO_2 did show some degradation effects arising from leakage current. When the test was conducted under similar conditions at a temperature of 300°C, the films on RuO_2 showed asymmetric degradation. As mentioned earlier, the asymmetric nature of the degradation arises form the difference in processing treatments of the top and bottom electrodes. The degradation essentially occured at the bottom electrode. When the same test was conducted on thinner PZT films (150 nm), no degradation was observed in the capacitor. We believe that this is a result of the improved adhesion of the thinner PZT films on the bottom electrode.

3.5 CONCLUSIONS

Based on the RBS, XRD and ESCA studies it can be concluded that RuO_2 is a better electrode material for PZT thin film devices when compared to ITO. The diffusion barrier properties of various ceramic thin films such as ZrN_x, TiN_x, TiO_x and ZrO_x were compared to that of RuO_2 and ITO. It was found that RuO_2 is a more effective barrier to the interdiffusion of Pb and Si at high temperatures. No intermixing was observed up to temperatures as high as 650°C in RuO_2/PZT samples while the intermixing was severe in ITO/PZT samples at temperatures above 500°C. It is possible to form the PZT perovskite phase on RuO_2 electrodes at temperatures where there is no serious interdiffusion of the constituent elements and therefore processing of the device at high temperatures is not a problem. In addition, PZT films annealed at high temperatures show good surface composition as determined from the ESCA studies. TEM studies showed that the interface between RuO_2 and PZT to be smooth with no chemical intermixing even at a temperature of 650 °C.

The ferroelectric properties of PZT films on RuO_2 electrodes was compared to the properties on metal (platinum) electrodes. PZT films with compositions close to the morphotropic phase boundary showed excellent hysteresis properties on RuO_2 electrodes. Films with a Zr/Ti ratio of 53/47 showed high remnant polarization (~20 $\mu C/cm^2$) and low coercive field (~30 kV/cm) values. The most significant improvement in properties was in the fatigue of PZT films. Under the given processing conditions, PZT films did not show any fatigue even up to $2x10^{11}$ cycles on RuO_2 electrodes while the films on Pt electrodes showed early fatigue. The improved fatigue properties of PZT thin films is explained on the basis of the increased stability of the ceramic electrode-ferroelectric interface. The interface between a ceramic electrode and an oxide ferroelectric is more stable on account of the reduced lattice mismatch and work function difference between the materials. Additionally, the oxide electrode can consume any oxygen vacancies at the electrode-ferroelectric interface, thus preventing the related development of space charge in these regions. As a result, domain pinning by space charge leading to loss of polarization is prevented. However, higher DC leakage current levels were observed in PZT films on RuO_2 electrodes when compared to Pt electrodes at room temperature. The mechanism for leakage current in PZT films has been explained on the basis of the Schottky limited currents. RuO_2/PZT capacitors have a lower Schottky barrier in comparison to Pt/PZT capacitors. Films on RuO_2 electrodes showed better TDDB characteristics under an AC field at high temperatures.

3.6 REFERENCES

1. D.W. Chapman, *J. Appl. Phys.*, 40, 2381 (1969).

2. R.B. Atkin, *Ferroelectrics*, 3, 213 (1972).

3. T. Nakagawa, J. Yamaguchi, T. Usuki, Y. Matsui, M. Okuyama and Y. Hamakawa, *Jpn J. Appl. Phys.*, 18, 897 (1979).

4. M. Sayer, *Proceedings of the 6th Symposium on Applied Ferroelectricity*, IEEE, New York, p. 559, (1986).

5. J.T. Evance and R. Wormack, *IEEE J. Solid State Circuits*, 23, 1171 (1988).

6. J.F. Scott and C.A. Paz De Araujo, *Science*, 246, 1400 (1989).

7. A. Tasch and L. Parker, *Proc. IEEE*, 77(3), 374 (1989).

8. D.B. Fraser and J.R. Maldonado, *J. Appl. Phys.*, 41(5), 2172 (1970).

9. I.S. Zheludev, *Physics of Crystalline Dielectrics, Electrical Properties*, Plenum, New York, Vol.2, 474 (1971).

10. A.Y. Kudzin, T.U. Panchenko and S.P. Yudin, *Sov. Phys. Solid State*, 16(8), 1589 (1975).

11. G. Rohrer, S. Narayan, L. McMillan and A. Kulkarni, *J. Vac. Sci. Technol. A*, 6(3), 1756 (1988).

12. H. M. Duiker, P.D. Beale and J.F. Scott, *Bull. Am. Phys. Soc.*, 33, 539 (1988).

13. I.K. Yoo and S.B. Desu, *Materials Science and Engineering*, B13, 319 (1992)

14. N.R. Parikh, J.T. Stephen, M.L. Swanson and E.A. Myers, *Mat. Res. Soc. Symp. Proc.*,200,193,(1990).

15. L. Krusin-Elbaum and M. Wittmer, *J. Electrochem. Soc. : Solid State Science and Technology*, 135 (10), 2610 (1988).

16. M.L. Green, M.E. Gross, L.E. Kappa, K.J. Schnoes and D. Barsen, *J. Electrochem. Soc.*, 132, 2677 (1985).

17. S. Saito and K. Kuramasu, *Jpn. J. Appl. Phys.*, 31, 135 (1992).

18. G. Yi and M. Sayer, *Ceram. Bull.*, 70(7), 1173 (1991).

19. I.M. Reaney and D.J. Barber, J. Microsc., 160, 213, (1993).

19. R.D. Standley and U. Ramaswamy, *J. Appl. Phys.*, 46, 4487, (1975).

20. S.B. Desu and C.K. Kwok, *Mat. Res. Soc. Symp. Proc.*, 200, 267 (1990).

21. J.M. Longo, P.M. Raccah, J.B. Goodenough, *Mat. Res. Bull.*, 4, 191 (1969).

22. Anonymous, *Microprocessors and Microsystems*, 13(4), 291 (1989).

23. J.F. Scott, C.A. Araujo, B.M. Melnick, L.D. McMillan and R. Zuleeg, *J. Appl. Phys.* 70 (1), 383 (1991).

24. I.M. Reaney, K.G. Brooks, R. Klissourka, C. Pawlaczyk, and N. Setter, J. Amer. Ceram. Soc. (in press).

25. C.K. Kwok and S.B. Desu, Appl. Phys. Lett., 60, 1430, (1992).

26. H.Y. Lee, K.C. Lee, J.N. Schunke and L.C. Burton, *IEEE Trans.*, CHMT-7 (4), (1984), pp.443.

27. I.K. Yoo and S.B. Desu, *Private Communication.*

This paper titled

"Multilayer Electrodes for Ferroelectric Thin Films"

has been submitted to

Applied Physics Letters (1995)

This paper is co-authored by Dr. S.B. Desu and Dr. H.D. Bhatt. The concept of using multilayer metal/metal oxide electrodes was proposed by both Dr. H.D. Bhatt and Dr. S.B. Desu. Dr. H.D. Bhatt was also involved the deposition of the electrodes by RF sputtering. My contributions included deposition of the ferroelectric thin films, characterization of the capacitors, analysis of the data and drawing conclusions from the study.

Chapter 4 : Minimization of Fatigue in Ferroelectric Thin Films II : Multilayer Metal/Metal Oxide Electrodes

4.1 ABSTRACT

Multilayer metal/metal oxide electrodes have been suggested as a possible means to reduce both fatigue and leakage current in PZT thin films. In this work, we have investigated the feasibility of using both Pt/RuO_2 and Pt/Rh_2O_3 as possible electrode structures for PZT films. The electrode films were grown by reactive sputtering on previously formed Si/SiO_2 substrates. PZT films were deposited by the sol-gel/spin coating method and characterized for their hysteresis and degradation properties on these electrodes. The films showed good ferroelectric properties, almost no fatigue and very good leakage current characteristics. In particular, PZT films annealed at 650 ^oC on $Pt-Rh/Rh_2O_3$ showed a $2P_r$ of 35 $\mu C/cm^2$, no fatigue up to 10^{10} cycles, a leakage current of the order of 1×10^{-8} A/cm^2 and very good TDDB characteristics (breakdown at 10^4 sec at 100 kV/cm). However, the ferroelectric of the films were found to be a strong function of the oxide layer thickness. The polarization was found to decrease with decreasing oxide layer thickness. The concept of multilayer electrodes was extended to develop a novel electrode system that overcomes the hillock formation problems in the existing Pt films. The commonly used Ti interlayer in the $Si/SiO_2/Ti/Pt$ was replaced by a Pt-Rh-O layer that provided the necessary adhesion between the electrode and the substrate and eliminated the hillock formation problems.

4.2 INTRODUCTION

Several of the investigations on ferroelectric materials for memory applications are focused on developing an electrode system for the ferroelectric capacitors [1-6]. Among other factors, the choice of an electrode material is based on its conductivity, its thermal and chemical stability and its amenability to dry etching [1-2]. It is desirable to use an electrode material that is a good diffusion barrier at high temperatures and does not react with the materials of the ferroelectric or the underlying substrate during high temperature processing. It is also now well known that the nature of the electrode-ferroelectric interface is critical in determining several degradation properties of the ferroelectric capacitors such as fatigue, leakage current, imprint, etc. [7-10].

Most of the work on ferroelectric capacitors has focused on the Pt electrode system. Platinum, if deposited directly on Si, reacts with the substrate material even at low temperatures to form a silicide layer thereby necessitating the growth of an intermediate SiO_2 barrier layer. However, the adhesion of Pt to SiO_2 is very poor and therefore a thin interlayer layer of Ti is normally used between Pt and SiO_2. Notwithstanding the good chemical and thermal stability of the Pt electrode system, it is well known that PZT capacitors with Pt electrodes show a progressive decrease in switched charge with increasing switching cycles (polarization fatigue). Fatigue has been attributed, among other reasons, to domain pinning by space charge build up at the Pt/PZT interface [1, 8-10]. Replacement of the Pt electrodes by conducting oxides such as RuO_2, LSCO etc. has served in minimizing this problem to a great extent [1-3]. It is believed that the oxide electrodes consume the mobile oxygen vacancies responsible for the space charge and reduce the Schottky depletion regions at the electrode-ferroelectric interfaces due to reduced work function differences [1]. However, Schottky emission in PZT films combined with lower effective Richardson constant values of the oxide electrodes may

also be responsible for the higher leakage current levels in oxide electrode/PZT capacitors [1, 11].

Noting this behavior, we propose multilayer metal/conducting oxide electrodes as a possible means to simultaneously reduce both fatigue and leakage current in PZT thin films. In this work, we have investigated the effectiveness of using Pt/RuO_2 as a possible multilayer electrode structure for PZT thin films. The conducting oxide was coated in the form of thin layers (< 100 nm) on previously formed $Si/SiO_2/Ti/Pt$ substrates. We believe that the thickness of the conducting oxide layer may play an important role in determining the electrical degradation properties of the ferroelectric films and therefore it was used as the primary variable in this study. PZT thin films with a composition close to the morphotropic phase boundary were then deposited on these electrodes and characterized for their hysteresis, fatigue and leakage current properties.

On a related topic, the adhesion of Pt to the underlying SiO_2 layer has been the focus of several recent studies [12-15]. Hillock formations are often found on the surface of Pt films during high temperature processing. The height of the Pt hillocks can be larger than the ferroelectric layer thickness resulting in very high leakage currents in very thin PZT films. One of the reasons for Pt hillock formation has been attributed to the difference in the thermal expansion coefficient of Pt ($9 \times 10^{-6}/^{o}C$) and of the underlying substrate (for e.g., Si : 2.5×10^{-6} $/^{o}C$) which results in a compressive stress in the Pt at elevated temperatures. The Pt relieves the stress by forming hillocks. The feasibility of using other oxide barrier layers including TiO_2, ZrO_2 etc. is now a subject of several investigations [16]. In this paper, we also propose an alternate device structure, that is essentially an extension of the concept of multilayer electrodes, to simultaneously improve: (a) the adhesion and associated hillock formation problems of Pt to the underlying oxide layer and (b) the degradation problems of fatigue and leakage current in

PZT thin films capacitors. For this study, the starting material for processing the bottom consisted of a Pt-10 % Rh alloy target. The electrode system was fabricated on Si/SiO_2 substrates using an *in-situ* three step sputtering process. The first step involved reactive sputtering of the alloy target in an Ar + O_2 ambient to form a thin Rh_xO_y (and/or PtO_z) on top of SiO_2 layer. This was followed (second step) by the sputtering of the metallic Pt-Rh layer itself in a pure Ar atmosphere. The Rh_xO_y layer was deposited in the first step to provide the necessary adhesion between the metallic Pt-Rh layer and SiO_2. The final step once again involved sputtering of the alloy target in a reactive O_2 + Ar atmosphere to form a surface Rh_xO_y layer. Rh_2O_3 is also a transition metal oxide that is conducting at room temperature [17]. This surface layer and the underlying metallic Pt-Rh layer formed the metal/conducting oxide multilayer electrode system for PZT deposition. A schematic of the electrode structure is shown in Fig. 4.1. There are several advantages in using this kind of a device structure for PZT capacitor applications: (a) it obviates the need for any kind of a metallic interlayer such as Ti and thereby prevents any associated hillock formation problems (b) the multilayer electrode structure is developed by an *in-situ* process and (c) the concept can be extended to other conducting transition metal/metal oxide systems such as Rh/Rh_2O_3, Ir/IrO_2 etc. We also provide the electrical characteristics of PZT films on these electrodes in the paper.

4.3 EXPERIMENTAL PROCEDURE

RuO_2 thin films were deposited to three different thickness' of 30 nm, 50 nm and 70 nm onto previously formed $Si/SiO_2/Ti/Pt$ electroded substrates. The sputtering process was conducted in a reactive atmosphere of O_2 and Ar using a Cooke Vacuum DC magnetron sputterer. The gas pressure during deposition was maintained at $2x10^{-4}$ Torr,

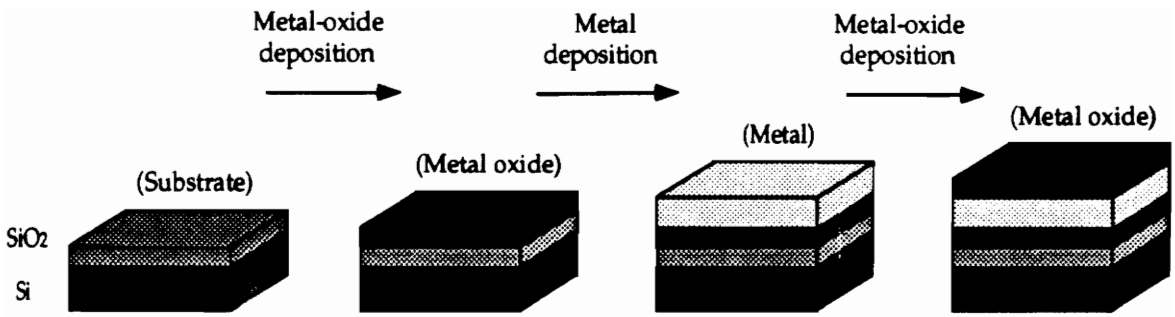

Figure 4.1 Schematic of the proposed multilayer metal/metal oxide electrode structure for PZT thin films

the O_2:Ar ratio at 1:4, and the substrate temperature at 200^{0}C. Sol-gel derived PZT films were then deposited onto these substrates. The PZT precursor (Zr:Ti = 53/47) was prepared from a metalorganic solution (0.4M) of lead acetate, zirconium n-propoxide and titanium iso-propoxide dissolved in acetic acid and n-propanol. The solution was hydrolyzed (R=10) to form the precursor. The method of preparing the precursor is similar to that suggested by Yi et al [18]. Ten percent excess lead was added to the solutions to compensate for the loss of lead during high temperature processing. Films were spin coated at 1500 rpm for 20 sec and subsequently dried at 150^{0}C for 5 min. The cycle was repeated once or twice (spin-bake cycle) to obtain the desired thickness (300-450 nm). The coated films were annealed at a temperature of 650^{0}C for 30 min in a quartz tube furnace under a controlled oxygen atmosphere. Top electrodes of RuO_2 (2.1 x 10^{-4} cm^2) were coated to the same thickness as the bottom electrodes through a shadow mask, under the same conditions as the bottom electrode. Before electrical characterization, the films were once again annealed at 650 ^{o}C for 30 min to ensure good contact between the top electrode and the ferroelectric film.

The sputtering process for Pt-Rh electrodes was conducted in an RF sputtering chamber (Denton Vacuum, Inc.) at a substrate temperature of 450 ^{o}C. The total gas pressure during all of the three stages of deposition was maintained at 5 mTorr while the RF power was kept at 50 W. The O_2 : Ar flow rate ratio used in the first and third stages of the deposition process was 1 : 4. The Pt-10 % Rh sputtering target was 2 inches in diameter and 0.125 inches in thickness; the substrates used were (100) Si with 100 nm SiO_2 oxide layer grown on it by thermal oxidation at 950 ^{o}C. The total deposition time was maintained at 22 min under these conditions and the deposition time for the first layer was also maintained at 3 min. However, the deposition time in the second and third stages were varied so as to grow surface oxide layers of different thickness'. The duration of the

final deposition in O_2+Ar was varied between 3 min, 6 min and 9 min and the deposition time of the intermediate Pt-Rh metallic was correspondingly reduced from 19 min to 16 min and 13 min. These samples will be referred to as 3/19/**3**, 3/16/**6** and 3/13/**9**, respectively, throughout the rest of this paper.

Both the electrodes and ferroelectric thin films were characterized for their phase formation and orientation by using x-ray diffraction (XRD). The adhesion of the films were tested by a simple tape peel test. Rutherford backscattering spectrometry was used to determine the thickness and stoichiometry of the oxide layers. The ferroelectric capacitors were characterized for hysteresis, fatigue and leakage current properties using a standardized RT66A ferroelectric tester (Radiant Technologies).

4.4 RESULTS AND DISCUSSION

4.4.1 Pt/RuO_2 Multilayer Electrodes :

Fig. 4.2 shows the x-ray diffraction patterns of PZT films deposited on the Pt/RuO_2 with various thickness' of the oxide electrode. The XRD pattern of bare RuO_2 deposited on Si/SiO_2 is also shown in the same figure to identify and separate the peaks from the electrode and the ferroelectric films. The PZT (53/47) thin films in this study were annealed at 650 ^oC for 30 min in O_2. It was found that the thickness of the RuO_2 films had a strong effect on the orientation of the overlying PZT films. From Fig. 4.2, it is clear that with decreasing thickness of the oxide film, there is an increase in the (100) orientation of PZT. It is important to determine the crystallographic orientation of the ferroelectric films because the measured polarization and coercive field values are a strong function of the orientation of the planes relative to the substrate. To obtain high

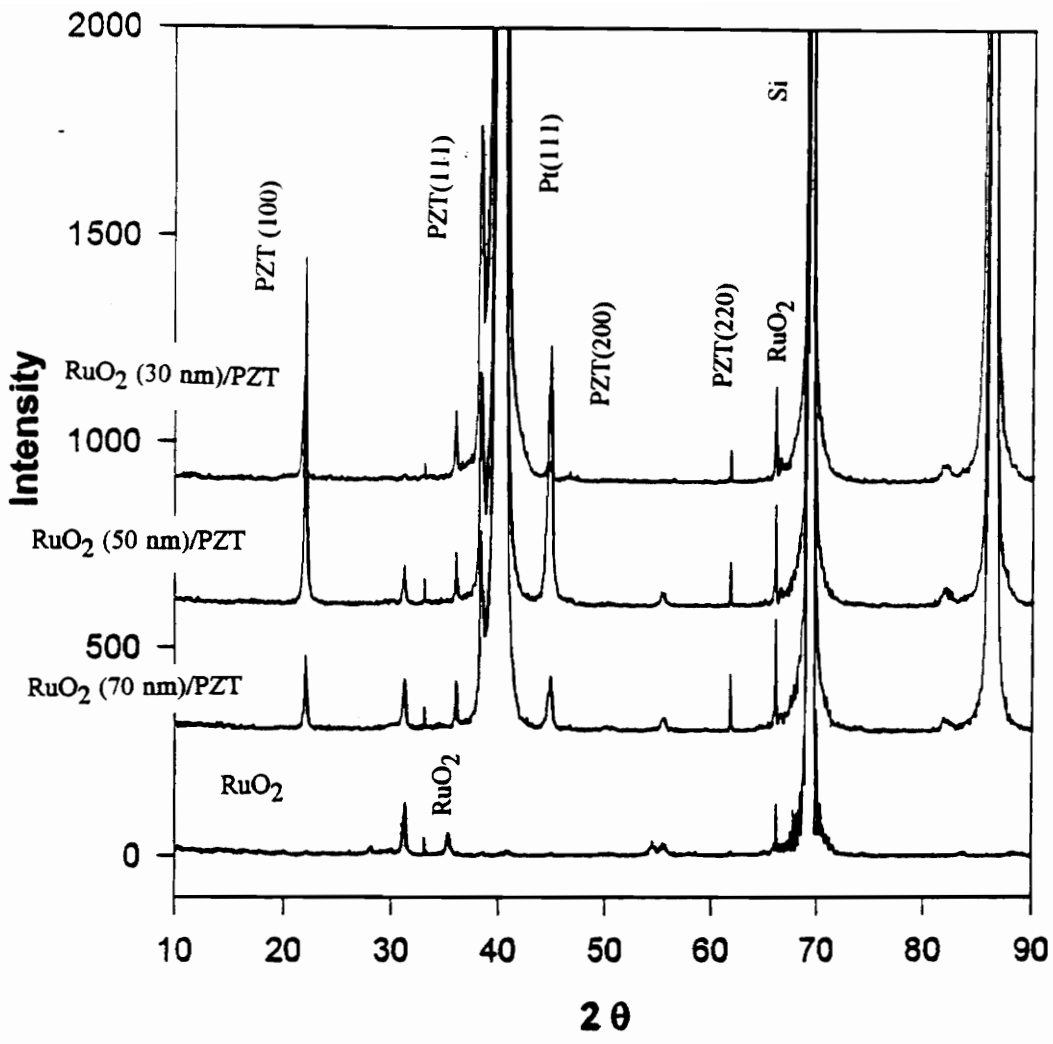

Figure 4.2 XRD pattern of PZT films deposited on Pt/RuO_2 electrodes with various thickness of the oxide electrode. PZT films were annealed at 650°C/30min.

polarization values, it is preferable to grow the ferroelectric films with the (111) and (110) perovskite planes parallel to the plane of the substrate. In the regular XRD pattern shown in Fig. 4.2, the (111) diffraction peak of PZT coincided with the (111) peak from the Pt films and therefore it was impossible to determine the absolute intensity of this diffraction peak.

To unequivocally determine the relative intensities of the (111) and (100) peaks from perovskite PZT, glancing angle incidence x-ray diffraction measurements were conducted. The glancing angle procedure eliminates diffraction from the substrate planes. The pattern obtained for the described samples is shown in Fig. 4.3. Qualitatively, it is now clear that there is an increase in the (100)/(111) peak intensity ratio with decreasing thickness of the RuO_2 thin films. One of the possible causes for this for this change in orientation of PZT films could be the thickness dependence of orientation in the RuO_2 films. There is a critical thickness above which the strain energy is to too large for the film to grow along a particular orientation. The XRD patterns of bare $Si/SiO_2/Ti/Pt/RuO_2$ substrates (i.e., without PZT) are shown as a function of RuO_2 thickness in Fig. 4.4. No diffraction peaks belonging to RuO_2 were detected from the $Si/SiO_2/Ti/Pt/RuO_2$(30 nm) and $Si/SiO_2/Ti/Pt/RuO_2$(50 nm) substrates. However, diffraction peaks from the (101) planes of RuO_2 were detected in the $Si/SiO_2/Ti/Pt/RuO_2$(70 nm) samples. It was thought that the diffraction volume of RuO_2 is too small in the 30 nm and 50 nm films for any diffraction peaks to be detected in the same. However, glancing angle studies also did not provide any diffraction peaks from the 30 and 50 nm RuO_2 films. Although at this point we do not have any conclusive explanation for this behavior, it is reasonable to state (with the available data) that the orientation of PZT films is dependent on the nature of the underlying RuO_2 electrodes, which is clearly a function of its thickness. Fig.4.5 compares the hysteresis properties of PZT films on these electrode structures. It can be seen that the

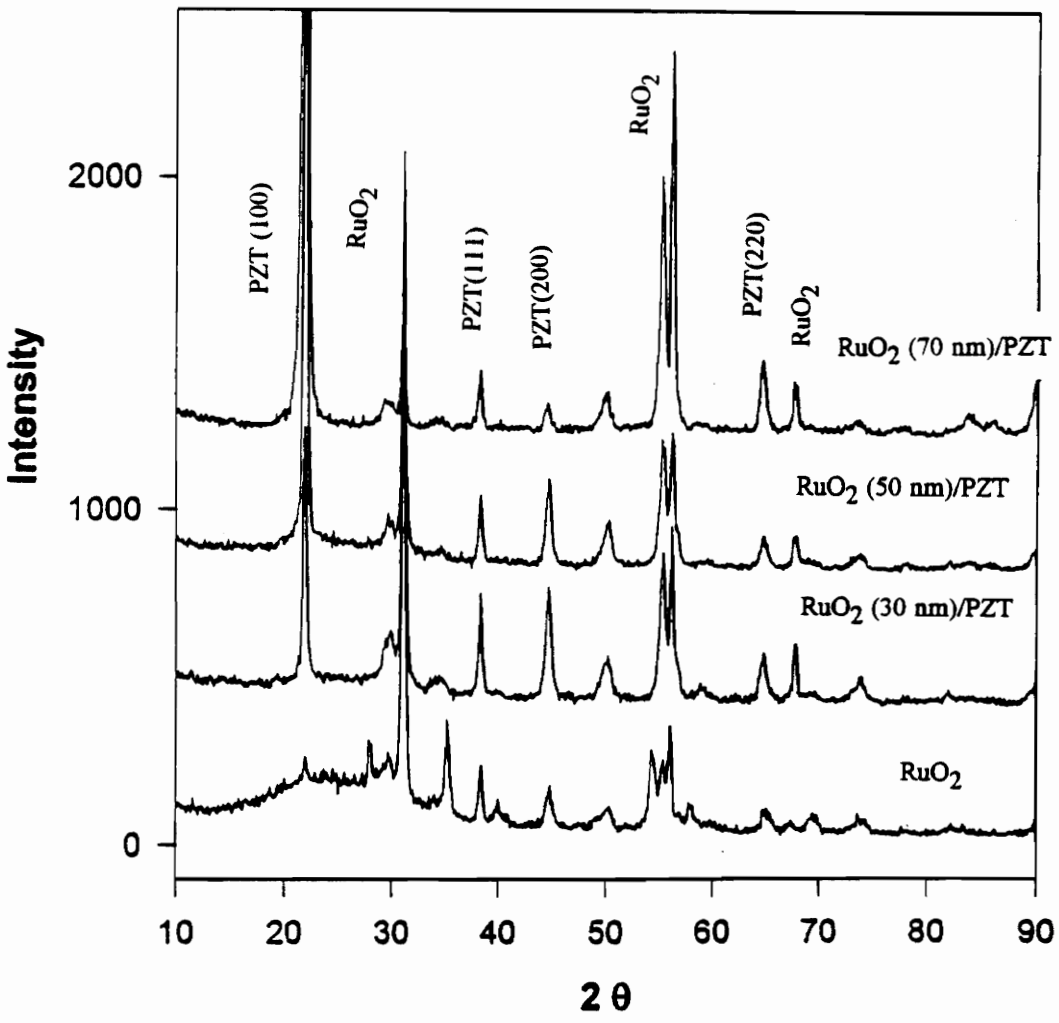

Figure 4.3 Glancing angle XRD pattern of PZT films on Pt/RuO_2 multilayer electrodes.

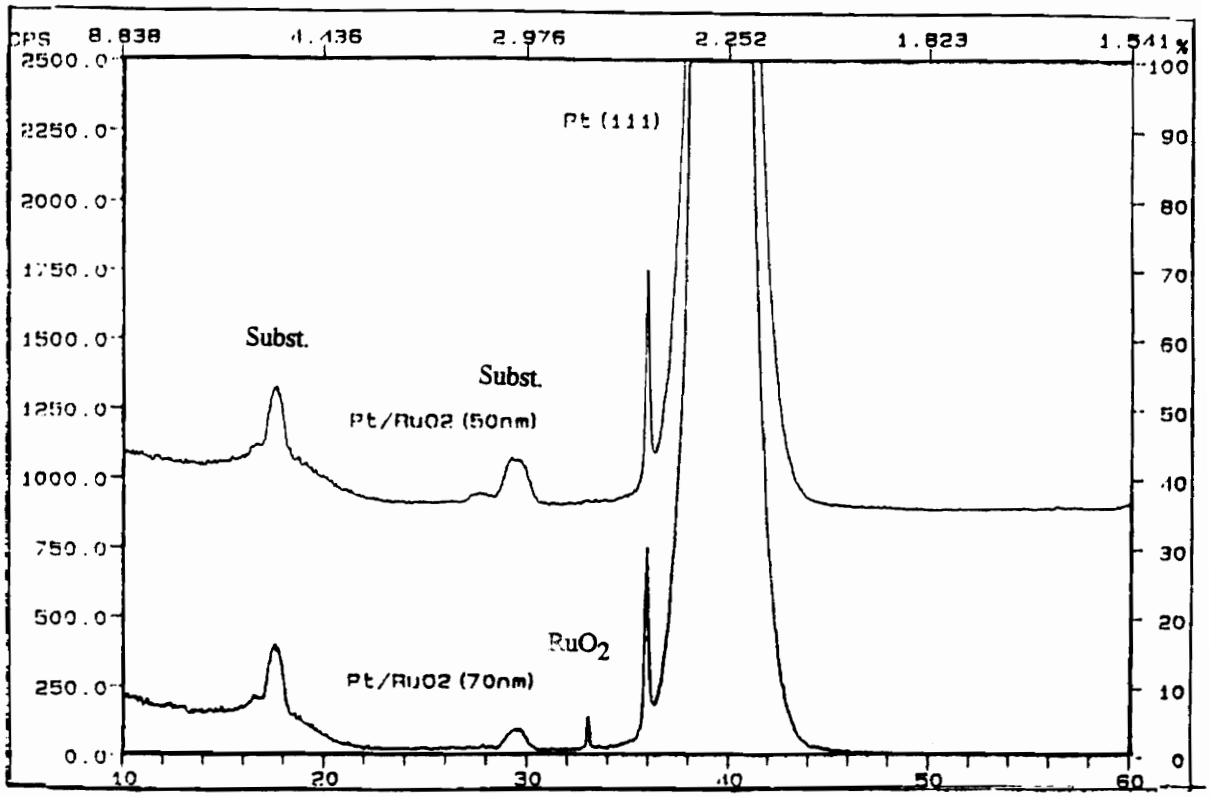

Figure 4.4 XRD pattern of Pt/RuO_2 as a function of RuO_2 thickness : (a) 70 nm (b) 50 nm.

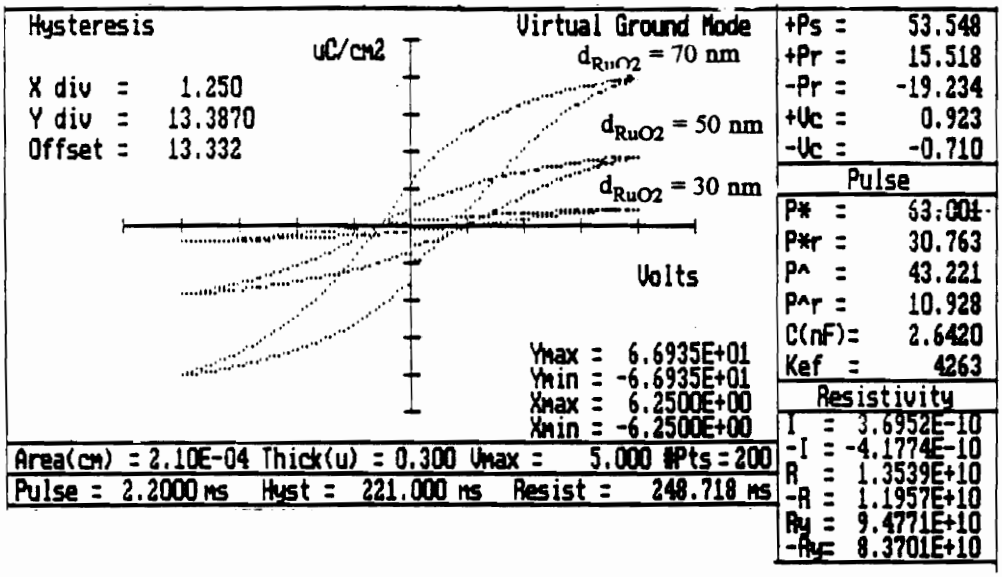

Figure 4.5 Hysteresis properties of PZT films on Pt/RuO_2 multilayer electrodes.

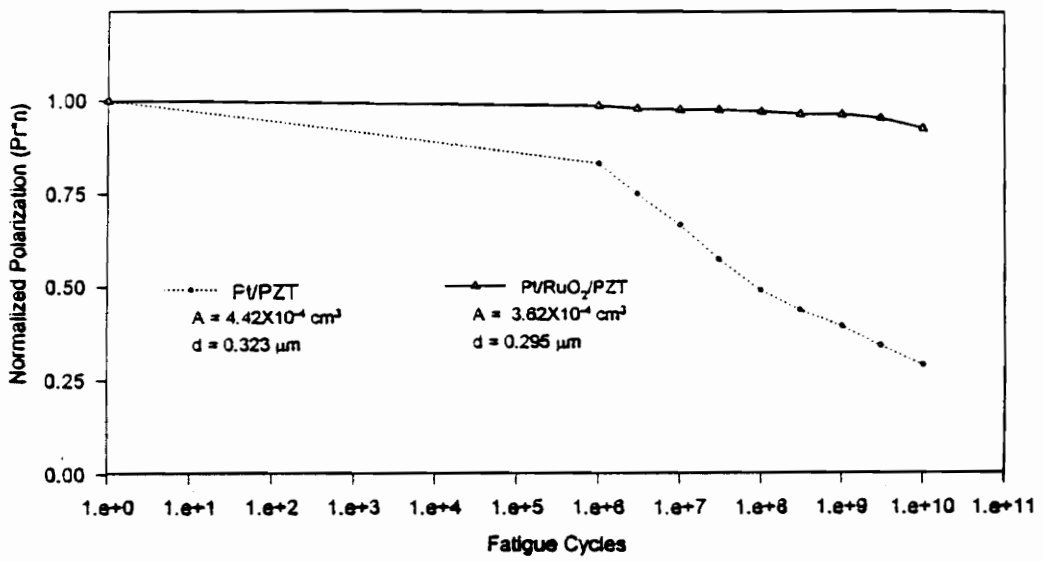

Figure 4.6 Fatigue properties PZT films on Pt/RuO_2 multilayer electrodes.

there is a significant difference in the polarization values. The lower polarization values with decreasing thickness of RuO_2 may be explained by the change in orientation of the PZT films from predominantly (111) to (100). Fig. 4.6 compares the fatigue results of Pt/RuO_2/PZT films as a function of RuO_2 thickness. None of the samples showed any fatigue up to the measured 10^{10} cycles indicating that a 30 nm thickness of RuO_2 is sufficient in preventing fatigue. Fig. 4.7 is plot of the leakage current of Pt/RuO_2 (50 nm)/PZT capacitors. As shown earlier, at an applied electric field of 3V, the PZT films on Pt electrodes typically show a leakage current density of 5×10^{-7} A/cm^2 while films on RuO_2 electrodes exhibit leakage current densities of the order of 4×10^{-4} A/cm^2. On comparison, we find that the leakage current density of PZT films of Pt/RuO_2 electrodes is 5×10^{-6} A/cm^2 which is definitely an improvement (by at least two orders of magnitude) over the bare RuO_2 electrodes. More importantly, the minimization of fatigue has been accomplished with a simultaneous reduction in leakage current.

In summary, Pt/RuO_2 multilayer electrodes show good promise for low fatigue and low leakage current applications. The polarization values obtained were low (but still within the requirements) on multilayer electrodes possibly due to a change in orientation in PZT from (111) to (100). The leakage current and fatigue have been simultaneously reduced. However, the leakage current values are still above acceptable limits and need improvement [19].

4.4.2 Pt-Rh Multilayer Electrodes :

The adhesion of the deposited films to the underlying substrates were tested qualitatively by a tape peel test. None of the films showed any peeling. The XRD analysis of the as-deposited electrode films indicated the formation of crystalline Pt-Rh structures

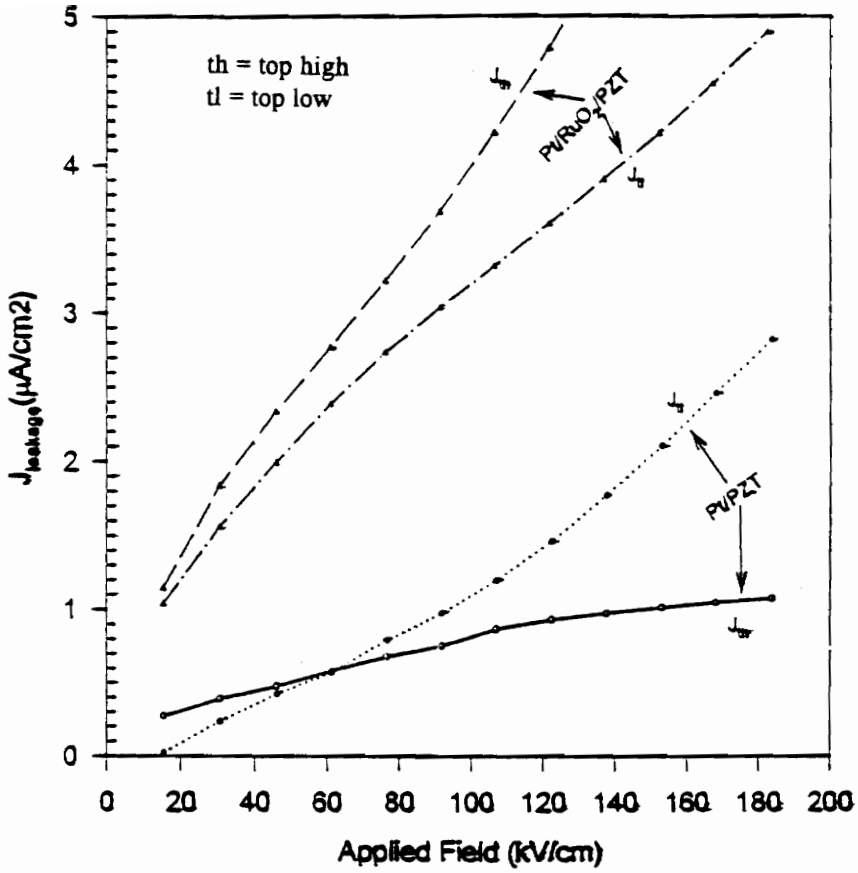

Figure 4.7 Current-Voltage characteristics of Pt/RuO_2 (50 nm)/PZT capacitors.

under these deposition conditions. Morphological examination of these films (using SEM) did not show any hillock formation on the surface. RBS measurements were conducted on the as-deposited films to determine the formation of the Rh_2O_3 layers. RBS also provides the composition and thickness of the layers comprising the multilayer structure. A 2 MeV He^{2+} beam was used as the reference. The sample sizes were typically 1 cm^2 in area. Sample normal tilts of -6^0 and 50^0 from the incident beam direction were used in the analysis with the detector placed at a backscattering angle of 165^0. A Win-spec (R) simulation program was used to obtain the concentration vs depth profile of the elemental distribution. Theoretical spectra were generated by varying the compositions of thin layers of the sample and compared to the experimental spectrum until a close match was obtained. Fig. 4.8 is a typical RBS plot obtained from the (3/19/3) Pt-Rh films. Although the starting composition of the alloy target contained 10 % Rh alloyed with 90 % Pt, quantitative analysis showed that the composition of Rh in the films was close to 13 %. This indicates that Rh is sputtered preferentially compared to Pt. The RBS simulation results indicate that there are three distinct layers in the deposited films. The first layer (nearest to the Si/SiO_2 substrate) is an oxide layer of composition Pt:Rh:O of 66:14:20, the second a metallic layer of composition Pt : Rh = 87:13 and finally a surface oxide layer of composition Pt:Rh:O = 50:20:30. The thickness of the layers were determined to 20 nm, 50 nm and 15 nm, respectively.

The important factor to note is that these results confirm the formation of the desired oxide layers at the surface and substrate-electrode interface. A small amount of Si diffusion into the electrode film was detected as evident from Fig. 4.8. However, the presence of Si at the surface could not be confirmed by this technique. It needs verification by a more sensitive technique such as Auger electron spectroscopy (AES). Based on the composition results, we cannot conclude if Pt has been oxidized during the sputtering

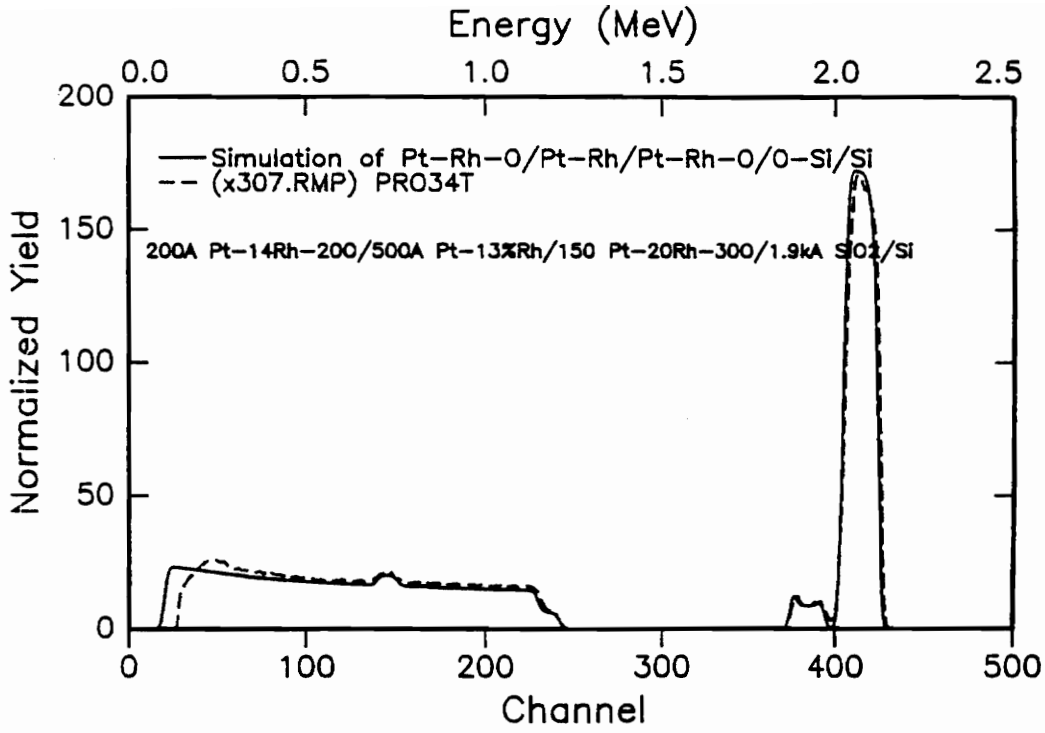

Figure 4.8 **RBS profile of Pt-Rh electrodes (3/19/3) multilayer electrodes deposited on Si/SiO_2 substrates by reactive sputtering in O_2 atmosphere at 450 ^oC.**

process. However, Rh certainly has a higher affinity for oxygen and is therefore likely to be oxidized to a greater extent relative to Pt during the sputtering process. PtO_2 is known to be a conductor at room temperature, but is unstable at temperatures above 600 °C. It is also known to provide good adhesion between SiO_2 and Pt layers.

PZT films were deposited onto these electrodes by the sol-gel spin coating process to a thickness of 300 nm. The as-deposited films were annealed at a temperature 650 °C for 30 min in a controlled O_2 atmosphere. The top Pt-Rh electrodes were deposited once again by reactive sputtering under conditions similar to that of the bottom electrodes and the samples were then annealed once again at 650 °C/30 min. Fig. 4.9 shows the XRD pattern of PZT annealed at 650 °C on (3/19/**3**), (3/16/**6**) and (3/13/**9**) Pt-Rh films. It was found that the intensity ratio of (100)/(110) peaks in the PZT increased with decreasing oxide layer thickness. This in turn means that the Rh_xO_y oxide layer formed over the Pt-Rh changes its orientation with increasing thickness as seen in the Pt/RuO_2 case.

Table 4.1 summarizes the electrical properties (hysteresis, fatigue and leakage current) of PZT films on the various Pt-Rh electrodes. As expected, with increasing surface oxide electrode layer thickness, the P_r value decreases. However, the difference in polarization values is not drastic as in the case of Pt/RuO_2 electrodes. A typical hysteresis plot obtained from 3/16/**6**/PZT samples is shown in Fig. 4.10. Fatigue measurements were performed on all the samples at an applied voltage of 5V and a frequency of 0.5 MHz. None of the PZT films showed any fatigue under these measurement conditions (see Fig. 4.11 for fatigue plot of the 3/16/**6**/PZT sample). It can also be seen from Table 1 that, in general, all of the samples showed very good leakage current density values at an applied field of 100 kV/cm. In particular, the 6 min sample (3/16/6) showed leakage current density in the range of 10^{-9} A/cm^2 which is one of the lowest values we have ever obtained for PZT thin films. Fig. 4.12 shows the time dependent dielectric breakdown

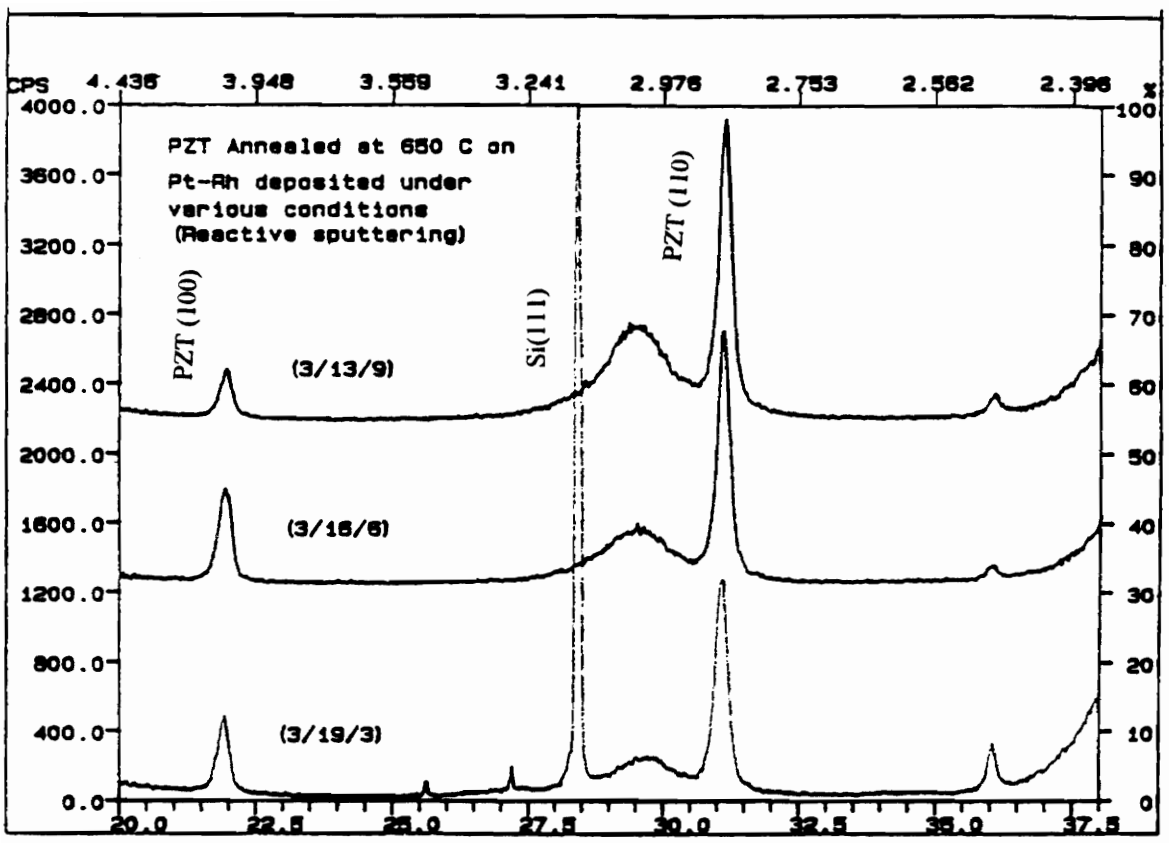

Figure 4.9 XRD pattern of PZT films deposited on $Si/SiO_2/Rh_xO_y/Pt\text{-}Rh/Rh_xO_y$ substrates. The patterns are shown as a function of surface Rh_xO_y layer thickness. PZT films were annealed at 650 ^oC for 30 min.

Table 4.1 Summary of the electrical properties (hysteresis, fatigue and leakage current) of PZT films on the various Pt-Rh electrodes.

Rh-Oxide Layer Thickness (given as time of sputt., of top oxide layer)	**PZT Annealing Conditions (°C/30 min)**	**$2P_r$ ($\mu C/cm^2$)**	**Leakage Current (A/cm^2) *at 100 kV/cm***	**Fatigue loss (%) *at 1 MHz, 5V***
(3/19/3)	650 + TE + 650	32	1.5×10^{-7}	5%
(3/16/6)	650 + TE + 650	35	9.9×10^{-9}	3%
(3/13/9)	650 + TE + 650	24	2×10^{-8}	3%

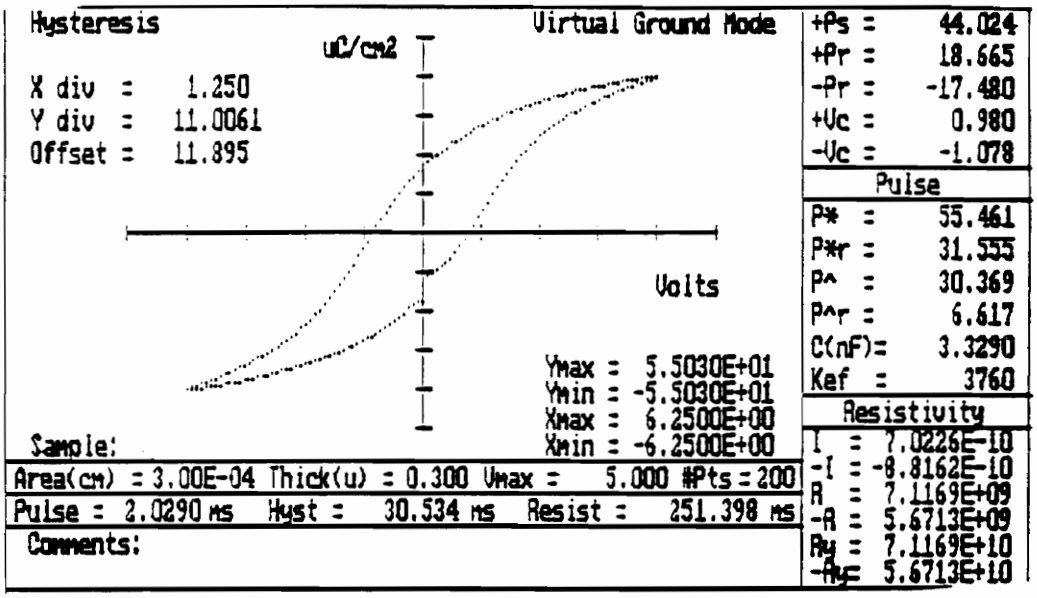

Figure 4.10 Typical hysteresis behavior of PZT films annealed at 650 ^{o}C for 30 min on 3/16/6 Pt-Rh multilayer electrodes.

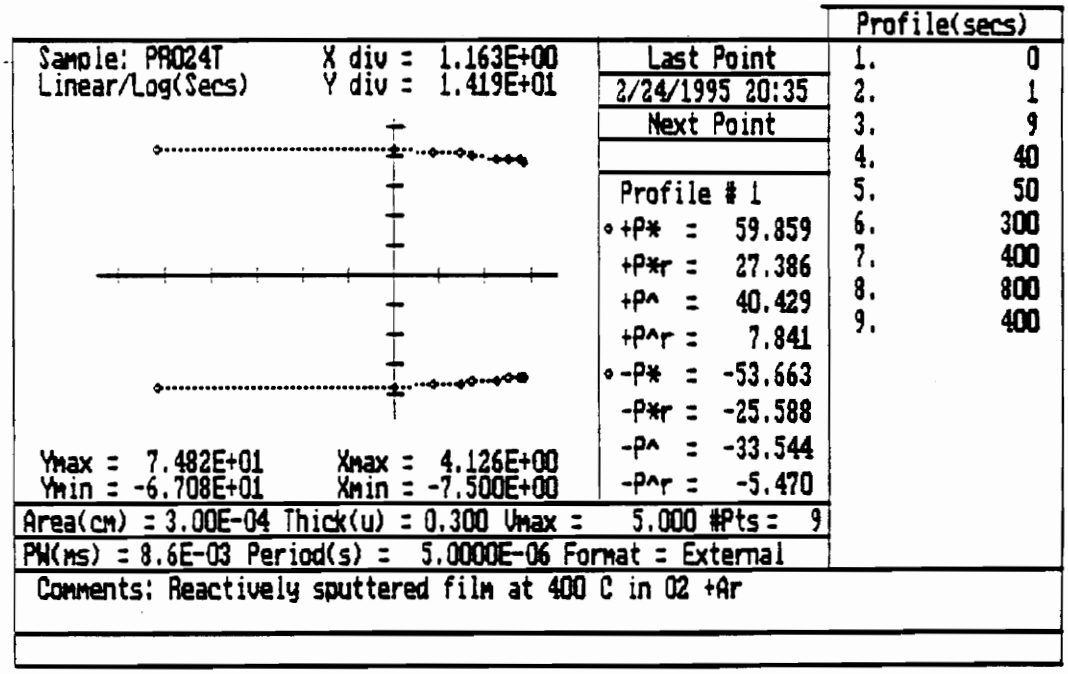

Figure 4.11 Fatigue behavior of PZT films annealed at 650 ^{o}C for 30 min on 3/16/6 Pt-Rh multilayer electrodes.

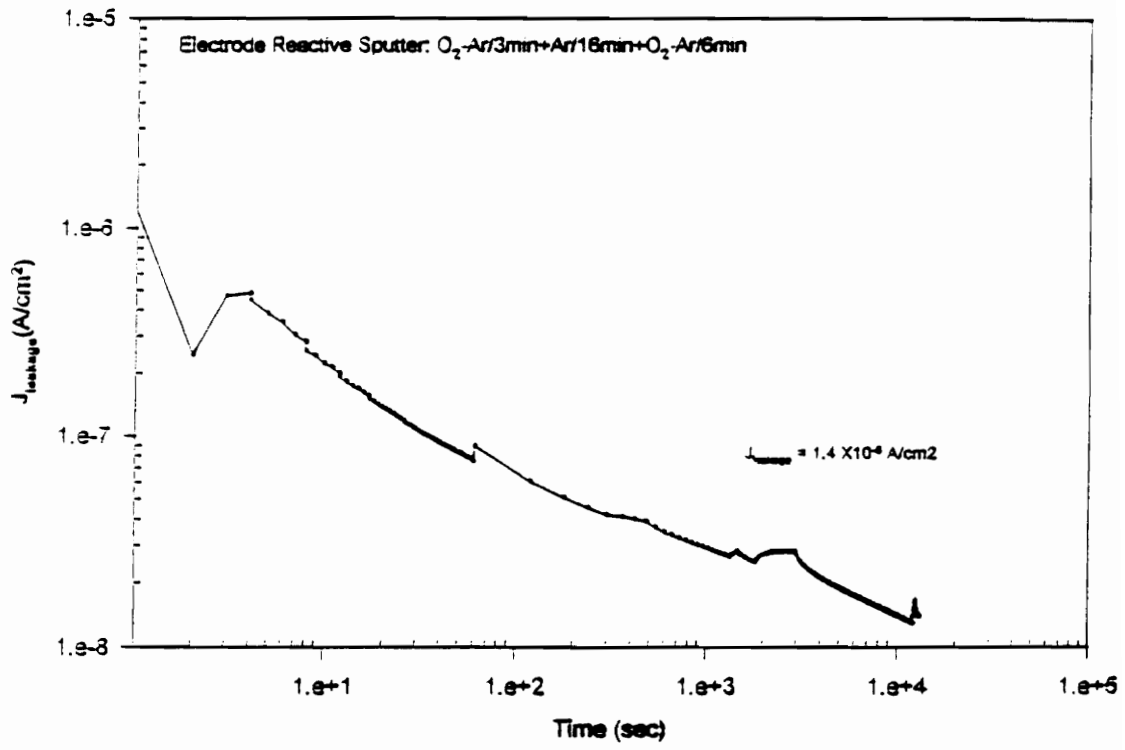

Figure 4.12 TDDB characteristics PZT films annealed at 650 ^{o}C for 30 min on 3/16/6 Pt-Rh multilayer electrodes.

characteristics (TDDB) of PZT samples (at 100 kV/cm) on Pt-Rh 3/16/6 electrode. Clearly, the sample shows very good TDDB characteristics; breakdown occurs only after 10^4 seconds.

For PZT thin films, the reasons for the improved fatigue properties on oxide electrodes and the better leakage current properties on metal electrodes have been discussed in previous reports [1-2]. While the improvement in fatigue as been attributed to reduced space charge entrapment at the oxide electrode-ferroelectric interface [1, 7-8], it has been suggested that the better leakage current properties of metal/PZT capacitors are due to the high Schottky barrier at the interface [1,11]. In this paper, we have shown that both fatigue and leakage current can be simultaneously reduced using metal/metal oxide multilayer electrodes. The improvement in fatigue properties is to be expected because of the surface oxide electrode layer. However, at this point of time, we do not have an explanation for the simultaneous improvement in leakage current. It is possible that the thickness of the oxide layer may control the Schottky barrier height at the interface. However, the determination of the exact mechanism needs further study.

4.5 CONCLUSIONS

Multilayer metal/metal oxide electrodes (Pt/RuO_2 and $Pt\text{-}Rh/Rh_2O_3$) have been shown to reduce both the fatigue and leakage current in PZT thin films. For example, PZT films annealed at 650 ^oC on $Pt\text{-}Rh/Rh_2O_3$ show good hysteresis behavior ($2P_r \sim 35$ $\mu C/cm^2$), no fatigue up to 10^{10} cycles, low leakage currents ($\sim 1 \times 10^{-8}$ A/cm^2) and very good TDDB characteristics (breakdown at 10^4 sec at 100 kV/cm). The thickness of the surface oxide electrode was found to critically determine the properties of the ferroelectric film. The decrease in polarization with decreasing oxide layer thickness has

been attributed to the change in orientation of the PZT films from predominantly (111) to (100). The concept of multilayer electrodes was extended to develop a novel electrode system that overcomes the hillock formation problems in the existing Pt films. The commonly used Ti interlayer in the $Si/SiO_2/Ti/Pt$ was replaced by a Pt-Rh-O layer that provided the necessary adhesion between the electrode and the substrate and eliminated the hillock formation problems.

4.6 REFERENCES

1. D.P. Vijay and S.B. Desu, *J. Electrochem. Soc*, 140, (1993), 2640.

2. C.K. Kwok, D.P. Vijay, S.B. Desu, N.R. Parikh and E.A. Hill, Integ. Ferroelect., 3, (1993), 121-130.

3. P.D. Hren et al., Integ. Ferroelect., 2, (1992), 311-326.

4. H.N. Al-Shareef, K.R. Bellur, O. Auciello, and A.I. Kingon, Proc. 5th Intern. Symp. on Integrated Ferroelectrics, edited by C.A. Paz de Araujo, University of Colorado Press, (1993).

5. 8. J.T. Cheung, *Proceedings of the 4th International Symposium on Integrated Ferroelectrics*, (1992), 158.

6. R.Ramesh, H. Gilchrist, T. Sand, V.G. Keramidas, R. Haakenaasen, and D.K. Fork, Appl. Phys. Lett., 63, (1993), 3592.

7. I.K. Yoo and S.B. Desu, Mat. Sci. and Eng., B13, (1992), 319.

8. I.K. Yoo and S.B. Desu, Phys. Stat. Sol., a133, (1992), 565.

9. H.M. Duiker, P.D. Beale, J.F. Scott, C.A. Paz de Araujo, B.M. Melnick, J.D. Cuchlaro and L.D. McMillan, J.Appl. Phys., 68(11), (1990), 5783.

10. S.B. Desu and I.K. Yoo, J. Electrochem. Soc., 140, (1993), L133.

11. I.K. Yoo and S.B. Desu, Integt. Ferroelect., 3, (1993), 365-376.

12. J.O. Olowolfe, R.E. Jones Jr. A.Campbell, R.I. Hedge, C.J. Mogab and R.B. Gregory, J. Appl. Phys., 73, (1993), 1764-1772.

13. P.D. Hren, H.N. Al-Shareef, S.H. Rou, A.I. Kingon, P. Buaud and E.A. Irene, Mat.Res.Soc. Symp. Proc., 260, (1992), 575-581.

14. H.N. Al-Shareef, K.D. Gifford, P.D. Hren, S.H. Rou, O. Auciello and A.I. Kingon, Integ. Ferroelect. 3, (1993), 259-263.

15. K. Sreenivas, I. Reaney, T. Maeder, N. Setter, C. Jagdish and R.G. Elliman, J. Appl. Phys., 75, (1994), 232-239.

16. S.C. Summerfelt, D. Kotecki, A. Kingon and H.N. Al-Shareef, preprint, (1995).

17. L. Krusin-Elbaum and M. Wittmer, *J. Electrochem. Soc. : Solid State Science and Technology,* 135 (10), 2610 (1988).

18. G. Yi and M. Sayer, *Ceram. Bull.*, 70(7), 1173 (1991).

19. 7. A. Tasch and L. Parker, *Proc. IEEE*, 77(3), 374 (1989).

This paper titled

"Novel Fatigue Free Layered Structure Ferroelectric Thin Films"

is published in

Materials Science and Engineering

B32 (1995) 75-81

This paper was co-authored by Dr. S.B. Desu (first author). My contributions included the experimental work, characterization, analysis of data and conclusions.

Chapter 5 : Minimization of Fatigue in Ferroelectric Thin Films III : Control of Defect Density

5.1 ABSTRACT

In earlier studies, the authors have attributed fatigue in ferroelectric thin films to domain pinning due to space charge caused by entrapment of defects such as oxygen vacancies at the electrode-ferroelectric interfaces [1-5]. In this work, we demonstrate that fatigue can be minimized by controlling the defect density in the ferroelectric films. The control of defect density has been achieved in two different ways : (a) donor doping to compensate for the vacancies (e.g., Nb and La doping in PZT) and (b) utilizing ferroelectric materials with a low intrinsic defect concentration. As a result of the latter approach, novel materials belonging to the layer-structure family of oxides have been identified as excellent candidates for fatigue free nonvolatile memory applications. Stoichiometric thin films of layer-structured $SrBi_2(Ta_xNb_{1-x})_2O_9$ ($0<x<1$) compounds were successfully deposited on platinized Si/SiO_2 wafers using the laser ablation technique. The identification of these fatigue free thin film materials and their processing, structure and properties are also discussed in this paper. The films show very good hysteresis characteristics with a remnant polarization value of 11 $\mu C/cm^2$ and no fatigue was observed up to 10^9 switching cycles.

5.2 INTRODUCTION

Degradation problems such as fatigue, leakage current and aging have been the major problems affecting the lifetime of ferroelectric thin films. There are several models

that have been proposed in the literature to explain these degradation phenomena [6-10]. For ferroelectric oxide films, Desu and Yoo [1-4] have proposed a unified model in which oxygen vacancies have been cited as the common source for most of these degradation phenomena. Their quantitative models [1-4] showed that both relative movement of oxygen vacancies and their entrapment at the electrode/ferroelectric interface (and/or at the grain boundaries and domain boundaries) are important contributing factors. The models offers two possible solutions to overcome fatigue : (1) reducing the tendency for entrapment by changing the nature of the electrode/ferroelectric interface and (2) controlling the defect density. Ceramic electrodes such as RuO_2 which minimize oxygen vacancy entrapment have been used to minimize fatigue problems in oxide ferroelectrics [5]. In this paper, we discuss the minimization of fatigue in ferroelectric materials based on strategies to control defect density. Two different approaches to the control of defect density are demonstrated : (a) donor doping to compensate for the vacancies (e.g., Nb and La doping in PZT) and (b) identifying alternate ferroelectric materials with a low intrinsic defect concentration.

5.3 DOPANT ADDITIONS

$PbZr_xTi_{1-x}O_3$ (PZT) is the most popular ferroelectric thin film material under investigation for nonvolatile memory applications. These ferroelectrics need to be crystallized in the perovskite phase (ABO_3) for them to exhibit ferroelectric behavior. In a tetragonal perovskite structure, the A^{2+} ions occupy the corners of the lattice, O^{2-} ions the face centers and the B^{4+} ions are located at the center. Spontaneous polarization in these materials is caused by the upward or downward displacement of the B^{4+} ions relative to the oxygen ions in the lattice; the oxygen ions are displaced in the direction opposite to the

displacement of the B^{4+} ions. In polycrystalline ferroelectric thin films, there are regions called ferroelectric domains that contain unit cells which all have the same polarization direction. On application of an electric field greater than E_c, all the domains switch to orient in the same direction.

In the processing of these films to obtain the desired ferroelectric phase, however, both intrinsic and extrinsic defects may be created. Extrinsic defects are the impurities that are incorporated in the films during processing and can be controlled by controlling the processing environment. Intrinsic defects can essentially be classified into two types : (a) defects such as Schottky defects that maintain stoichiometry and (b) defects that alter stoichiometry in the materials. Schottky defects in perovskite (ABO_3) ferroelectrics may be represented by a quasi-chemical reaction (in Kroger-Vink notation) as :

$$A_A + B_B + 3O_O \text{ ---------- } V_A^{''} + V_B^{''''} + 3V_O^{oo} + A_S + B_S + 3O_S \qquad (5.1)$$

where A_A, B_B, $3O_O$ represent respectively occupied A, B and O sites; $V_A^{''}$, $V_B^{''''}$, V_O^{oo} represent vacancies of A, B and O atoms; and A_S, B_S, $3O_S$ are the respective Schottky defects. A typical example of defects that alter the stoichiometry are vacancies that are formed due to the vaporization of one or more volatile components in multicomponent oxide materials. In the case of PZT, for example, a processing temperature of at least 600 °C is required to form the ferroelectric perovskite phase. However, the PbO component begins evaporating at temperatures as low as 550 °C, resulting in the formation of oxygen and lead vacancies as shown below [11]:

$$Pb_{Pb} + Ti_{Ti} + Zr_{Zr} + 3O_O \text{ ------- } xPbO + xV_{Pb}^{''} + xV_O^{oo} + (1-x)\,Pb_{Pb} + Ti_{Ti} + Zr_{Zr} + (1-x)\,O_O \qquad (5.2)$$

Studies on bulk PZT materials have also shown that 3+ ions which substitute for $(Zr,Ti)^{4+}$ (acceptors) also create vacancies [12]. This process can be represented as :

$$A_2O_3 \rightarrow 2A_{Ti,Zr}' + 3O_O + V_O^{00} \qquad (5.3)$$

where A_2O_3 is a trivalent oxide, and $A_{Ti,Zr}'$ represents a 3+ ion at $(Ti,Zt)^{4+}$ site. If the processing conditions are limited to high oxygen activities ($p_{O2} > 10^{-4}$ atm), then reduction can be eliminated as a source of oxygen vacancies [13]. Although such studies have not been carried out for thin films, it may be assumed that the loss of PbO and the presence of acceptors are the two major source of oxygen vacancies for thin films also. Since the vacancy concentrations resulting from PbO volatilization cab be very high, techniques for controlling the PbO activities during film formation are important for minimizing the defect concentrations. One common technique is to provide excess PbO during film formation to compensate the loss. However, precise control is often very difficult and chemical segregation problems at various structural interface sites such as grain boundaries are commonly observed.

In addition to compensating the PbO loss, another technique that can be used to lower the oxygen vacancy concentration is the introduction donor dopants. (e.g., Nb^{5+} at Zr or Ti sites). The consumption of oxygen vacancies can then be written as :

$$Nb_2O_5 + V_O^{oo} \rightarrow 2Nb_{Ti,Zr}^{o} + 5O_O \qquad (5.4)$$

where $Nb_{Ti,Zr}^{o}$ represents a Nb^{5+} ion at $(Ti,Zr)^{4+}$ site in PZT. In addition to compensating for the oxygen vacancies, the donor dopants can also compensate for any kind of acceptors present in the films as shown below :

$$A_2O + Nb_2O_5 \rightarrow 2A_{Pb}' + 2Nb_{Ti}^{o} + 6O_O \qquad (5.5)$$

The critical donor concentration above which the effects of donor dopants will become evident is dependent on the acceptor concentration and the nature of the heat treatment process. Although theoretical calculations of the critical donor concentration will require a knowledge of the defect reaction constants, an experimental study will yield valuable information.

Using this approach, Nb doped PZT (PNZT) films were fabricated by the sol-gel spin coating method on both Pt and RuO_2 electroded Si/SiO_2 substrates. The details of the solution coating process can be found elsewhere [14]. The films were annealed at 650 ^oC for 30 min in a controlled O_2 atmosphere. Fig. 5.1 depicts the fatigue and leakage current behavior of undoped PZT films with both Pt and RuO_2 electrodes. Fatigue of Pt can be seen from Fig.5.1(a) as the drastic decrease in the normalized polarization at around 10^7 switching cycles. This behavior has been modeled quantitatively and a fatigue equation has been derived as [1-4]:

$$P = P_o\,(An + 1)^m \qquad (5.6)$$

where P_o is the initial polarization, P is the polarization after n switching cycles, A is the piling constant and m is the decay constant. As shown in Fig. 5.1(a), no fatigue was found up to 10^{10} switching cycles for PZT capacitors with RuO_2 electrodes. However, increased leakage currents were observed when compared to Pt electroded PZT films at similar electric fields (Fig. 5.1(b)). The primary charge carriers responsible for electrical conductivity in PZT thin films are holes [15]. Since oxygen vacancies contribute to fatigue and holes contribute to leakage current in PZT films, it is expected that both fatigue and leakage current can be minimized by donor doping.

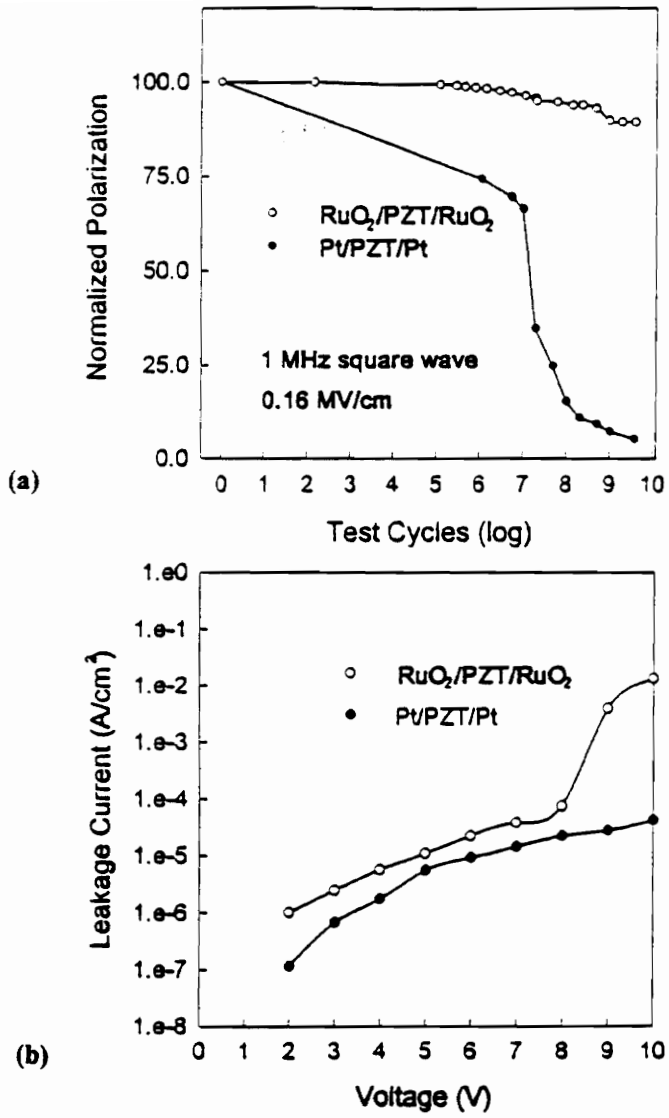

Figure 5.1 (a) Fatigue and (b) leakage current properties of undoped Pt/PZT and RuO_2/PZT capacitors

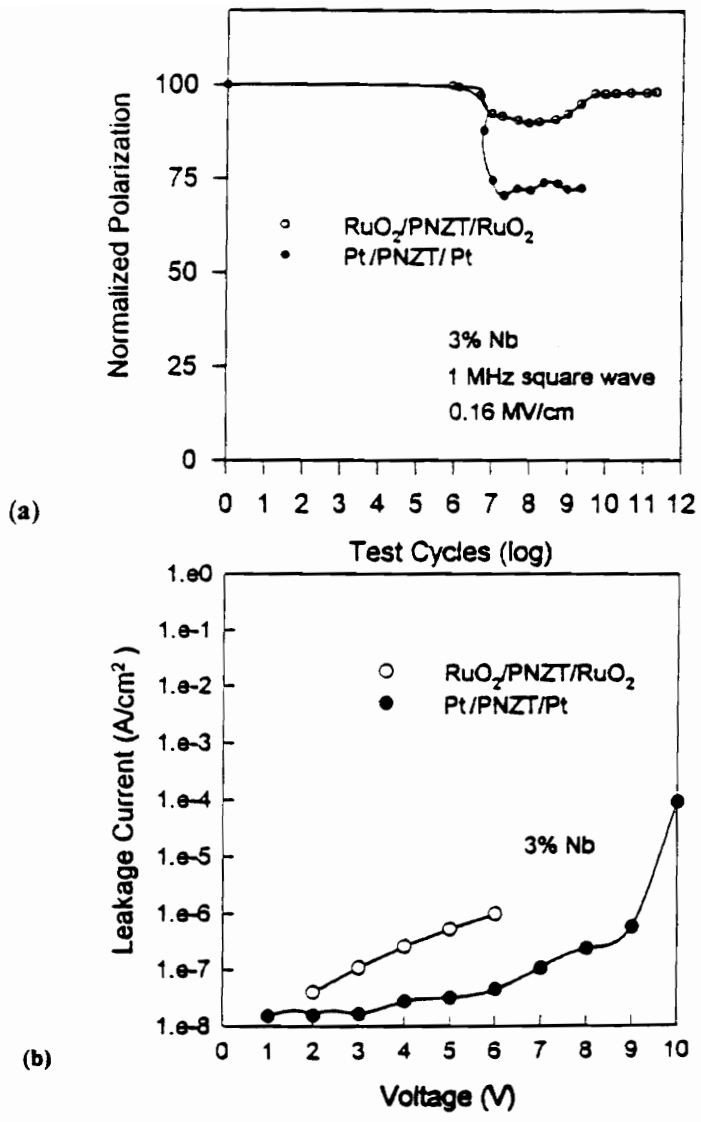

Figure 5.2 (a) Fatigue and (b) leakage current properties of Nb-doped Pt/PZT and RuO_2/PZT capacitors

Fig. 5.2 depicts the fatigue and leakage current behavior of 3 % Nb-doped PZT films for both RuO_2 and Pt electrodes. It is clear that the leakage currents of PNZT films are lower than those of PZT films for both Pt and RuO_2 electrodes(compare Fig. 5.2(b) and Fig. 5.1(b)). Furthermore, it can also be noticed that the fatigue behavior of Pt electroded PNZT films is far better than that of Pt electroded PZT films. In the case of RuO_2 electroded PNZT films, although they do not show overall fatigue, a slight decrease in polarization at around 10^7 switching cycles and recovery around 10^{10} was observed. At this point, we do not have an explanation for this behavior.

5.4 ALTERNATE MATERIALS

The minimization of intrinsic defect concentration may also be accomplished by choosing ferroelectric materials with inherently high defect formation energies or compounds that have no volatile components in their lattice. A careful analysis of the fatigue model reveals that it is *not* presence of points defects in the lattice of the ferroelectric as a whole that is responsible for fatigue, it is only the formation of defects in the *sublattice exhibiting ferroelectric properties* that causes fatigue. In the case of perovskite type ferroelectrics such as PZT, the entire lattice is responsible for the ferroelectric phenomena; the volatile PbO component is part of the perovskite lattice contributing to the polarization. The search for alternate ferroelectric materials was therefore also directed towards other structure type ferroelectrics that contain separate sublattices exhibiting polarization. The chosen ferroelectric material should also satisfy basic criteria such as room temperature stability, high curie temperature, large P_r and P_s, low E_c, low dielectric constant, low dielectric loss and finally, easy thin film processibility using standard VLSI processing techniques.

In addition to perovskite type ferroelectric oxides, other structure types that exist include : pyrochlore, tungsten bronze and layer-type bismuth compounds [14]. Using the criteria stated above and noting the presence/absence of any volatile component in the ferroelectric sublattice, all but a few oxides belonging to the $Sr_2Nb_2O_7$ (pyrochlore) family, $YMnO_3$ (perovskite) family and the layer-structure family were rejected. Although $Sr_2Nb_2O_7$ and $La_2Ti_2O_7$ are promising candidates for this application as a result of their high curie temperature, high spontaneous polarization and low coercive field values in the bulk form, we have had difficulty in obtaining the ferroelectric phase at low temperatures in the thin film processing of these oxides. The ferroelectric properties of $YMnO_3$ thin films deposited by sol-gel/spin coating was investigated in our laboratory. Although we have obtained the required ferroelectric phase and the desired stoichiometry, the films were found to be highly leaky which is possibly due to the multiple oxidation states of manganese.

In the layer-structure family, a large number of compounds of the general form $(Bi_2O_2)^{2+}$ $(M_{n-1}R_nO_{3n+1})^{2-}$, where M= Ba, Pb, Sr, Bi, K, or Na, n= 2,4, or 5 and R = Ti, Nb or Ta, are known to be ferroelectric [14-17]. These compounds have a pseudo-tetragonal symmetry and the structure is comprised of stacking of n perovskite-like units of nominal composition MRO_3 between Bi_2O_2 layers along the pseudo-tetragonal c-axis [14-17]. For our investigation, Pb-based (e.g., $PbBi_2Nb_2O_9$, $PbBi_2Ta_2O_9$) compounds were not considered because Pb atoms are a part of the perovskite sublattice responsible for spontaneous polarization in these materials. PbO volatility at high temperatures is therefore still a problem. The K and Na based oxides were eliminated because of their poor room temperature stability. Furthermore, compounds that contain Bi^{3+} ions in the perovskite-like units were also not considered because Bi_2O_3 could volatilize during high temperature processing and undesirable oxygen vacancies could be created in the

perovskite lattice leading to fatigue. For example, $Bi_4Ti_3O_{12}$ is a well characterized layer-structure ferroelectric oxide in both the bulk and thin film form. However, thin films of $Bi_4Ti_3O_{12}$ need to be processed at high temperatures (> 700 °C) to obtain the ferroelectric phase. At these temperatures, Bi_2O_3 (part of the perovskite-like units in this compound) is volatile, resulting in creation of oxygen vacancies in the material. This compound is known to show fatigue on Pt electrodes [18]. The investigation of possible fatigue free ferroelectrics was thus restricted to compounds that contained Ba or Sr in the M site with Ta or Nb in the R site and solid solutions of these compounds. The Sr based compounds have higher Curie temperatures than Ba based compounds and therefore, show the stronger domain interactions that are needed to overcome certain degradation problems such as retention.

Hence, in this work, we have chosen to investigate the thin film ferroelectric properties of compounds that are solid solutions of $SrBi_2Nb_2O_9$ and $SrBi_2Ta_2O_9$ i.e., $SrBi_2(Ta_xNb_{1-x})_2O_9$ with $0 < x < 1$ for fatigue free nonvolatile RAM applications. The crystal lattice of these compounds consists of two connected layers TaO_6 (or NbO_6) octahedrons (perovskite-like layers) alternating with Bi_2O_2 layers [16-19]. The Sr cations are located inside the perovskite-like layers in the space between the TaO_6/NbO_6 octahedrons. The perovskite-like units are continuous only in the planes perpendicular to the c-axis. Along the c-axis, they are broken in their continuity by the presence of Bi_2O_2 layers. However, spontaneous polarization has been observed along the c-axis also indicating that the (Bi_2O_2) layers participate in the cooperative phenomenon that is responsible for ferroelectricity in these materials [16]. Therefore, as observed in the case of $Bi_4Ti_3O_{12}$, the measured spontaneous polarization values in these materials, are expected to depend on the orientation of the unit cells.

In what follows, we describe the details of the thin film processing and characterization of the $SrBi_2(Ta_xNb_{1-x})_2O_9$ ferroelectric compounds. The newly emerging technique of pulsed laser deposition was used deposit thin films of these compounds. The films were characterized by x-ray diffraction (XRD) for their structure and orientation, scanning electron microscopy (SEM) for microstructure, electron spectroscopy for chemical analysis (ESCA) to determine composition, spectroscopic ellipsometry for their thickness and refractive index and the standardized RT66A ferroelectric tester (Radiant Technologies, Inc.) for ferroelectric properties.

Currently, sputtering, sol-gel, metalorganic decomposition (MOD), and metalorganic chemical vapor deposition are the most common deposition techniques in fabrication of ferroelectric thin films. Recently, there has been considerable interest in the technique of pulsed laser ablation for the deposition of ferroelectric thin films. This technique has become particularly attractive ever since it was used to successfully deposit *in situ* multicomponent high temperature superconducting oxide thin films [20]. It offers the advantages of multicomponent composition and phase control in complex oxides, *in-situ* epitaxial growth of thin films, compatibility with semiconductor technology and ability to deposit a wide variety of materials over a broad pressure regime [21].

In our study, thin films of $SrBi_2(Ta_xNb_{1-x})_2O_9$ (SBTN) were fabricated by pulsed laser deposition (PLD) on $Si/SiO_2/Pt$ substrates. A schematic of the pulsed laser deposition chamber is shown in Fig. 5.3. A Lambda Physik LPX 300 excimer laser utilizing KrF radiation (248 nm) was focused onto a rotating target of the starting material with a 50 cm UV graded plano-convex lens. The energy of the incoming beam was 600 mJ/pulse and the laser was operated at a frequency of 10 Hz. The beam was incident on the target at an angle of 45° ; the target was rotated at a speed of 10-13 rpm. The targets were processed by mixing $SrCO_3$, Bi_2O_3, Ta_2O_5 and Nb_2O_5 powders in stoichiometric

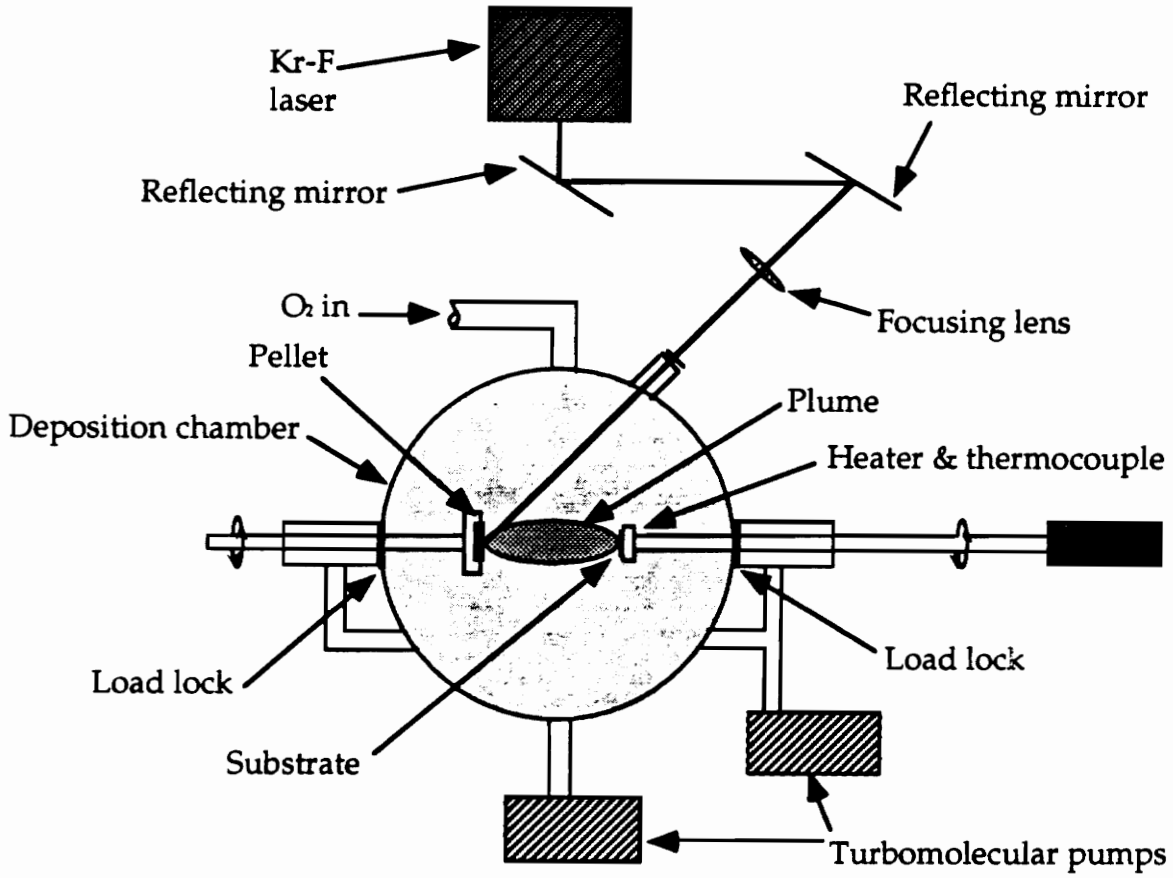

Figure 5.3 Schematic of the pulsed laser deposition chamber used for the growth of $SrBi_2Ta_2O_9$ thin films.

ratios by ball milling, followed by calcination of the mixed powders at 1000 °C, pressing of the calcined powders at 10000 psi in a circular die and sintering of the pressed pellets at 1100 °C for 1hr in a regular box furnace. Substrates of $Si/SiO_2/Ti/Pt$ were mounted onto a heated stainless steel block using thermally activated silver paint and placed parallel to the target at a distance of 4-5 cm. The substrate holder was also rotated to ensure uniform deposition across the wafer surface. The depositions were carried out under an oxygen ambient of 200 mTorr and a substrate temperature of 700 °C. Top electrodes of Pt were then deposited onto the samples through a shadow mask by RF sputtering to complete the device structure.

Variable angle spectroscopic ellipsometry was used to determine the thickness and the optical constants of the deposited films. The delta and psi coefficients were measured as a function of wavelength (200 nm-1000 nm) at angles of 70°, 75° and 80°. A Cauchy dispersion relation was assumed and used to calculate the thickness and refractive index of the films. The plots of refractive index and extinction coefficient as a function of wavelength for SBTN films with a composition of x = 0.8 are shown in Fig. 5.4(a) ; the thickness of the films was determined to be 200 nm. These refractive index values (e.g., 2.25 at 640 nm) were close to that observed for the corresponding bulk compound as shown in Fig. 5.4 (b) (2.45 at 640 nm) and thus indicate very good packing density of the films (~ 96 %). This was further confirmed by observing the surface microstructure of the films using scanning electron microscopy. Fig. 5.5 shows a typical SEM micrograph obtained from the films deposited at 700 °C. The films showed a fine-grained structure with very good packing density and almost negligible porosity. Typically, the grain size varied between 150-200 nm. The dense microstructure is probably due to the large average kinetic energy of the depositing species that is inherent in the pulsed laser deposition process and the high density of the target material that was used. The surface

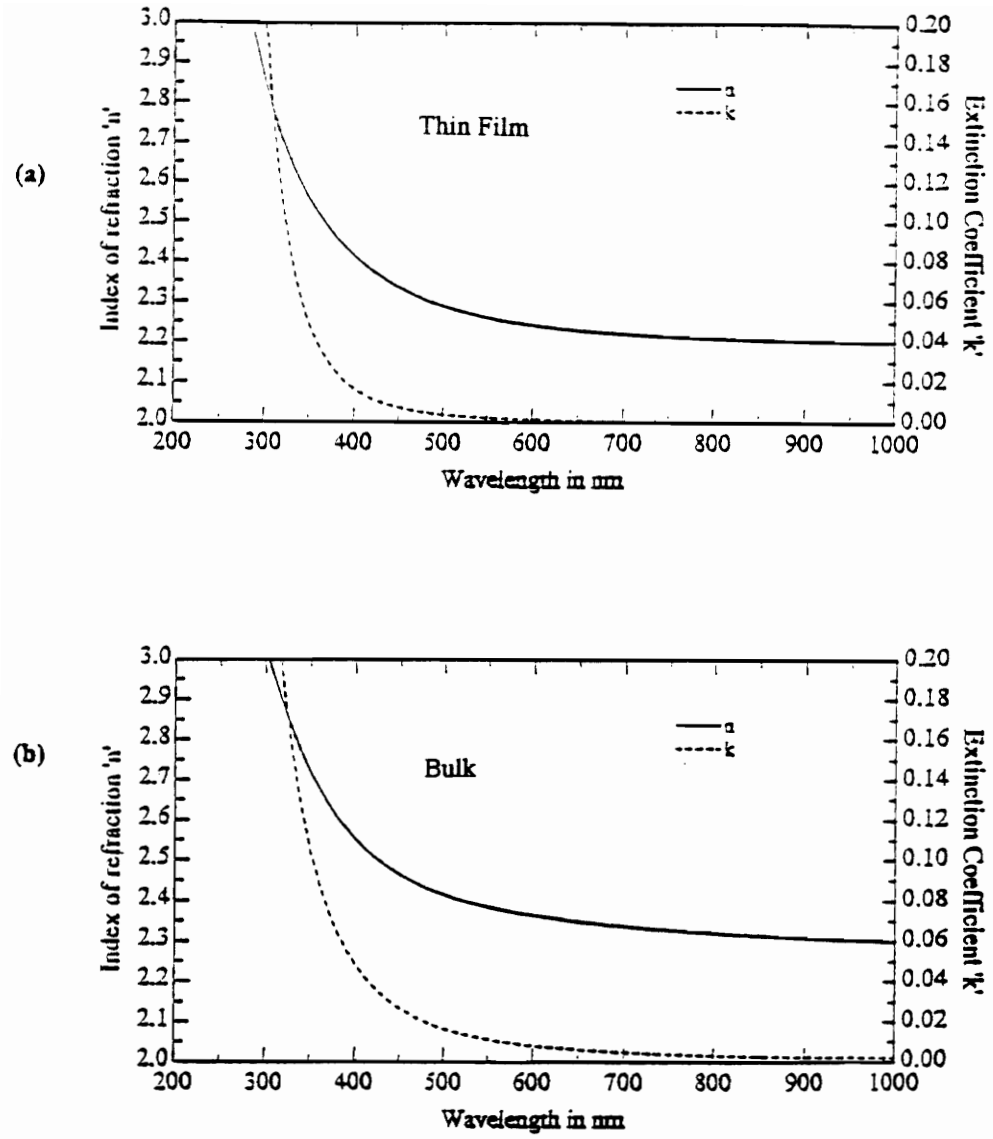

Figure 5.4 The plots of refractive index and extinction coefficient as a function of wavelength for SBTN films with a composition of x = 0.8. The measurements were done using spectroscopic ellipsometry.

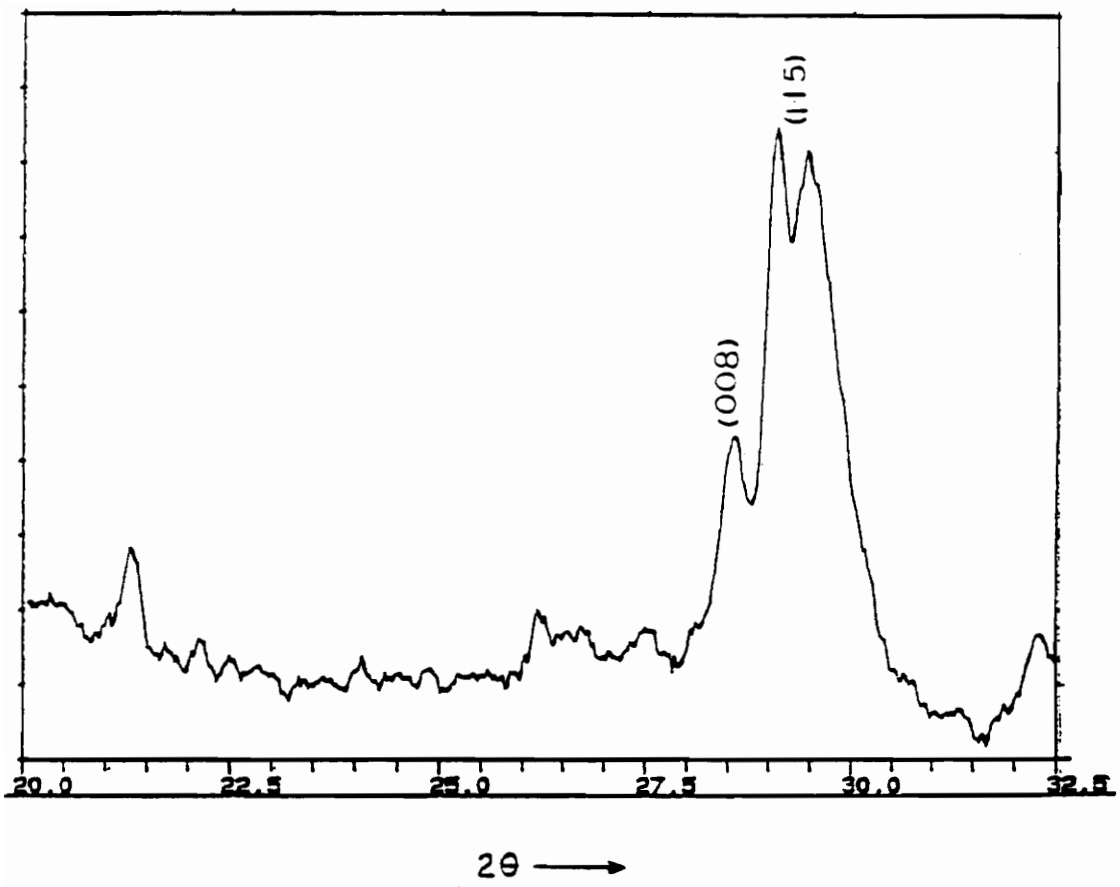

Figure 5.5 XRD pattern of $SrBi_2(Ta_{0.4}\ Nb_{0.6})_2O_9$ films grown on $Si/SiO_2/Ti/Pt$ at 700 °C by laser ablation

composition of the deposited films were analyzed using electron spectroscopy for chemical analysis and were found to be close to the desired stoichiometry.

X-ray diffraction studies were conducted to determine the phases that were formed under these deposition conditions. Fig. 5.6 shows the diffraction pattern obtained from these SBTN (x =0.8) films between 2θ angles of 20 and 30 degrees. Compounds with layered structure apparently have a face-centered orthorhombic unit cell. However, we have identified the diffraction peaks in our analysis by considering the unit cell to be body-centered tetragonal [16-18] which is true to a first approximation. As-deposited films show strong diffraction from the (115) and (00*l*) planes. The diffraction peak from the (115) planes is a doublet indicating that there is a strong distortion in the unit cell and a deviation from the actual symmetry. As mentioned earlier, the polarization in layered structure compounds are dependent on the orientation. It is reasonable to expect the polarization in any direction to be a vectorial sum of the polarizations along the a-axis (or b-axis) and the c-axis in the unit cells. It is well known that $Bi_3Ti_4O_{12}$ thin films (layered structure) exhibit larger spontaneous values when oriented along the a-axis compared to orientation along the c-axis [22]. However, the coercive field values along the a-axis are also very large compared to the c-axis orientation which makes the switching process in these materials difficult. In our case, since we have strong (115) and (00*l*) orientations, the resultant polarization is a combination of the c and a-axis polarizations. The polarization values could change with the degree of orientation.

The hysteresis properties of the films with were measured with Pt top electrodes using the standardized RT66A ferroelectric tester (Radiant Technologies). The top electrodes were deposited by RF sputtering using a shadow mask to an area of 2.1×10^{-4} cm^2. Figure 5.7(a) shows the hysteresis characteristics of as-deposited SBTN (x=0.8) films at an applied voltage of 5V. The hysteresis loop is well saturated at this voltage; a $2P_r$

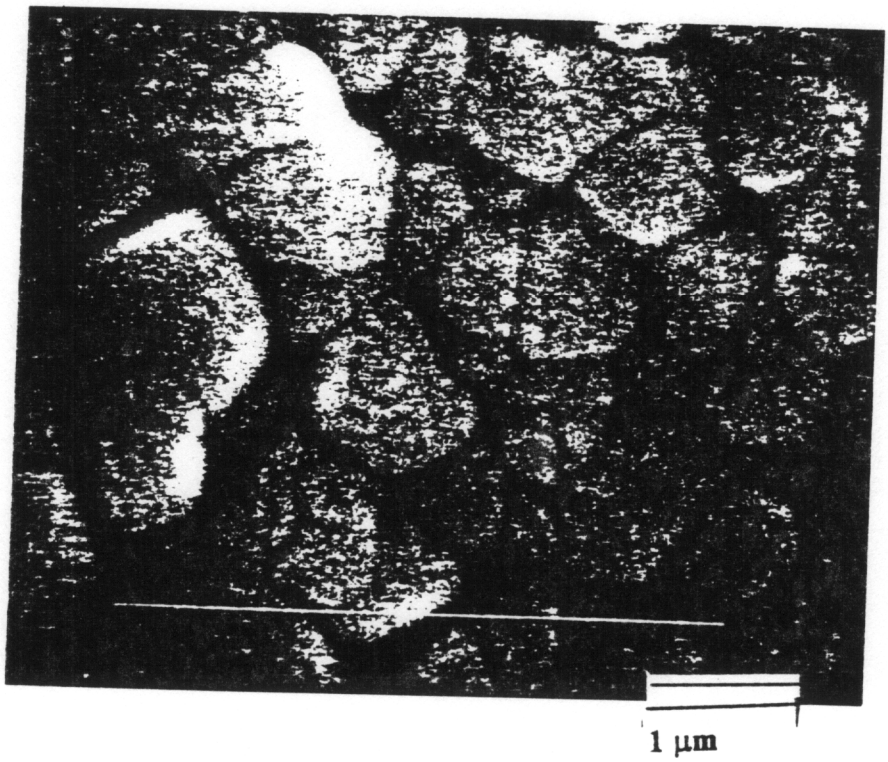

Figure 5.6 **Microstructure of SBTN films deposited using PLD at 700°C on Pt electrodes by laser ablation.**

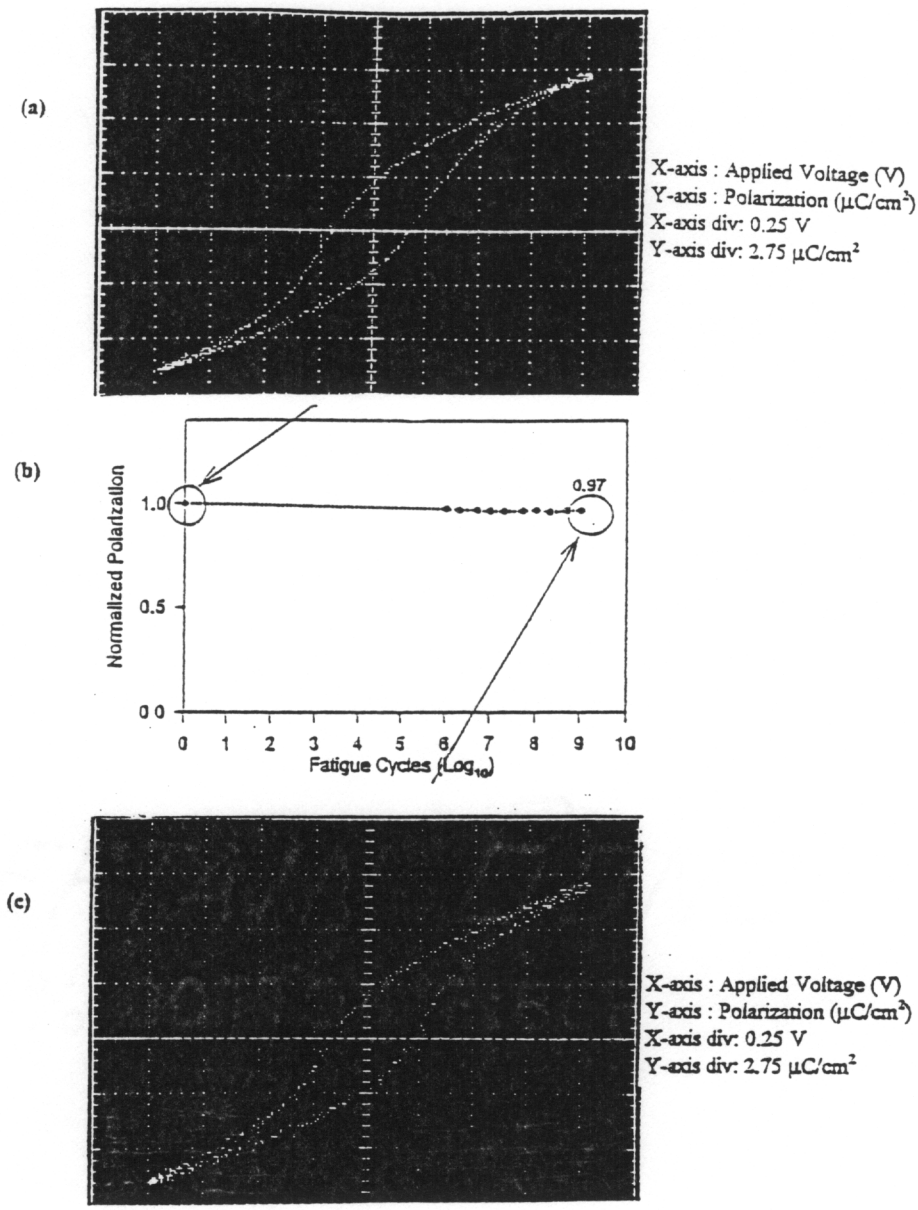

Figure 5.7 (a) Hysteresis properties of $SrBi_2(Ta_{0.4}\ Nb_{0.6})_2O_9$ films grown on $Si/SiO_2/Ti/Pt$ at 700 °C before fatigue cycling (b) the fatigue behavior of Pt/SBTN/Pt capacitors at 5V and 1 MHz (bipolar square wave) frequency (c) hysteresis characteristics of Pt/SBTN(x=0.8)/Pt films after fatigue cycling

value of 22 $\mu C/cm^2$ and an E_c value close to 60 kV/cm were obtained. These values are well within the requirements for nonvolatile memory device applications. The fatigue test on the films were performed using a 5V square wave a.c. signal at a frequency of 1 MHz input through a pulse generator. Figure 5.7(b) shows the results of the fatigue study performed up to 10^9 cycles. The films do not show any significant fatigue up to this cycling; there is only a 3 % loss in polarization after 10^9 cycles. This was confirmed by measuring the hysteresis properties of the films after fatigue as shown in Figure 5.7(c); the hysteresis properties of the films before and after fatigue cycling were similar. The leakage current density values for these films were measured as a function of applied voltage. At an applied voltage of 3V, the films showed a leakage current density value less than 10^{-7} A/cm^2. The measured resistivity of films were typically of the order of 5×10^{-12} ohm-cm.

5.5 SUMMARY

Based on a quantitative fatigue model, it has been shown that fatigue can be minimized by controlling the defect density. The control the defect density in ferroelectric thin film capacitors has been achieved in two ways : (a) addition of donor dopants to compensate for the oxygen vacancies in oxide ferroelectric films. It has been shown that Nb donor dopant additions to PZT films can reduce both the fatigue and leakage current on Pt and RuO_2 electrodes, respectively. (b) utilizing ferroelectric materials that have a low intrinsic defect concentration. On this basis, several ferroelectric oxides belonging to the pyrochlore, layered structure and tungsten bronze families were considered for possible memory applications. It was found that $SrBi_2(Ta_xNb_{1-x})_2O_9$ family of layered structure compounds are very good candidates for fatigue free ferroelectric thin film applications. The fundamental criterion for the selection of this family of compounds was

that fact the lack of any volatile species which could cause the formation of intrinsic defects such as oxygen vacancies in the ferroelectric sublattice that is responsible for the spontaneous polarization. High quality stoichiometric thin films of these compounds with a dense microstructure have been deposited on platinized Si/SiO_2 wafers using laser ablation. The films showed excellent hysteresis characteristics and no fatigue up to 10^9 cycles. For example, SBTN films with composition of x =0.8 , showed 2Pr values close to 22 $\mu C/cm^2$, a coercive field of 65 kV/cm and a leakage current density of less 10^{-7} A/cm^2 at 3V.

5.6 REFERENCES

1. I.K. Yoo and S.B. Desu, Mat. Sci. and Eng., B13, (1992), 319.

2. I.K. Yoo and S.B. Desu, Phys. Stat. Sol., a133, (1992), 565.

3. I.K. Yoo and S.B. Desu, J. Int. Mat. Sys., 4, (1993), 490.

4. S.B. Desu and I.K. Yoo, J. Electrochem. Soc., 140, (1993), L133.

5. D.P. Vijay and S.B. Desu, J. Electrochem. Soc, 140, (1993), 2640.

6. B. Jaffe, W. Cook and H. Jaffe, Piezoceramics, Academic Press, New York, 1971, pp. 10-13

7. I.S. Zheludev, Physics of Crystalline Dielectrics, Electrical Properties, Plenum, New York, Vol.2, 1971, pp. 474-490.

8. A.Y. Kudzin, T.U. Panchenko and S.P. Yudin, Sov.Phys. Solid State, 16(8), (1975), 1589.

9. H.M. Duiker, P.D. Beale, J.F. Scott, C.A. Paz de Araujo, B.M. Melnick, J.D. Cuchlaro and L.D. McMillan, J.Appl. Phys., 68(11), (1990), 5783.

10. W.H. Shepherd, Mat.Res.Soc. Symp., 200, (1990), 277.

11. S.B. Desu, D.P. Vijay and I.K. Yoo, Mat. Res. Soc. Symp., 335, (1994), 53.

12. J.J. Dih and R.M. Fulrath, J.Am. Ceram. Soc., 61, (1978), 448.

13. C.K. Kwok and S.B. Desu, Mat. Res. Soc. Symp. Proc., 243, 91992), 393.

14. G. Yi and M. Sayer, *Ceram. Bull.*, 70(7), 1173 (1991).

15. V.V. Priedsky, V.I. Shishkovsky and V.V. Klimov, Ferroelectrics, 17, (1978), 465.

16. E.C. SubbaRao, J. Phys. Chem. Solids, 23, (1962), 665.

17. B. Aurivillius, Arkiv Kemi, 1[54], (1949), 463.

18. E.C. SubbaRao, J. Chem. Phys., 34 [2], (1961), 695.

19. G.A. Smolenski, V.A. Isupov and A.I. Agranovskaya, Fiz Tverdogo Tela, 3[3], (1961), 895.

20. P.C. Joshi and S.B. Krupanidhi, J. Appl. Phys., 72(12), (1992), 5827.

21. D. Dijkkamp, T. Venkatesan, X.D. Wu, S.A. Saheen, N. Jisrawi, Y.H. Min-Lee, W.L. Mclean and M. Croft, Appl. Phys. Lett., 51, (1987), 619.

22. N. Maffei and S.B. Krupanidhi, J. Appl. Phys, 72(8), (1992), 3617.

This paper titled

"Formation and Properties of $SrBi_2Ta_2O_9$ Thin Films"

has been submitted to

Physica Status Solidi

(1995)

The co-authors in this manuscript are Masaya Nagata, Xubai Zhang and Dr. S.B. Desu. Xubai Zhang fabricated the bulk targets for the laser ablation process, Masaya Nagata characterized the films for their composition using x-ray photoelectron spectroscopy and Dr. S.B. Desu provided useful insights into the analysis and presentation of the data. My contributions included conducting the experiments, characterization, analysis of the data and conclusions. The authors would also like to gratefully acknowledge the useful suggestions and discussions provided by Dr. W.T. Reynolds, Jr. during the course of this work.

Chapter 6 : Formation and Properties of $SrBi_2Ta_2O_9$ Thin Films

6.1 ABSTRACT

Layered structure $SrBi_2Ta_2O_9$ thin films were grown on $Pt/Ti/Si/SiO_2$ substrates by laser ablation. The films were deposited at temperatures ranging from 500 ^oC to 750 ^oC and characterized for their phase formation, microstructure, composition and ferroelectric properties. Although crystalline phase formation was observed at temperatures as low as 500 ^oC, well defined saturated hysteresis loops were observed only in films deposited at temperatures of 700 ^oC or above. The transition in ferroelectric properties between 650 and 700 ^oC was associated with a change in orientation and grain size. The orientation of the films changed from highly c-axis oriented at 650 ^oC to randomly polycrystalline at 700 ^oC, while the grain size of the films increased from an average value of 80 nm (at 650 ^oC) to 160 nm (at 700 ^oC). An understanding of process-structure relationships is required in order to fabricate high quality films at lower temperatures.

6.2 INTRODUCTION

$SrBi_2(Ta_xNb_{1-x})_2O_9$, $0<x<1$ (SBTN) solid solutions belong to the Aurivillus family of bismuth layered structure ferroelectric compounds of the general formula $(Bi_2O_2)^{2+}$ $(M_{n-1}R_nO_{3n+1})^{2-}$ where M= Ba, Pb, Sr, Bi, K, or Na, n= 2,4, or 5 and R = Ti, Nb or Ta. [1-3]. These compounds have pseudo-tetragonal symmetry and the structure is comprised of n perovskite-like units of nominal composition MRO_3 between Bi_2O_2 layers along the pseudo-tetragonal c-axis [1-3]. These materials may be good candidates for nonvolatile

memory applications [4-7]. Currently, $PbZr_xTi_{1-x}O_3$ (PZT) has been considered to be the promising material for ferroelectric random access memory (FRAM) applications. However, one of the major disadvantages in using PZT films for FRAM applications is its high dielectric constant. Additionally, PZT films are known to suffer from significant polarization loss with increasing switching cycles (fatigue) on Pt electrodes [8,9]. In contrast, bismuth layered structure ferroelectric oxides such as $SrBi_2Ta_2O_9$-$SrBi_2Nb_2O_9$ solid solutions exhibit a low dielectric constant (~300 at 10 kHz), almost no fatigue on Pt electrodes and very low leakage currents (~ 10^{-8} A/cm^2 at 100 kV/cm) [4,5].

The high temperatures (~700°C) required for processing of these materials, however, is a major limitation for VLSI fabrication. There are few reports on the thin film processing of SBTN solid solutions for memory applications. Araujo et al .[4] and Ammanuma et al. [6] have used metalorganic decomposition (MOD). They found an annealing temperature of 800 °C was required to obtain good ferroelectric properties on $Pt/Ti/SiO_2/Si$ substrates. Desu and Li [7] have obtained good ferroelectric properties processed by MOD at 750 °C. Recently, Desu and Vijay [5] have reported fabrication by laser ablation. The inherently high energy available in this process permitted them to reduce temperatures to 700 °C. In all these studies, the crystalline phase formation occurred at temperatures far lower than that at which good ferroelectric properties were observed. For VLSI fabrication, it is important to understand the reasons for this in order to reduce the final processing temperature for device fabrication. In PZT thin films, the temperature and kinetics of the metastable pyrochlore phase to perovskite phase transformation are the most crucial factors determining final processing temperatures [12-14]. In layered structure SBTN thin films, no such intermediate phases have yet been observed. XRD studies on MOD films have shown the onset of crystalline phase formation to be as low as 550-600 °C [6-7] and the temperature of complete phase formation to be

around 700 °C. The fact that processing temperatures to obtain good ferroelectric properties are at least 50-100 °C higher than the complete phase formation temperature indicates that complete crystallinity alone is not a sufficient condition for obtaining good ferroelectric properties. Some other possible factors are : (a) stoichiometry of the deposited films, (b) their crystallographic orientation, (c) size effects and (d) the presence of defects structures at lower processing temperatures. In this work, we investigated the effect of these parameters on the ferroelectric properties of SBTN thin films.

6.3 EXPERIMENTAL PROCEDURE

The studies were conducted by depositing the films at various deposition temperatures onto $Pt/Ti/SiO_2/Si$ substrates using the laser ablation technique. Bulk pellets of SBT were made by conventional ceramic powder processing and used as targets for laser ablation. A Lambda Physik LPX 300 excimer laser utilizing KrF radiation (248 nm) was focused onto the rotating target with a 50 cm UV graded plano-convex lens. The energy of the incoming beam was 600 mJ/pulse and the laser was operated at a frequency of 10 Hz. The depositions were carried out under oxygen at 200 mTorr and at substrate temperatures ranging from 500 °C to 750 °C in 50 °C intervals. Top electrodes of Pt were then deposited onto the samples by RF sputtering (dot area : 2×10^{-4} cm^2). As-deposited films were characterized for thickness by variable angle spectroscopic ellipsometry, for phase formation by x-ray diffraction (XRD), for microstructure by scanning electron microscopy (SEM), for surface composition by electron spectroscopy for chemical analysis (ESCA) and for their ferroelectric properties using a Sawyer-Tower circuit.

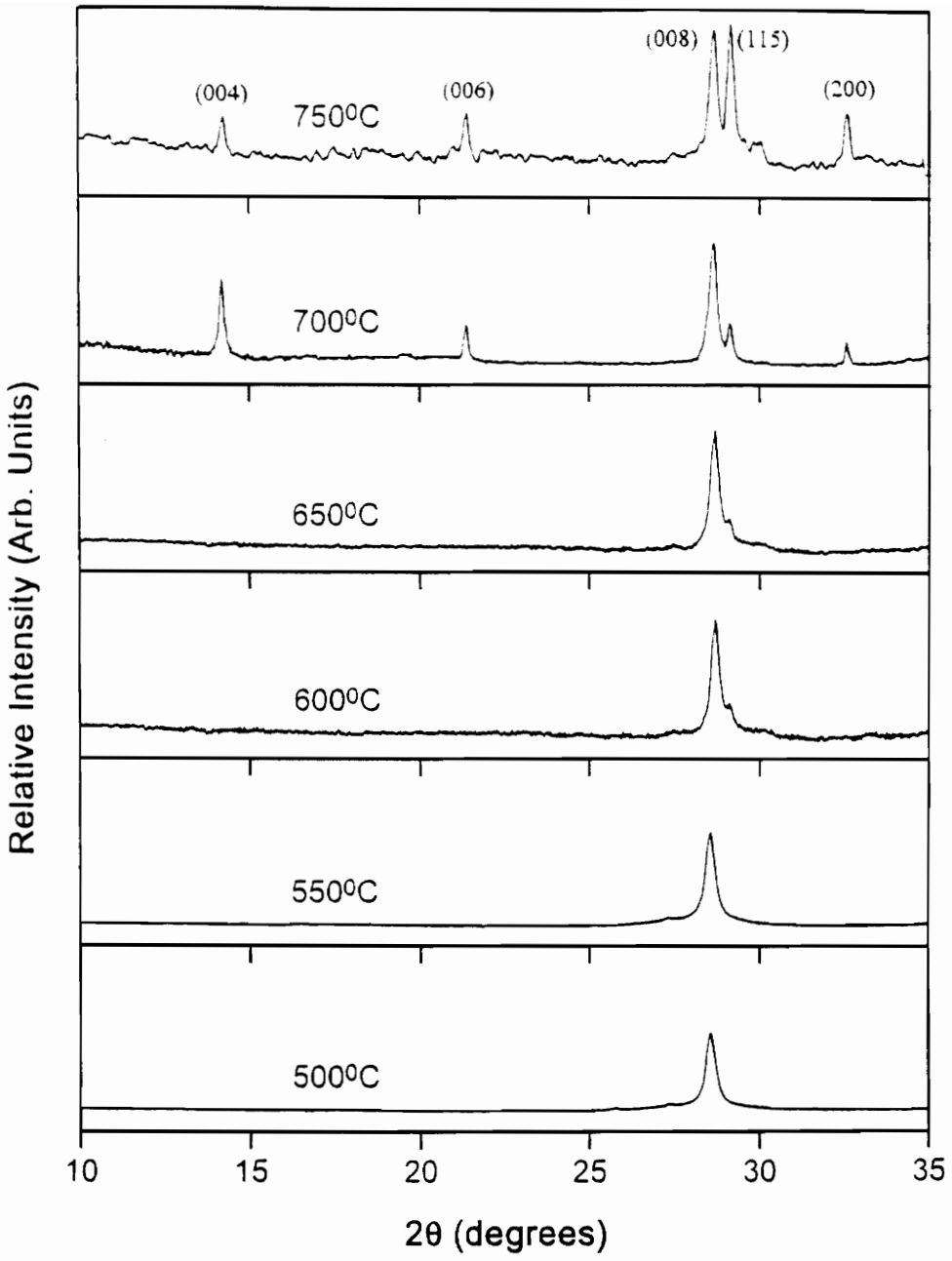

Figure 6.1 **XRD pattern of $SrBi_2Ta_2O_9$ films as a function of deposition temperature.**

6.4 RESULTS AND DISCUSSION

Each film was around 200 nm thick. Fig. 6.1 shows the XRD patterns of the films as a function of deposition temperature. In the deposition temperature range between 500°C and 650 °C, a strong diffraction peak can be observed at a 2θ value close to 28.5°. Analysis showed this peak to coincide with the diffraction peak from the (008) crystal planes of the pseudo tetragonal SBT films. However, no other peaks belonging to the (00l) family of crystal planes (e.g., (004), (006) etc.) were detected. At temperatures of 600°C and 650°C, a low intensity peak belonging to (115) planes was observed in addition to the peak at 28.5°. At temperatures of 700 °C and 750 °C, we observe sharp peaks from the SBT phase. It may be possible that the high intensity peak at 2θ = 28.5°, up to a deposition temperature of 650 °C, is a result of diffraction from crystal planes belonging to one or more other phases such as Sr-Ta-O, Bi-Ta-O and Bi_2O_3 in addition to SBT. However, if this is the case, it should be possible to observe multiple peaks belonging to the different phases. Clearly, no such peaks are visible in the data shown in Fig. 6.1. The other possibility is that up to deposition temperatures of 650 °C, there is some kind of a nanocrystalline compositional disorder along certain *a-b* planes in the films. If this is the case, either no diffraction peaks or diffraction peaks of only very low intensity will be visible from these planes even though they are oriented parallel to the film surface. We are currently investigating this possibility.

Composition studies conducted using ESCA did not show any deviation from the overall stoichiometry on the surface of SBT films. The standardless ratio method was used for quantitative analysis of the composition. Throughout the deposition temperature range between 500 and 750 °C, the overall surface composition of the films was close to desired stoichiometry. A plot of the measured bismuth concentration as a function of deposition

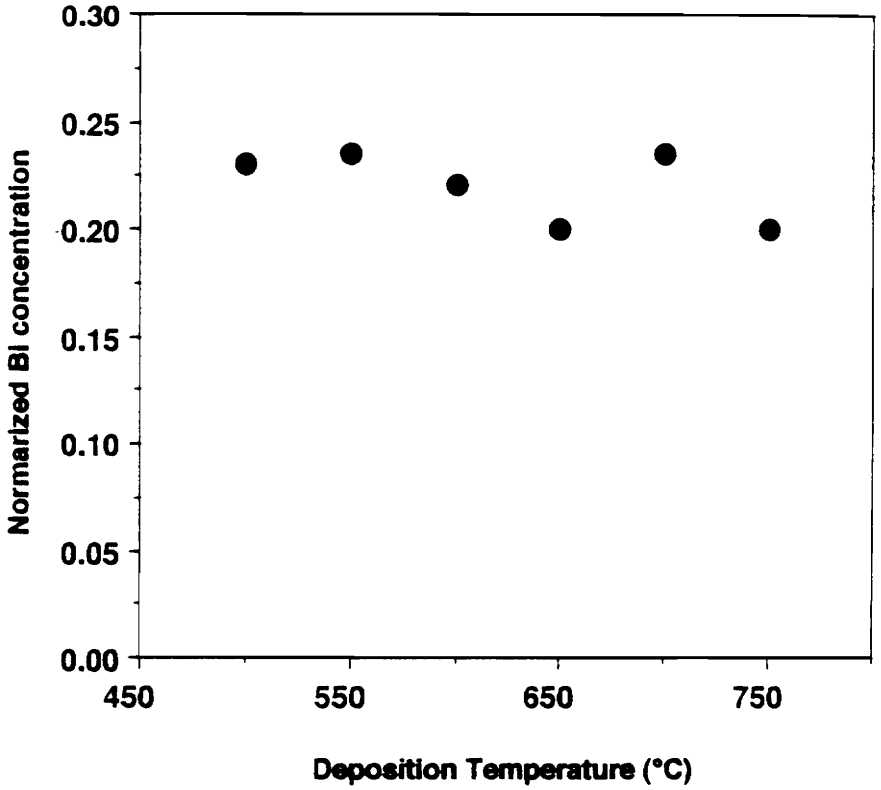

Figure 6.2 Bi concentration of $SrBi_2Ta_2O_9$ films as a function of deposition temperature.

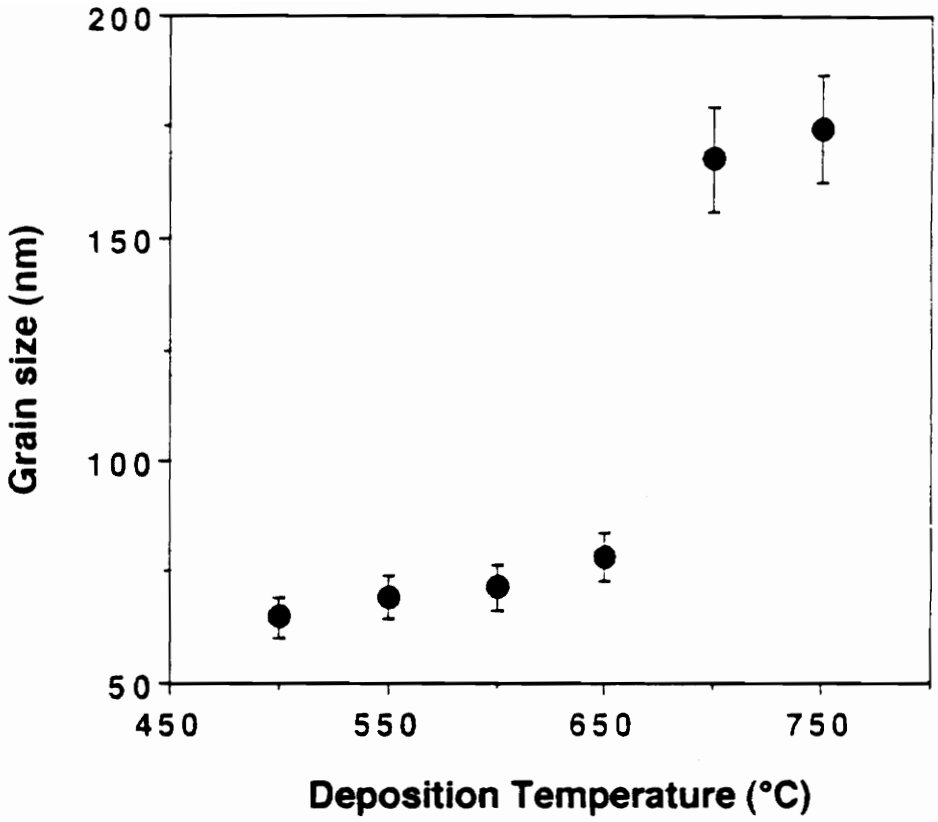

Figure 6.3 (a) Grain size of $SrBi_2Ta_2O_9$ on $Pt/Ti/SiO_2/Si$ substrates. Results were taken from SEM photographs using the linear intercept method.

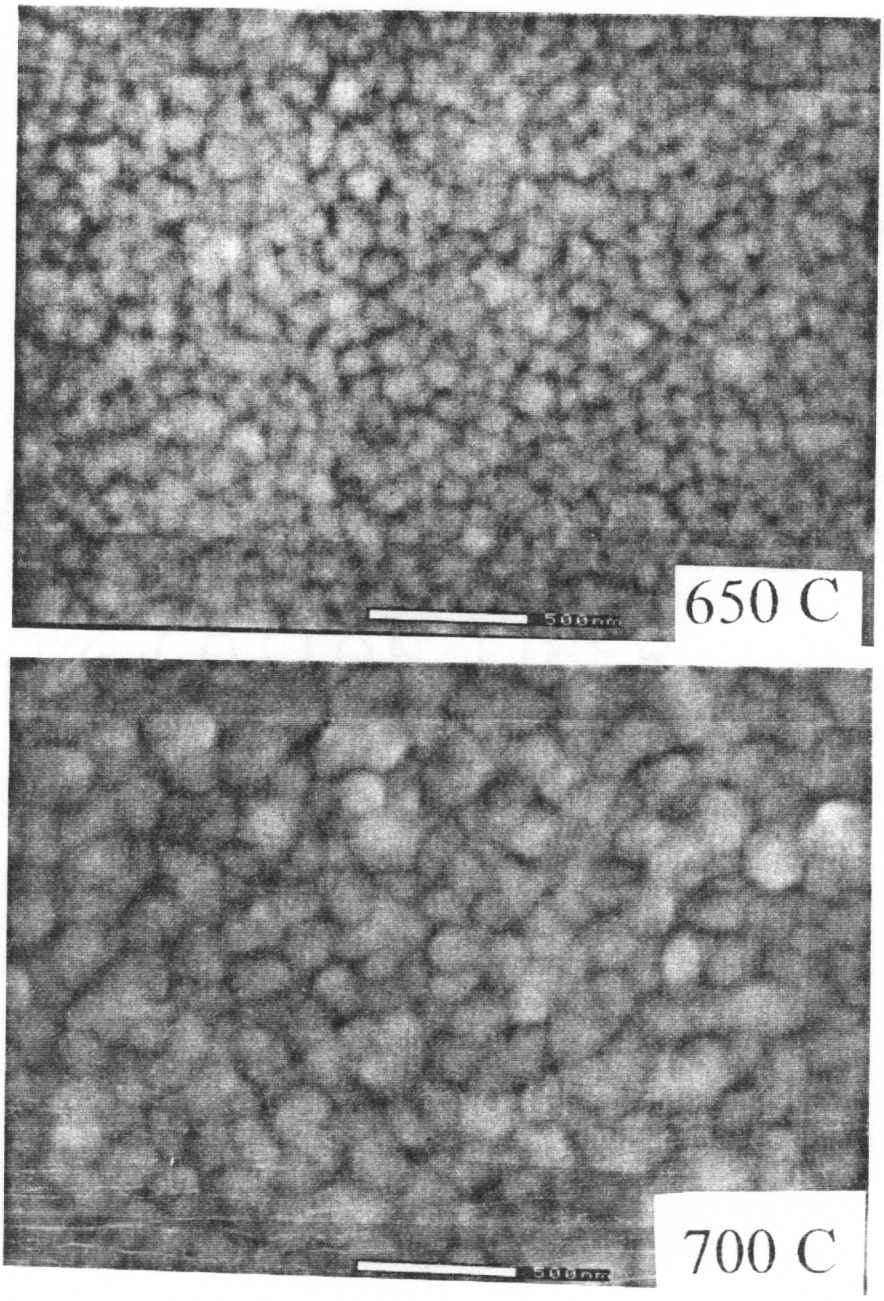

Figure 6.3 (b) the SEM micrographs of $SrBi_2Ta_2O_9$ film fabricated at deposition temperatures of 650 ^oC and 700 ^oC.

temperature is shown in Fig. 6.2. The ESCA data, however, can only provide the overall composition of the film surface and cannot discern any local compositional inhomogenities.

Figure 6.3(a) shows grain size of SBT films as a function of temperature. Results were taken from SEM photographs using the linear intercept method. In the deposition temperature range between 500 and 650 ^{o}C, all the films showed a uniform grain size of around 80 nm. However, in the temperature range between 650 ^{o}C and 700 ^{o}C, a twofold increase in grain size was observed (Fig.6.3(b)). Although we do not have an explanation for this change in grain size at this point in time, we certainly can eliminate the possibility of thickness effects since the ellipsometry results have shown the thickness of all the films to be around 200 nm.

The hysteresis properties of the films were measured using a Sawyer-Tower circuit at a frequency of 100 Hz and an applied voltage of 5V. Fig. 6.4 shows the measured ferroelectric properties as a function of deposition temperature. Films deposited at 500 and 550 ^{o}C did not exhibit any hysteresis behavior. Although hysteresis was observed at deposition temperatures of 600 and 650 ^{o}C, the loops were poorly saturated. However, at deposition temperatures of 700 ^{o}C and 750 ^{o}C, well defined hysteresis properties were obtained. The films exhibited a $2P_r$ value of nearly 10 $\mu C/cm^2$ and a coercive field of 60 kV/cm. Additionally, we found excellent fatigue endurance; after 10^{11} switching cycles using a 5V, 0.5 MHz square wave, the switchable polarization decreased by a factor of only 5 %.

It is clear that good ferroelectric properties at 700 ^{o}C are caused by several factors. XRD results indicate a change in orientation from possibly c-axis dominated to polycrystalline in the temperature range between 650 and 700 ^{o}C. We have demonstrated recently that SBT films oriented completely with the c-axis perpendicular to the plane of

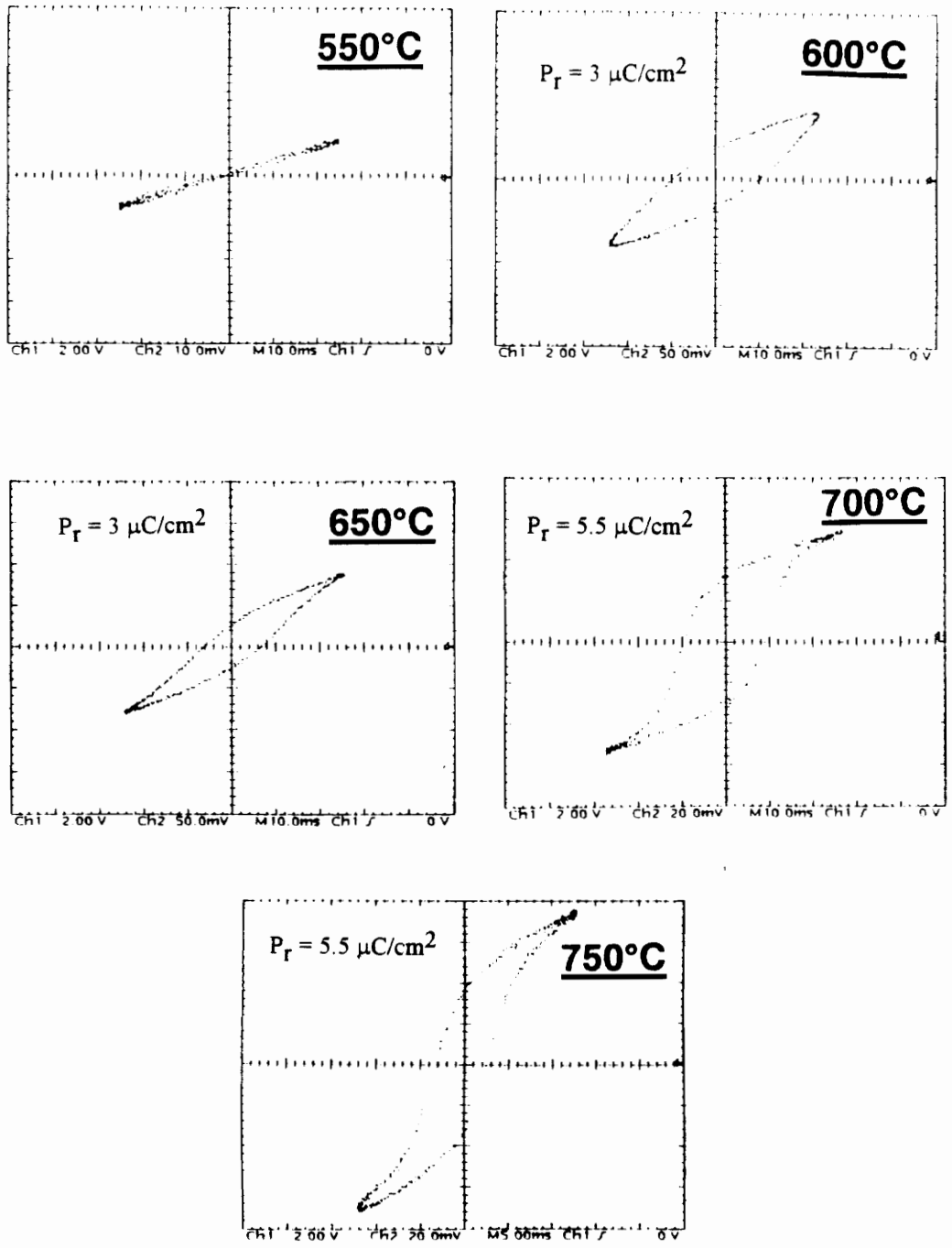

Figure 6.4 **Hysteresis properties measured at a frequency of 100Hz and an applied voltage of 5V for 200nm thick $SrBi_2Ta_2O_9$ films fabricated at various deposition temperature.**

substrate show little or no polarization [15]. However, Fig. 6.1 shows a diffraction peak of relatively low intensity from the (115) planes at deposition temperatures of 600 and 650 ^{o}C. The hysteresis loops observed from the films deposited at these temperatures can be explained by the polarization components from this crystallographic plane. The absence of peaks other than from (008) planes at temperatures below 600 ^{o}C explains the absence of ferroelectric properties in the corresponding films. Nonetheless, the fact that the hysteresis loops are well defined and saturated only at temperatures at or above 700 ^{o}C suggests that there are additional effects determining the properties of these materials. One of these effects could be grain size. The transition in ferroelectric properties between 650 and 700 ^{o}C is concurrent with an increase in the grain size from 80 to 160 nm. Because the ferroelectric properties are due to a cooperative phenomenon, it has been argued that materials below a certain critical size cannot exhibit ferroelectric properties [16]. Additionally, this critical size is dependent on the property and the material itself. The significance of size effects in controlling ferroelectric properties has been documented for fine grained ceramics, finely dispersed powders and small crystals [17-20]. Unlike perovskite ferroelectrics such as PZT and $BaTiO_3$, SBT is a layered structure two dimensional ferroelectric material. Therefore, the critical grain size for ferroelectric properties is expected to be higher than in these materials than in three-dimensional ferroelectrics such as PZT. These results suggest that to obtain good ferroelectric properties at lower processing temperatures, it may suffice to devise processing methods that can provide a grain size above the observed critical value (160 nm) at lower temperatures. Some of these methods may include the addition of dopants, addition of excess Bi, seeding layers etc.

6.5 SUMMARY

In summary, we have investigated the processing temperature effects on the ferroelectric properties of layered structure $SrBi_2Ta_2O_9$ thin films grown by laser ablation. Up to deposition temperatures of 550 ^oC, the films were completely c-axis oriented; no hysteresis properties were detected in these films. At deposition temperatures of 600 and 650 ^oC, additional diffraction peaks from the (115) planes were also observed. We have attributed the observed ferroelectric properties (albeit poorly saturated) in these films to be a result of the polarization from these (115) planes. SBT films oriented completely with the c-axis perpendicular to the plane of substrate are not known to show any polarization. Good ferroelectric properties were observed only in films deposited above 700 ^oC. There was an observed transition in ferroelectric properties from poorly saturated hysteresis loops in the films deposited at 650 ^oC to well defined and saturated hysteresis properties in 700 ^oC deposited films. The reason for this transition in ferroelectric properties has been ascribed to grain size effects; the grain size increased from an average value of 80 nm to 160 nm between 650 and 700 ^oC. These results suggest that to obtain good ferroelectric properties at lower processing temperatures, it may suffice to devise processing methods that can provide a grain size above the observed critical value (160 nm) at lower temperatures.

6.6 REFERENCES

1. B. Aurivillus, Arkiv Kemi, 1 (1949), 463.

2. G.A. Smolenski, V.A. Isupov and A.I. Agranovskaya, Fiz Tverdogo Tela, 3, (1961), 895.

3. E.C. Subba Rao, J. Chem. Phys., 34, (1961), 695.

4. C.A. Paz de Araujo, J.D. Cuchlaro, L.D. McMillan, M.C. Scott, J.F. Scott, Nature, 374, (1995), 627.

5. S.B. Desu and D.P. Vijay, Mat. Sci. Eng. (B), in press, (1995).

6. K. Ammanuma, T. Hase and Y. Miyasaki, Appl. Phys. Lett., 66(2), (1995), 221.

7. S.B. Desu and T.K. Li, Mat. Sci. Eng. (B), in press, (1995).

8. C.E. Land, J. Am. Ceram. Soc. 71, (1988), 905

9. Katsuhiko Aoki, Yukio Fukuda and Akitoshi Nishimura, J. Appl. Phys. 32, (1993) 4147

10. D.P. Vijay and S.B. Desu, J. Electrochem. Soc., 140, (1993), 2640.

11. J.T. Cheung, Proceedings of the 4th International Symposium on Integrated Ferroelectrics, (1992), 158.

12. R. Roy, K. Etzold and J. Cuomo, Mat. Res. Soc. Symp. Proc., 200, (1990), 141.

13. A. Okada, J. Appl. Phys., 49(8), (1978), 4495.

14. C.K. Kwok and S.B. Desu, Ceramic Transactions, 25, (1992), 73-84.

15. S.B. Desu, D.P. Vijay and M. Nagata, work in progress, (1995).

16. F.P. Jona and G. Shirane, "Ferroelectric Crystals", Pergamon, (1962).

17. S.B. Desu, C.H. Peng, L. Kammerdiner and P.J. Schuele, Mat.Res. Soc.Symp. Proc., 200, (1990), 319.

18. M. Anliker, H.R. Brugger and W. Kanzig, Helv. Phys. Acta., 27, (1954), 99.

19. G. Arlt, D. Hennings and G. De With, J. Appl. Phys., 58, (1985), 1619.

20. W.J. Mertz, J. Appl. Phys., 27, (1956), 938.

This paper titled

"Oriented Growth of $SrBi_2Ta_2O_9$ Ferroelectric Thin Films on Platinum Electrodes"

has been accepted in

Applied Physics Letters

(1995)

The co-authors in this manuscript were Dr. Baoping He, Xubai Zhang and Dr. S.B. Desu. Dr. Baoping He conducted all of the x-ray diffraction analysis and pole figure analysis. Xubai Zhang fabricated the targets for the laser ablation process. The authors also wish to gratefully acknowledge the useful insights provided by Dr. R.W. Hendricks into the analysis of the data in this work. My main contribution was in developing the basis for this work. Additionally, I also conducted the deposition processes, electrical characterization, and analysis of the data.

Chapter 7 : Oriented Growth of $SrBi_2Ta_2O_9$ Ferroelectric Thin Films

7.1 ABSTRACT

Recent reports on the identification of novel bismuth layered perovskite (e.g., $SrBi_2Ta_2O_9$) ferroelectrics has spurred renewed interest in ferroelectric materials for destructive read out (DRO) nonvolatile memory applications [1-4]. $SrBi_2Ta_2O_9$ thin films show almost no fatigue up to 10^{12} switching cycles, very good retention properties and low leakage current densities on Pt electrodes. Structurally, the bismuth layered perovskite ferroelectrics are highly anisotropic in nature and therefore the ferroelectric properties (spontaneous polarization, coercive field, dielectric constant etc.) are strongly dependent on the orientation of the films with respect to the underlying substrate materials. We have identified a novel device structure wherein the layered oxide ferroelectric thin films can be crystallographically oriented along different directions relative to the underlying platinum electrode in the capacitor structure. This permits the tailoring of the ferroelectric properties of the capacitor structure and has important technological implications in device application of these materials. Additionally, we also report for the first time, the ferroelectric properties of c-axis oriented ferroelectric $SrBi_2Ta_2O_9$ thin films. $Pt/SrBi_2Ta_2O_9/Pt$ capacitors were grown on single crystal MgO (and/or $SrTiO_3$) substrates using pulsed laser ablation. These substrates provide the necessary template for (100) texture in platinum due to their close lattice matching . This in turn facilitates the c-axis orientation in the ferroelectric films. The degree of orientation in the layered structure ferroelectric film was systematically varied from highly c-axis oriented to random polycrystalline by varying the growth conditions of the bottom metal electrode. The polarization and coercive field values were found to decrease with increasing degree of c-

axis orientation; while the randomly oriented films exhibited a remnant polarization of 5 $\mu C/cm^2$, a coercive field of 70 kV/cm, and a dielectric constant of 320, the c-axis oriented films exhibited very low polarization (~ 1 $\mu C/cm^2$), coercivity (22 kV/cm) and dielectric constant (~ 200) values. The results of this study has shown that, in addition to DRO memory applications, these capacitors are also attractive candidates for low voltage switching memory applications and metal-ferroelectric-semiconductor transistor (MFST) nondestructive memory applications.

7.2 INTRODUCTION

Semiconductor memories utilizing ferroelectric thin film capacitors can potentially satisfy the high speed, nonvolatile, low cost and low power requirements sought in computer memories today [5-6]. Nonetheless, the commercial development of these ferroelectric memories, in general, has been plagued mainly by reliability problems such as fatigue, retention, leakage current and imprint. Until recently, $Pb(Zr,Ti)O_3$ (PZT) was considered to be the primary candidate ferroelectric material for this application as a result of its excellent ferroelectric properties and high Curie temperature. It is now well known that PZT thin film capacitors with platinum electrodes suffer from severe loss of polarization with cumulative switching (fatigue). Although fatigue has been circumvented by replacing the metal electrodes with conductive oxides, the leakage current levels in oxide electrode/PZT thin film capacitors are far too high for memory applications [7-8]. Some of the other ongoing approaches to minimization of this problem include the use of multilayer metal/metal oxide electrodes and donor doping of the ferroelectric materials [9-11].

Recently, alternate ferroelectric oxides belonging to the family of layered perovskites were identified as promising candidates for degradation free nonvolatile memory applications; $SrBi_2Ta_2O_9$ (SBT) thin films were found to exhibit no fatigue up to 10^{12} cycles, excellent retention characteristics and very low leakage currents on Pt electrodes [1-4]. The promise that these materials hold for memory applications can be realized by the fact there are ongoing efforts to fabricate fully functional 256-kb and higher density RAMs [12]. But the application of these materials to memories on a large scale is not without problems. In particular, the processing of these layered perovskite structure oxides is not as straightforward as in the case of perovskite ferroelectrics such as PZT and is in the incipient stages of understanding. Higher processing temperatures (> 700 ^{o}C) are required to obtain good ferroelectric properties in these materials which is a major limitation in terms of VLSI processing [1-4]. The values of the remnant polarization and coercive field commonly exhibited by these materials are on the lower limit of that required for nonvolatile memory applications. Furthermore, these ferroelectric properties (e.g., remnant polarization, coercive field, dielectric constant etc.) are highly sensitive to the processing conditions and the processing method. This is because bismuth layered structure ferroelectric oxides are highly anisotropic in nature and therefore the crystallographic orientation, which is extremely process dependent, can strongly affect the measured ferroelectric properties.

The ferroelectric properties along the major axes are fairly simple to characterize in bulk compound ferroelectric materials since crystal sections can be cut in such a way as to facilitate the application of high fields along different crystallographic directions. However, the properties in bulk compounds can never be truly replicated in the corresponding thin films. For the case of $SrBi_2Ta_2O_9$ thin films, the ferroelectric properties along the different crystallographic orientations have not been characterized so

far. This is primarily because of the difficulty in orienting these thin films along the different crystallographic directions relative to the underlying substrate materials. For memory applications, as mentioned before, the SBT films are usually grown on top of the Pt bottom electrodes. The bottom Pt layer is grown on oxidized single crystal silicon substrate with a Ti interlayer for adhesion purposes (Fig. 7.1(a)). However, in this structure, the Pt films are almost always oriented with the (111) planes parallel to the film surface at any given deposition temperature. This poses a severe limitation on controlling the orientation of the ferroelectric film on top of the Pt layer as exemplified by the case of SBT films grown on Pt electrodes by the metalorganic decomposition method wherein, the films are almost always polycrystalline at the final processing temperatures [1,3,4]. The occurrence of a favorable orientation during film growth is critically controlled by the lattice parameter ratio of the film and substrate material. In this work, we have devised a novel device structure for growth of Pt/SBT/Pt capacitors, that provides us with the flexibility of varying the orientation in the ferroelectric film with minor changes in the processing conditions. This not only has important technological implications in the fact that it permits the tailoring of the ferroelectric properties of the capacitor structure but also provides opportunities now to understand, at a fundamental level, the ferroelectric behavior of these materials.

In the proposed device structure, the SBT film and the underlying Pt electrode is grown on top of a highly oriented or epitaxial MgO (100) [and/or $SrTiO_3$] layer as shown in Fig. 7.1(b). SBT belongs to the Aurivillus family of mixed bismuth oxides with the general formula $(Bi_2O_2)^{2+}[A_{m-1}B_mO_{3m+1}]^{2-}$, where A and B are metal ions and m is a numeral: $A = Sr^{3+}$, $B=Ta^{4+}$ and m=2 for $SrBi_2Ta_2O_9$ [13-14]. These compounds have a pseudotetragonal symmetry (actually orthorhombic) and the unit cell consists of stacking two perovskite-like units of nominal composition ABO_3 between Bi_2O_3 layers (Fig. 7.2).

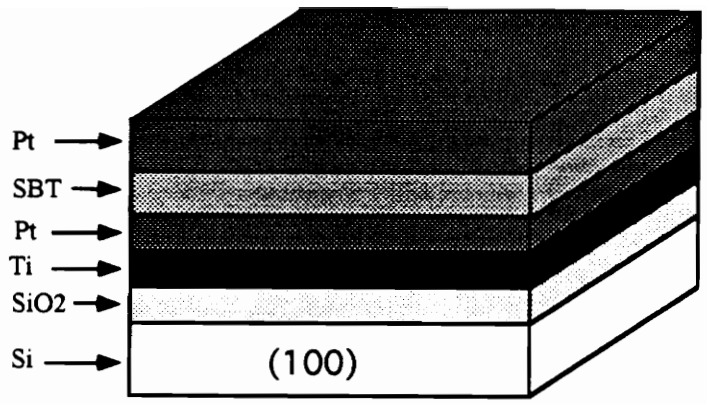

(a)

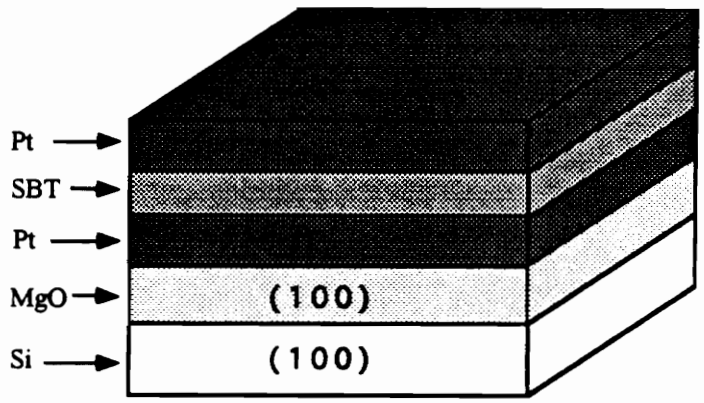

(b)

Figure 7.1 (a) Schematic of the currently used capacitor structure for nonvolatile memory applications of SBT films. (b) Schematic of the device structure proposed in this paper.

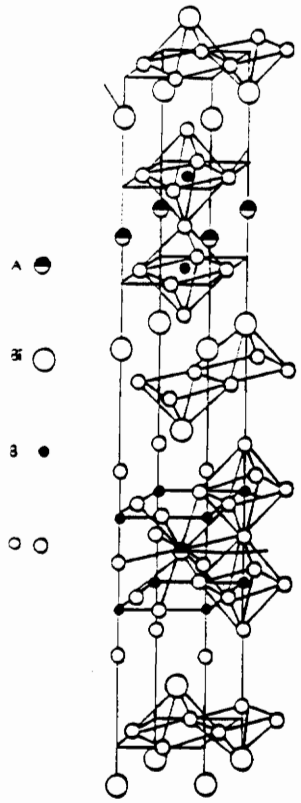

Figure 7.2 Schematic of the unit cell of $ABi_2B_2O_9$ layered structure oxides; for $SrBi_2Ta_2O_9$, A = Sr and B= Ta

The reported value for the *a* (or *b*) parameters for SBT films is 0.389 nm and the *c* parameter is at least five times this value [15]. F.C.C. Pt has the same lattice constant as that reported for SBT films (a = 0.389 nm). This indicates that for favorable growth of SBT films along the c-axis, the underlying Pt films need to be grown with a (100) preferred orientation. MgO(100) or $SrTiO_3$ (100) can be chosen as template layers in this device structure because of their close lattice match to Pt. MgO is a highly insulating crystalline solid with the NaCl structure and has only a 7.4 % mismatch in lattice constant with platinum while $SrTiO_3$ has an even lower lattice misfit of only 0.4 %. Therefore, it is possible to grow highly oriented Pt(100) on MgO(100) or $SrTiO_3$ albeit at a high deposition temperature (600-700 ^oC). The preferred growth of substrates such MgO(100) on Si(100) has been reported previously for both epitaxial and nonepitaxial depositions [16]. Thus the complete device structure can be grown on the preferred single crystal Si(100) substrates for VLSI applications.

7.3 EXPERIMENTAL PROCEDURE

In this study, the Pt films were grown on top single crystal MgO(100) substrates by the sputtering process. The films were deposited at three different substrate temperatures - room temperature, 600 ^oC and 700 ^oC under the conditions of argon gas pressure = 5 mTorr and RF power = 10 W. The deposition rate at high temperatures was typically in the range of 0.1 nm/sec-0.3 nm/sec. After deposition, the films were cooled at a rate of 20 ^oC/min to room temperature in the sputtering chamber itself.

$SrBi_2Ta_2O_9$ films were deposited, for the first time, by the technique of pulsed laser ablation on these platinum coated MgO substrates. The polycrystalline bulk target for the ablation process was fabricated by conventional ceramic processes and sintered at a

temperature of 1150 ^{o}C for 3 hours in a conventional box furnace to a relative density of around 98 %. A 248 nm KrF laser was focused onto these targets with a 50 cm UV-grade planoconvex lens. The targets were placed in a target holder that was rotated at a speed of 10-13 rev/min. The energy of the incoming beam was 700 mJ/pulse and the laser was operated at a frequency of 10 Hz. The beam was incident on the target at an angle of 45^{o} in a vacuum chamber held at an oxygen pressure of 200 mTorr. The resulting plume was caught on the substrates held onto a substrate holder heated to a temperature of 700 ^{o}C. The substrate surface temperature was about 40 ^{o}C lower than the substrate heater temperature. The growth rate of the films under these conditions was typically 0.2 nm/sec and the thickness of the all the films were 200 nm as verified by spectroscopic ellipsometry.

7.4 RESULTS AND DISCUSSION

Fig. 7.3 shows the XRD pattern of the Pt films on MgO(100) substrates as a function of deposition temperature. As expected, the room temperature deposited films showed a strong (111) texture with no reflections from the (200) planes. With increasing deposition temperature, additional reflections were also gathered from the (200) diffraction planes until at a deposition temperature of 700 ^{o}C the Pt films were almost completely oriented with the (100) planes parallel to the substrate surface. Furthermore, rocking curve scans around 2θ peak position of the (200) planes (on the films deposited at 700 ^{o}C) showed a full width at half maximum value of only 1.4^{o} indicating a very strong (100) preferred orientation.

Fig. 7.4 shows the XRD pattern of the SBT films deposited on the various MgO/Pt substrates. The SBT films deposited on the (111) textured Pt films are randomly

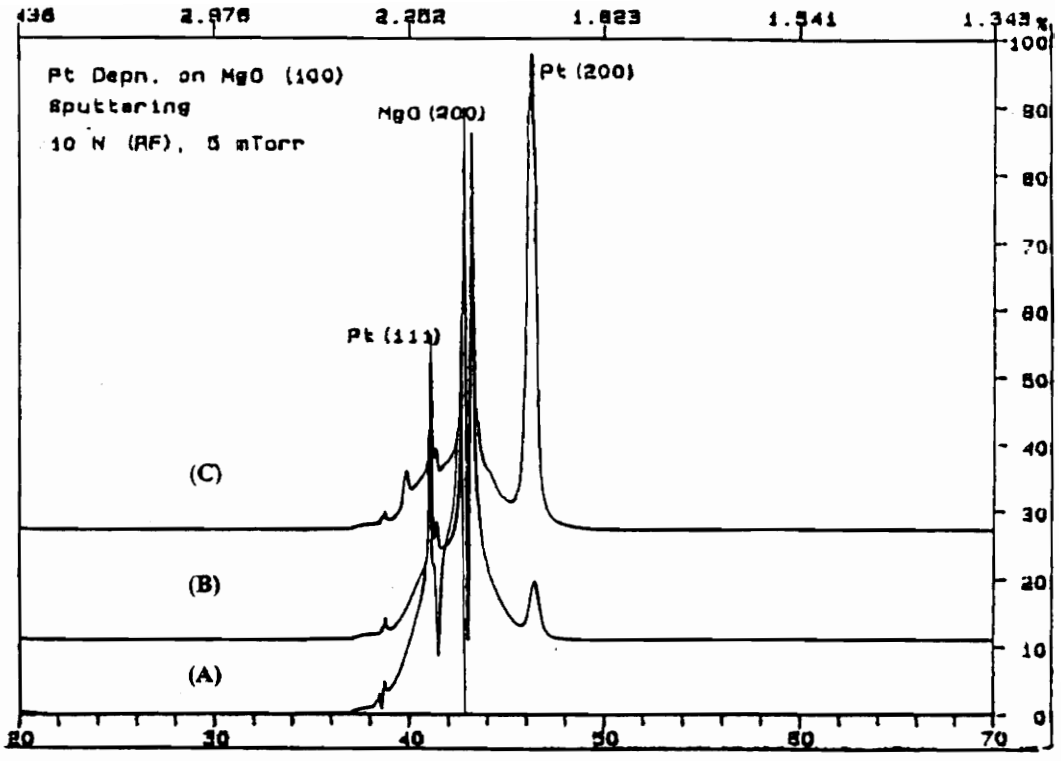

Figure 7.3 X-ray diffraction patterns of Pt films sputter deposited on single crystal MgO (100) substrates as a function of deposition temperature; (a) room temperature deposition, (b) 600 °C deposition and (c) 700 °C deposition.

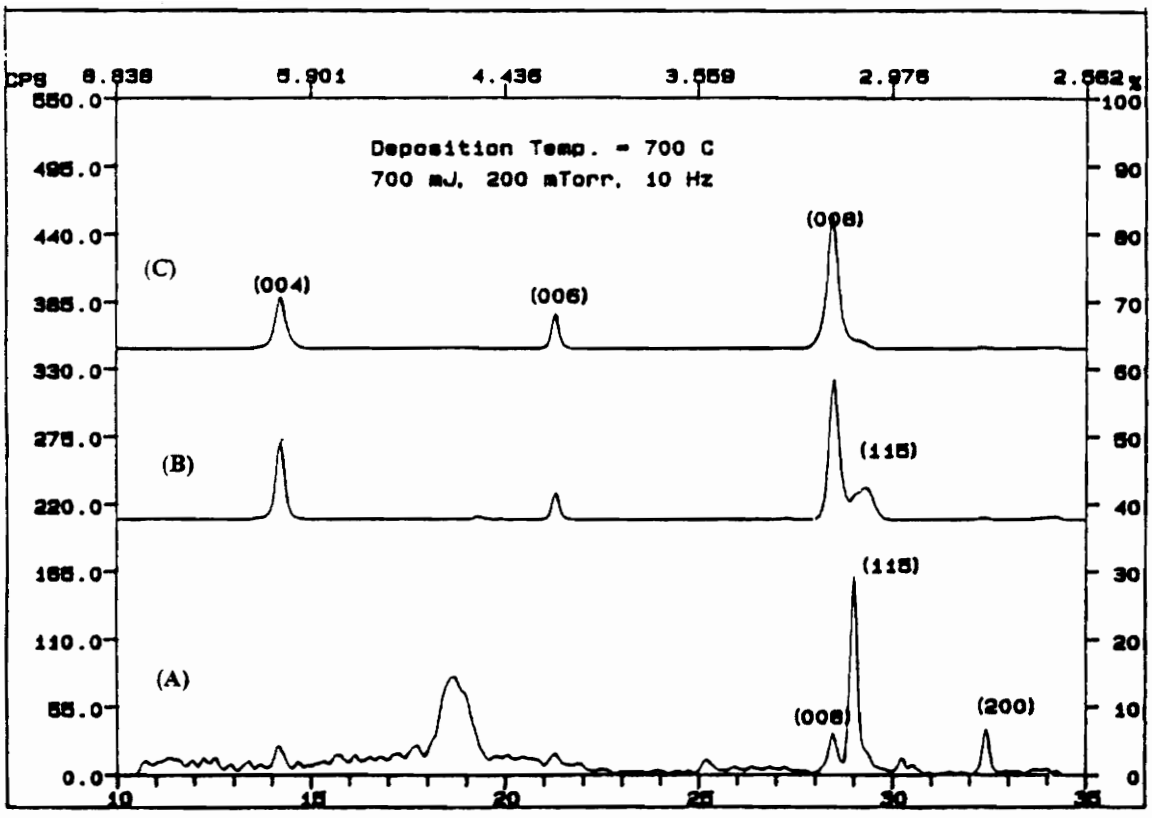

Figure 7.4 X-ray diffraction patterns of $SrBi_2Ta_2O_9$ thin films deposited on (a) MgO/Pt (RT), (b) MgO/Pt(600 °C) and (c) MgO/Pt(700 °C) substrates at a substrate temperature of 700 °C.

polycrystalline under these deposition conditions with predominant diffraction occurring form the (115) planes; also observable are reflections from the (00*l*) and (200) planes. However, the films deposited on MgO(100)/Pt(100) substrates show a strong (00*l*) texture as indicated by reflections from only the (004), (006) and (008) planes. For the intermediate case of the films deposited on substrates containing both (100) and (111) oriented Pt films, the predominant orientation in the ferroelectric was still (00*l*); however, diffraction peaks of significant intensity were also observed form the (115) planes. In effect, these results indicate that simply by increasing the (100) texture in the underlying Pt bottom electrode, the degree of c-axis orientation in the ferroelectric can be increased for the same processing conditions.

Pole figure measurements were made to determine the degree of orientation of the SBT film and the relative orientations of the ferroelectric film and underlying Pt electrode. These measurements were conducted over the tilt range of χ =0 to 80^{o} in steps of $\Delta\chi$ = 5^{o} and azimuth angle steps of $\Delta\phi$ = 5^{o}. The pole figures for the three samples are presented in Fig. 7.5. For the randomly polycrystalline sample, the pole figure shows no texture as indicated the pole density value of one, in large range of tilt angle up to 70^{o}. For SBT films deposited on MgO(100)/Pt(100) substrates, the pole figures indicate a strong texture. In both these samples, the diffraction intensity from the (008) planes is concentrated in the vicinity of χ =0. For the case of MgO/Pt(600 ^{o}C)/SBT films, the (115) intensity is localized within several spots in the tilt angle of 54^{o} and form a circle around the (008) spot indicating that all the crystals are not aligned in the same orientation in three dimensions. In contrast, the measurements on SBT films deposited on MgO/Pt(700 ^{o}C) substrates show only four (115) satellite spots making an angle of χ = 54^{o} from the sample normal in addition to the (008) intensity concentrated at the center. Since the (115) planes have a 4-fold symmetry above the c-axis, this pole figure shows that all the crystals

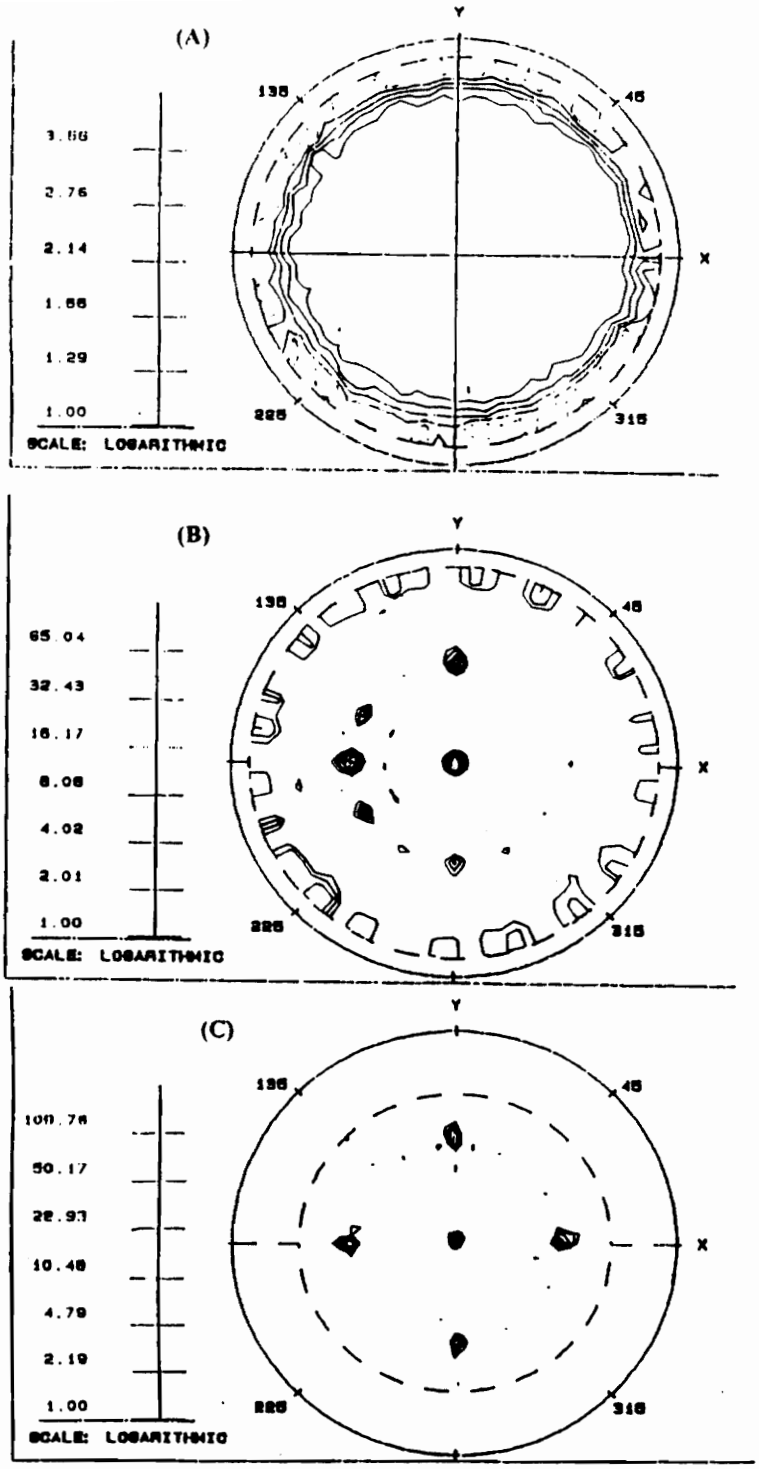

Figure 7.5 Pole figures of $SrBi_2Ta_2O_9$ thin films deposited on (a) MgO/Pt (RT), (b) MgO/Pt(600 °C) and (c) MgO/Pt(700 °C) substrates at 700 °C.

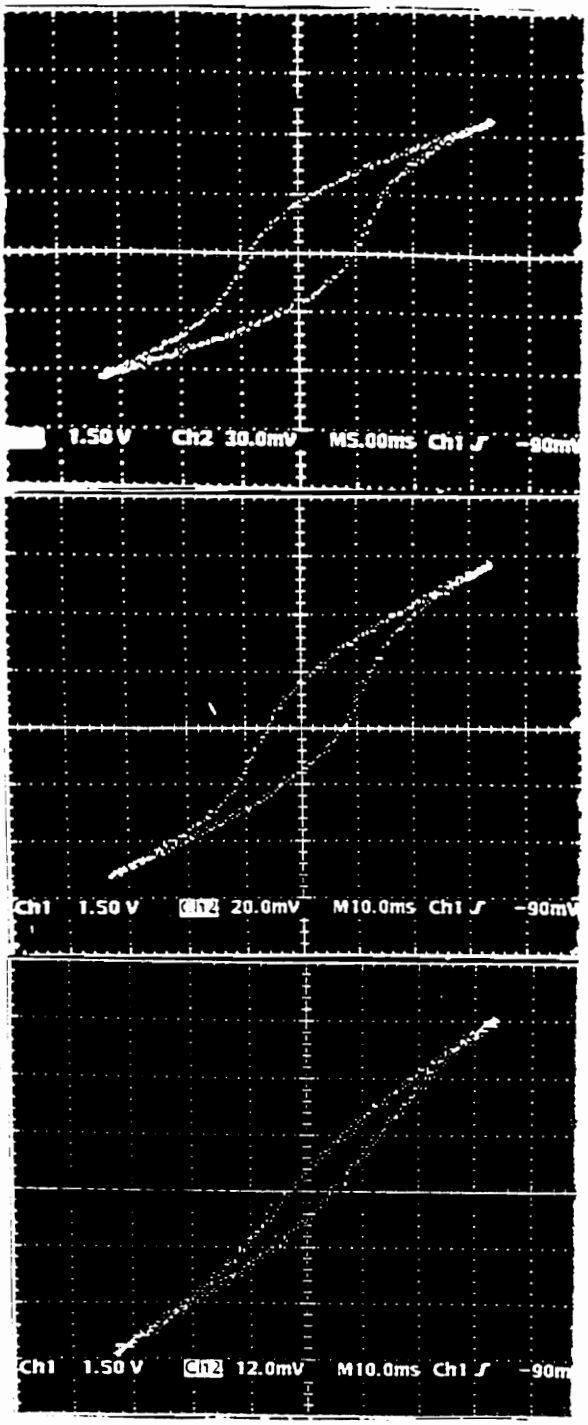

Figure 7.6 The hysteresis characteristics of $MgO/Pt/SrBi_2Ta_2O_9/Pt$ capacitors as a function of degree of c-axis orientation; (a) MgO/Pt (RT)/SBT, (b) MgO/Pt(600 °C)/SBT and (c) MgO/Pt(700 °C)/SBT.

are aligned in three-dimensions. Furthermore, higher pole density values were obtained from the latter films (Fig. 7.5) indicating a greater degree of texture.

The electrical properties of the respective films were measured using a simple Sawyer-Tower circuit [17]. Circular Pt counter electrodes (2 x 10^{-4} cm^2 in area) were deposited onto the samples through a shadow mask by sputtering. Fig. 7.6 shows the hysteresis plots as a function of degree of c-axis orientation in the ferroelectric films. These measurements were conducted at a frequency of 800 Hz and at an applied voltage of 5V. Clearly, the polarization and coercive field values decrease systematically with increasing degree of c-axis orientation. More importantly, the c-axis oriented films show extremely low polarization values (P_r ~ 1 $\mu C/cm^2$) and coercive field (22 kV/cm) values. These results suggest that the Bi_2O_2 layers intervening the perovskite-like units along the c-axis may not be participating in the cooperative phenomenon responsible for ferroelectricity in these materials. The polarization vector, most likely, lies close to the a-b plane wherein all the perovskite-like layers are continuous. The random polycrystalline films exhibited the highest value of remnant polarization (~ 5 $\mu C/cm^2$); however, they also showed the highest coercivity (72 kV/cm). For nonvolatile memory applications, it is preferable to use a ferroelectric material that exhibits high remnant polarization ($2P_r$ > 10 $\mu C/cm^2$) along with low coercivity (< 50 kV/cm). But none of the ferroelectric films reported in this study satisfy this criterion. Nonetheless, it is known from previous studies that polycrystalline solid solutions of $SrBi_2Nb_2O_9$- $SrBi_2Ta_2O_9$ with a composition close to 40/60 exhibits higher polarization values. Therefore, similar device structures can be fabricated with this material as the ferroelectric layer. The results of dielectric constant measurements as a function of frequency are shown in Fig. 7.7; the dielectric constant was found to decrease with increasing degree of c-axis orientation. For the c-axis oriented films, a dielectric constant value of 200 was obtained at room temperature in the

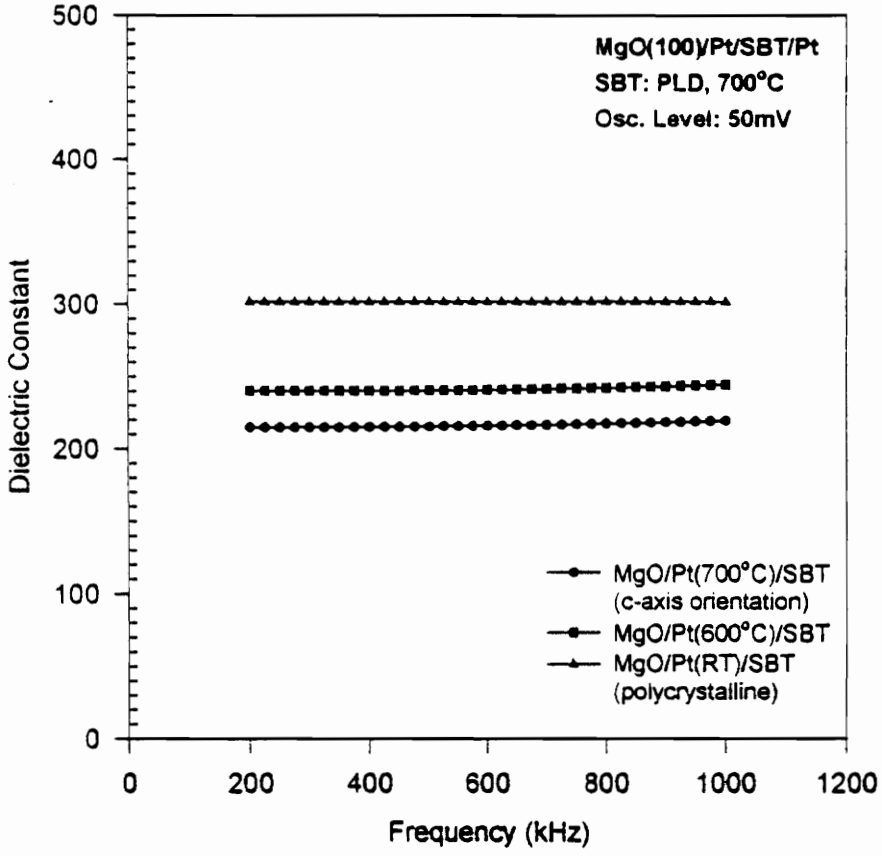

Figure 7.7 The dielectric properties of $MgO/Pt/SrBi_2Ta_2O_9/Pt$ capacitors as a function of degree of c-axis orientation.

frequency range measured (200-1200 kHz).

7.5 SUMMARY

For the first time, the ferroelectric properties of $SrBi_2Ta_2O_9$ ferroelectric thin film capacitors have been characterized as a function of crystallographic orientation using a novel device structure; the remnant polarization, coercivity and dielectric constant were found to decrease with increasing degree of c-axis orientation. Technologically, it has been shown that the structural flexibility of these materials can now be used for a wide variety of nonvolatile memory applications ranging from high voltage (5V) DRO NvRAMs to low voltage memory applications (single transistor-single capacitor) and nondestructive readout MSFT applications (single transistor). It has also been shown for the first time that highly c-axis oriented or epitaxial layered structure SBT films exhibit very small polarization, coercivity and dielectric constant values and are thereby attractive candidates for NDRO MSFT applications.

7.6 REFERENCES

1. C.A-Paz de Araujo, J.D. Cuchlaro, L.D. McMillan, M.C. Scott, J.F. Scott, *Nature*, 374, (1995), 627.

2. K. Ammanuma, T. Hase and Y. Miyasaki, *Appl. Phys. Lett.* 66(2), (1995), 221.

3. S.B. Desu and D.P. Vijay, *Mat. Sci. Engg. (B)*, in press, (1995).

4. S.B. Desu and T.K. Li, *Mat. Sci. Engg. (B)*, in press, (1995).

5. J.F. Scott and C.A. Paz de Araujo, *Science*, 246, (1989), 1400.

6. R. Ramesh, A. Inam, W.K. Chan, B. Wilkens, K. Myers, K. Remschnig, D.L. Hart and J.M. Tarascon, *Science*, 252, (1991), 944.

7. D.P. Vijay and S.B. Desu, *J. Electrochem. Soc.*, 140 (1993) 2640.

8. R. Dat, D.J. Lichtenwalner, O. Auciello, and A.I. Kingon, *Appl. Phys. Lett.*, 64(20), (1994), 2673.

9. R. Ramesh, H. Gilchrist, T. Sands, V.G. Keramidas, R. Haakenaasen and D.K. Fork, *Appl. Phys. Lett.* 63, (1993), 3592.

10. S.B. Desu, D.P. Vijay and I.K. Yoo, *Mat. Res. Soc. Symp. Proc*, 335 (1994), 53.

11. H.D. Bhatt, D.P. Vijay, S. B. Desu, X. Zhang and C.L. Thio, *in preparation.*

12. C.A-Paz de Araujo, J.D. Cuchlaro, L.D. McMillan and M.C. Scott, International Patent Publication No. WO 93/12542 (24 June 1993).

13. B. Aurivillus, *Arkiv Kemi*, 1 (1949), 463.

14. G.A. Smolenski, V.A. Isupov and A.I. Agranovskaya, *Fiz Tverdogo Tela*, 3, (1961), 895.

15. E.C. SubbaRao, *J. Chem. Phys.*, 34, (1961), 695.

16. D.K. Fork, F.A. Ponce, J.C. Tramontana and T.H. Geballe, *Appl. Phys. Lett.* 58(20), (1991), 2294.

17. C.B. Sawyer and C.H. Tower, *Phys. Rev.* 35, (1960), 239.

This paper titled

"Reactive Ion Etching of Lead Zirconate Titanate (PZT) Thin Film Capacitors"

is published in

Journal of The Electrochemical Society
140 (9), (1993), 2635

This co-authors in this publication are Dr. S.B. Desu and Dr. W. Pan. Dr. W. Pan conducted the measurements on the thickness for etch rate determination using profilometry. My contributions included the experimental work, analysis of the data and conclusions.

Chapter 8 : Reactive Ion Etching of Lead Zirconate Titanate (PZT) Thin Film Capacitors

8.1 ABSTRACT

One of the key processing concerns in the integration of $PbZr_xTi_{1-x}O_3$ (PZT) thin film capacitors into the existing VLSI for ferroelectric or dynamic random access memory applications is the patterning of these films and the electrodes. In this work, we have identified a suitable etch gas (CCl_2F_2) for dry etching of PZT thin films on RuO_2 electrodes. The etch rate and anisotropy have been studied as a function of etching conditions. The trends in the effect on the etch rate of the gas pressure, RF power and O_2 additions to the etch gas have been determined and an etching mechanism has been proposed. It was found that ion bombardment effects are primarily responsible for the etching of both PZT and RuO_2 thin films. Etch rates of the order of 20-30 nm/min were obtained for PZT thin films under low gas pressure and high RF power conditions. The etch residues and the relative etch rates of the components of the PZT solid solution were determined using XPS. The results show that the etching of PbO is the limiting factor in the etch process.

8.2 INTRODUCTION

There has been a renewed interest in ferroelectric thin films for dynamic and nonvolatile RAM applications because of their high dielectric constant and bistable nature of polarization [1]. Lead Zirconate Titanate (PZT) ferroelectric thin films are potential candidates for these applications as a result of their promising electrical properties and applicability in a wide range of temperatures. However, several problems need to be

overcome before the integration of a ferroelectric thin film capacitor into the existing semiconductor VLSI. Some of these issues include the degradation of the ferroelectric capacitor and the need for improvement of the existing processing techniques to obtain the optimum properties.

One of the key processing issues involved in the integration of PZT thin film based capacitors (electrode/PZT/electrode) into the existing VLSI is the etching of these films and the associated electrodes. It is preferable to use dry etching techniques for VLSI applications because of the large etch anisotropy, high resolution and the high etch uniformity that they offer [2]. For dry etching of PZT thin films, it is important to identify a suitable etch gas that can etch all three components of the PZT solid solution- PbO, ZrO_2 and TiO_2- at reasonable etch rates. It is also convenient to use an etch gas that can etch the both the electrodes and the ferroelectric material, so that the ferroelectric stack capacitor can be etched in a single run.

Recently, there has been a considerable amount of interest in conductive oxides such as RuO_2 for electrodes in PZT thin film capacitors [3]. This interest arises from the excellent diffusion barrier properties and the reduced fatigue of the ferroelectric films on these electrodes. We have therefore chosen to use RuO_2 electrodes for PZT thin film capacitors. There have been only very few reports on the etching of PZT and RuO_2 thin films in the literature. Poor et al. [4] have reported plasma etching of PLT thin films in CF_4 and HCl plasmas. However, to obtain high etch rates, substrate heating was necessary in their process. Saito et al.[5] have etched RuO_2 using Reactive Ion Etching with a CF_4/O_2 plasma. In this study, we have examined the feasibility of using CCl_2F_2/O_2 as an etch gas for dry etching of PZT thin film capacitors. An attempt has been made to provide a guideline to the mechanism of etching in these materials by determining the trends in the etch rates of these films as a function of etch parameters such as RF power, gas pressure,

gas flow rate and percentage O_2 content in the chamber . The etch residues at the end of the etch process have been studied using surface analysis.

8.3 EXPERIMENTAL PROCEDURE

Thin films of PZT (53/47) were deposited on Pt coated Si/SiO_2 substrates using the sol-gel method. The Si substrates were oxidized at 950°C for 1 hr in wet O_2 to obtain 100 nm of SiO_2. 500 nm of Pt was then deposited onto these substrates. The PZT precursor was prepared from a metallorganic solution (0.4M) of lead acetate, zirconium n-propoxide and titanium iso-propoxide dissolved in acetic acid and n-propanol. The solution was hydrolyzed (R=10) to form the precursor. The method of preparing the precursor is similar to that suggested by Yi et al [6]; more details regarding the method of preparation can be obtained from this reference. The films were spin coated at 2000 rpm for 30 seconds and subsequently dried at 150°C for 5 min. The cycle (spin-bake) was repeated to obtain the desired thickness of 180-200 nm. The coated films were annealed at 600°C for 30 min to form the PZT perovskite phase.

RuO_2 thin films were reactively sputtered onto Si/SiO_2 in an argon-oxygen ambient at a gas pressure of 10 mTorr and a substrate temperature of 200°C. The films were deposited to a thickness of 200 nm. The films were etched after suitable masking using positive photoresist in a RIE-1C etcher. The typical etch structures used in the etching of PZT and RuO_2 thin films are shown schematically in Figure 8.1. The thickness of material etched was determined using a WYKO 3D profilometer. The surface composition before and after the etch was determined using XPS and the etch anisotropy was evaluated using SEM.

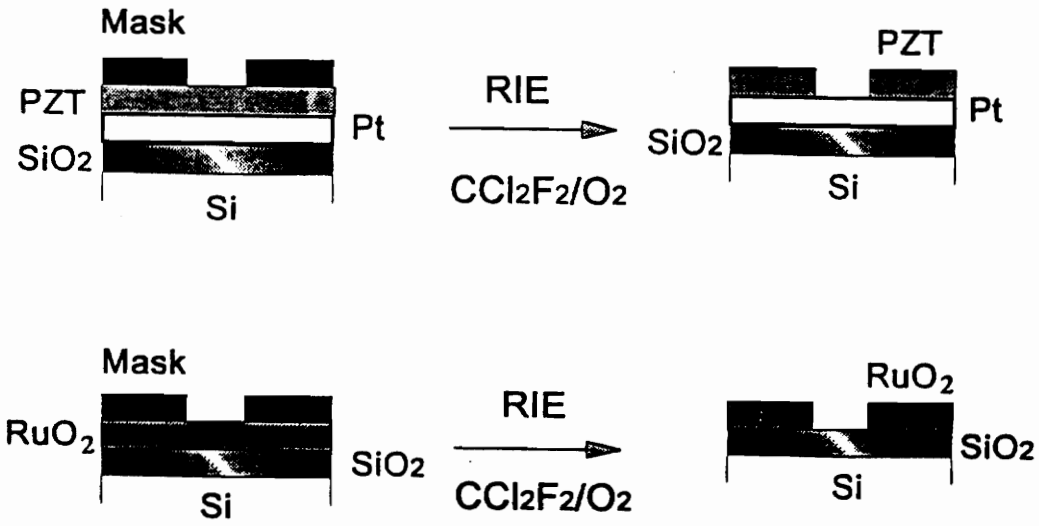

Figure 8.1 Schematic of the etch structures used in the etching of PZT and RuO_2 thin films.

8.4 RESULTS AND DISCUSSION

PZT thin films are solid solutions of lead zirconate and lead titanate. Since the material consists of three components (PbO, ZrO_2 and TiO_2), the overall etch rate is dependent on the Zr/Ti ratio and the concentration of excess lead because of the differing volatilities of the fluorides and chlorides of the constituent elements. However, in this study we have only examined the etch characteristics of PZT films with compositions close to the morphotrophic phase boundary. No substrate heating was used to avoid the loss of lead from the masked areas which could result in degradation of the films at high temperatures. The etching was performed on water cooled substrate holders to avoid excessive heating from the plasma. The critical etch parameters studied were the gas pressure, RF power and the effect of O_2 addition to the CCl_2F_2 plasma. Since the objective was to etch the complete ferroelectric stack capacitor in a single run, the etch rate of RuO_2 was also studied under the same conditions as the PZT films. The range of the values of the parameters were chosen so as to observe the general trends in etching of these films with varying conditions. The parameter values were also limited by the stability of the plasma.

Figure 8.2 shows the trend in etch rate of PZT films with increasing flow rate of CCl_2F_2 gas in the etch chamber. The flow rate of the gas in the chamber was not independent of the gas pressure and therefore its effect on the etch rate is a direct indication of the gas pressure effects. The flow rate of CCl_2F_2 and O_2 were calibrated for gas pressure before the etching process. The etching was performed at fixed RF power values of 150 W and 200 W. As can be seen from Figure 8.2, the etch rate decreases with increasing flow rate of the gas. Also, at low flow rates, higher etch rates are observed at higher RF power. The RF power does not have any significant effect on the etch rate at

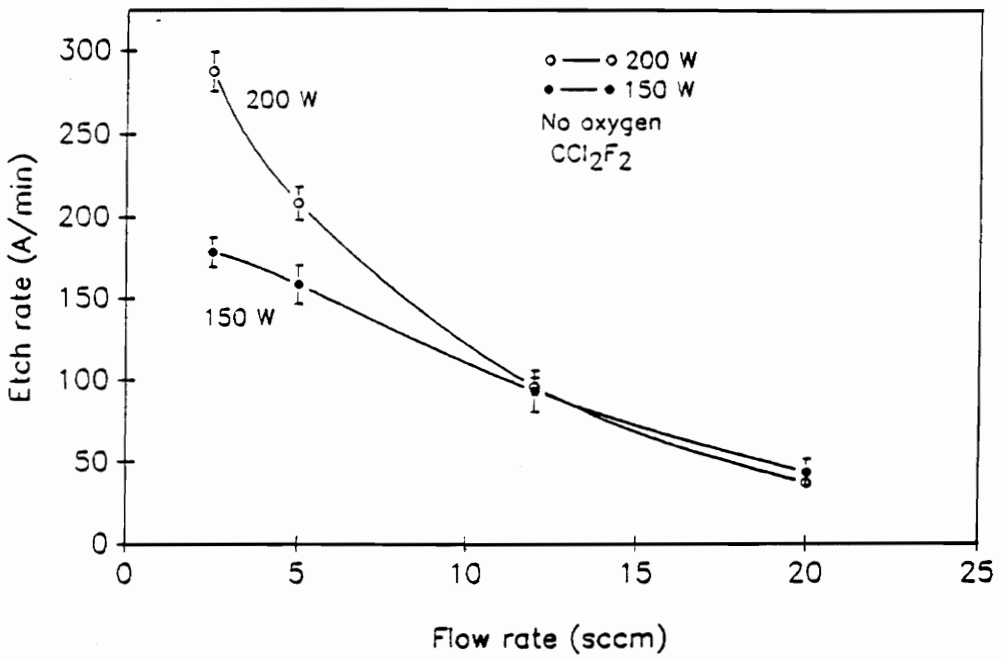

Figure 8.2 The etch rate of PZT thin films as a function of CCl_2F_2 gas flow rate.

high flow rates. Typical etch rates obtained under conditions of low flow rates and high power were in the range of 20-30 nm/min. The decreasing trend of the etch rate with increasing flow rate indicates that the primary mechanism of etching in these films is by ion bombardment. In general, with increasing gas pressure, there are two effects : an increase in the neutral and ion species concentration and a decrease in the sheath potential[2]. Since we observe a decrease in etch rate with increasing gas pressure, the latter should have a more pronounced effect. This indicates that the etching mechanism is ion-induced. With increasing gas pressure, the interionic collision rate increases in the sheath region, thereby reducing the number of ions participating in the etch process. In effect, this decreases the energy of ion bombardment and consequently, the etch rate.

The effect of RF power on the etch rate of PZT films is shown in Figure 8.3. For each of the O_2 concentrations studied, the etch rate increased with increasing RF power. It is well known that with an increase in the RF power, the sheath potential and the concentration of the reactive ions increase [2]. The effect of gas pressure on the etch rate at different power values (Figure 8.1) does suggest that the increase in etch rate with RF power is due to the increase in sheath potential. As a result, the energy of the bombarding ions increases causing an increase in the etch rate. The notable feature however is the actual value of the etch rate. At a gas pressure of 100 mTorr, O_2 content of 15 % and RF power as high as 200 W, an etch rate of the order of 30 nm/min was obtained. At lower gas pressures and higher power, however, the plasma was very unstable.

Figure 8.4 shows the effect of O_2 addition on the etch rate of PZT films at various gas pressures. In general, there is a peak in the etch rate with varying O_2 content at a particular gas pressure. At low gas pressures, it was found that the etch rate dropped significantly with increasing O_2 content in the chamber. O_2 addition in small amounts is known to enhance the etch rate in the case of SiO_2 etching [7]. In the case of CF_4 plasma,

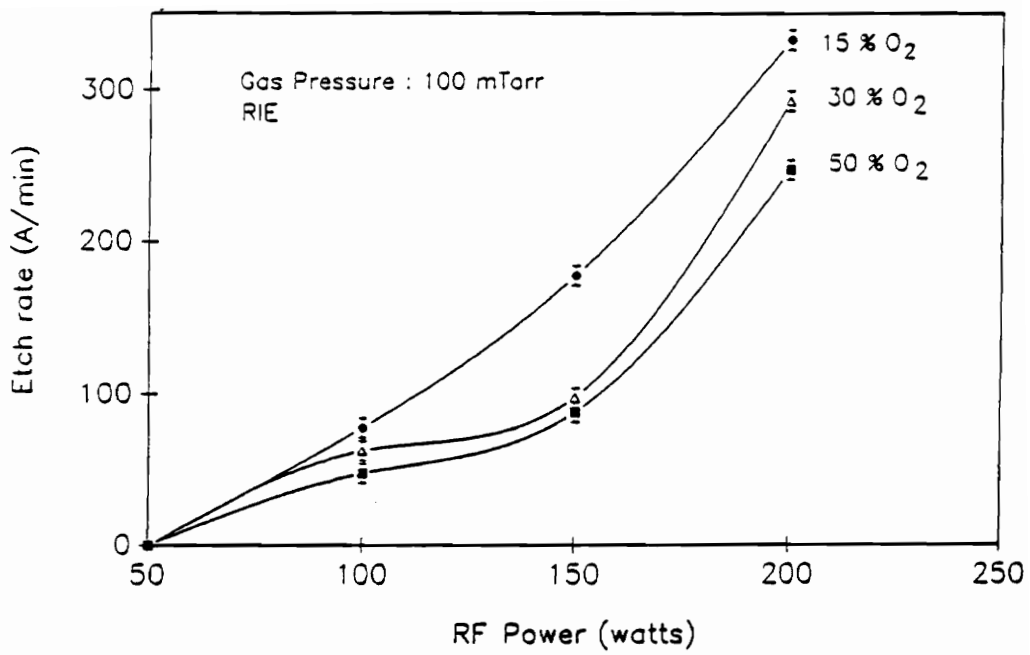

Figure 8.3 **The effect of RF power on the etch rate of PZT thin films at constant gas pressure.**

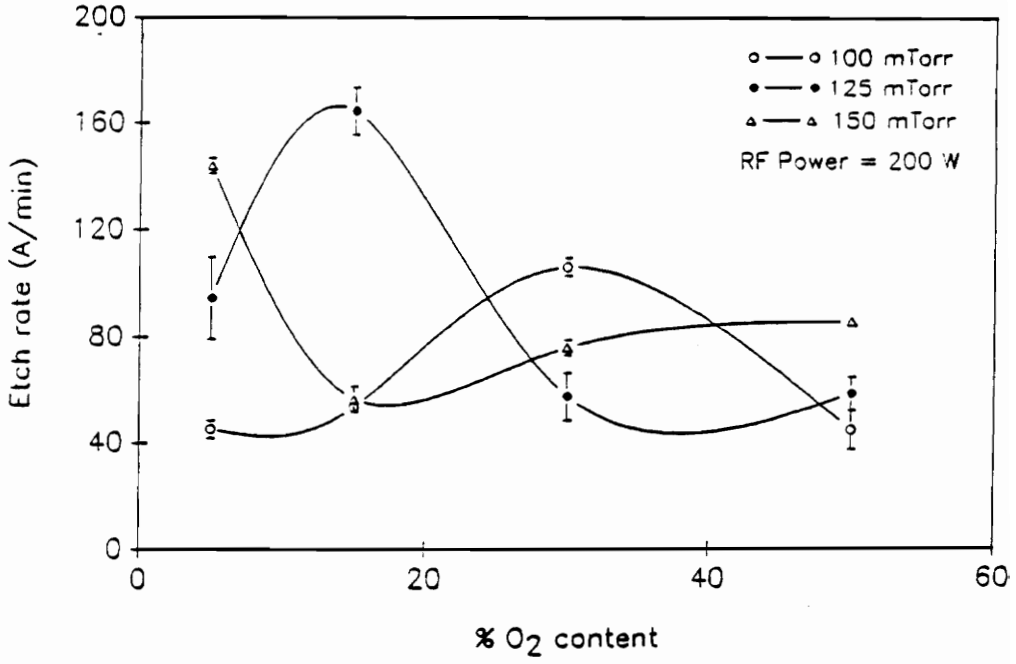

Figure 8.4 The etch rate of PZT films as a function of % O_2 in the etch gas.

addition of O_2 reduces the recombination rate of the CF_x and F radicals by reacting with CF_x to form other by products and thereby increases the available active F radicals for etching [7]. In our case, we can expect a similar mechanism of etching. The gas pressure effects do indicate that the process is ion induced and therefore the surface reactivity of the radicals increases with increasing ion bombardment. At lower gas pressures, the addition of small amounts of O_2 enhances the etch rate of the films possibly by causing reduction in the recombination of the radicals. However, at higher O_2 content, the etch gas is diluted and therefore the etch rate is reduced. As discussed before, at higher gas pressures, there are strong interionic collisions taking place near the sheath region that cause a reduction in the etch rate. Addition of O_2 to the etch gas at these pressures, tends to reduce the number of these radicals near the sheath region. Although the O_2 ions do not participate in the etch process directly, they assist in reducing the density of ions, radicals and neutral species of the primary etch gas at higher gas pressures. Since the species of the primary etch gas have a higher molecular weight in comparison to the oxygen radicals, they play a greater role in the sputtering process. The effective impact energy of the ions participating in the sputtering is increased as a result of reduced collisions.

The etch anisotropy under various etching conditions was studied using the SEM. Figure 8.5 is an SEM micrograph of a sample etched under conditions of low gas pressure and low RF power. Under these conditions we found the etch profile to be anisotropic. At high gas pressures and high RF power, the etch profile was more isotropic. Since the primary etch mechanism is by ion bombardment, one can expect high anisotropy at low gas pressures. However, at high RF power, the energy of the bombarding ions are very high, leading to significant damage of the etched surface. The composition of the etched surface was determined as a function of etch time using XPS.

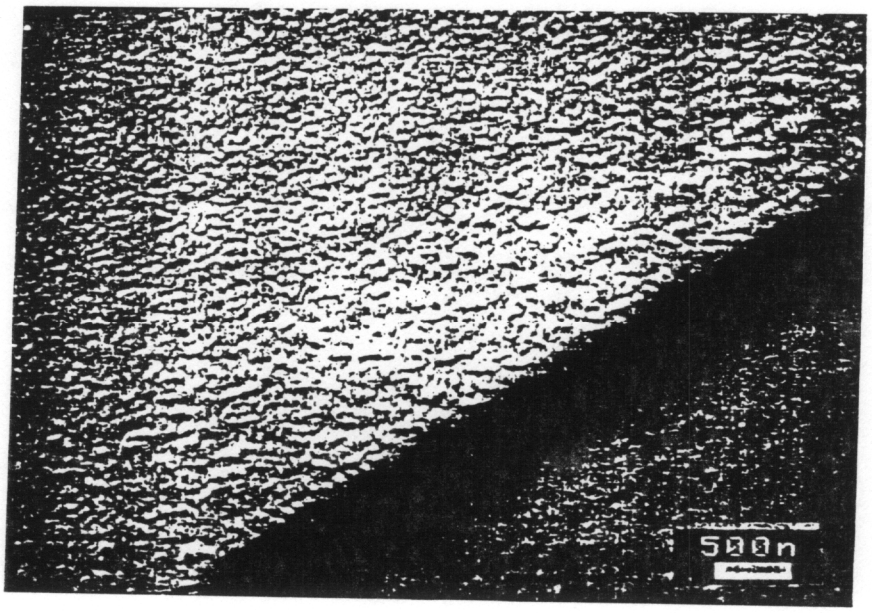

Figure 8.5 **SEM micrograph of PZT thin film sample showing the high etch anisotropy obtained under conditions of low gas pressure and low RF power.**

For this study etching was performed on a single sample (1cm x 1cm) without any overlying mask. The etching was done under the conditions of 150 W RF power, 100 mTorr gas pressure and 15 percent O_2 content in the chamber. An initial surface analysis was performed on the sample before the etching process and subsequent analyses was done at predetermined intervals during etching. Figure 8.6(a) is a comparison of the ESCA wide scan before and after the etch process. The components of the PZT solid solution clearly seem to be completely etched out at the end of the etch process. However, at the end of this process, Cl and F residues are present on the surface of the sample. Figure 8.6(b) is an ESCA wide scan of the sample after 4 min of etching. The wide scan spectrum after 4 min shows a higher F concentration and a lower Cl concentration when compared to the concentrations at the end of the process. Figure 8.6 (c) is a plot of the relative atomic concentration of Pb, Zr and Ti as a function of etch time. The concentrations of these elements were determined using the standard-less ratio method and more details regarding this method can be obtained from Ref 8. This plot is a clear indication of the relative etch rates of the three components in the PZT solid solution. Initially, the relative atomic concentration of Zr and Ti decreases quite rapidly. The narrow scan results show that after the first 30 seconds of etching under these conditions, there is a continuos decrease in the Zr concentration while the relative Ti concentration appears to be nearly constant. It is evident from Fig. 8.6 (c) that the etch rate of PbO is the limiting factor in the etching of PZT thin films and therefore any post etch residues are primarily due to the PbO.

The vapor pressures of fluorides of Pb, Zr and Ti are too low in the temperature range ($< 100^0$C) in which the etching was done to permit significant vaporization of these fluoride by-products. The chlorides of Zr, Ti and Pb, on the other hand, have reasonably high vapor pressures at these temperatures; the vapor pressure decreases in the order of

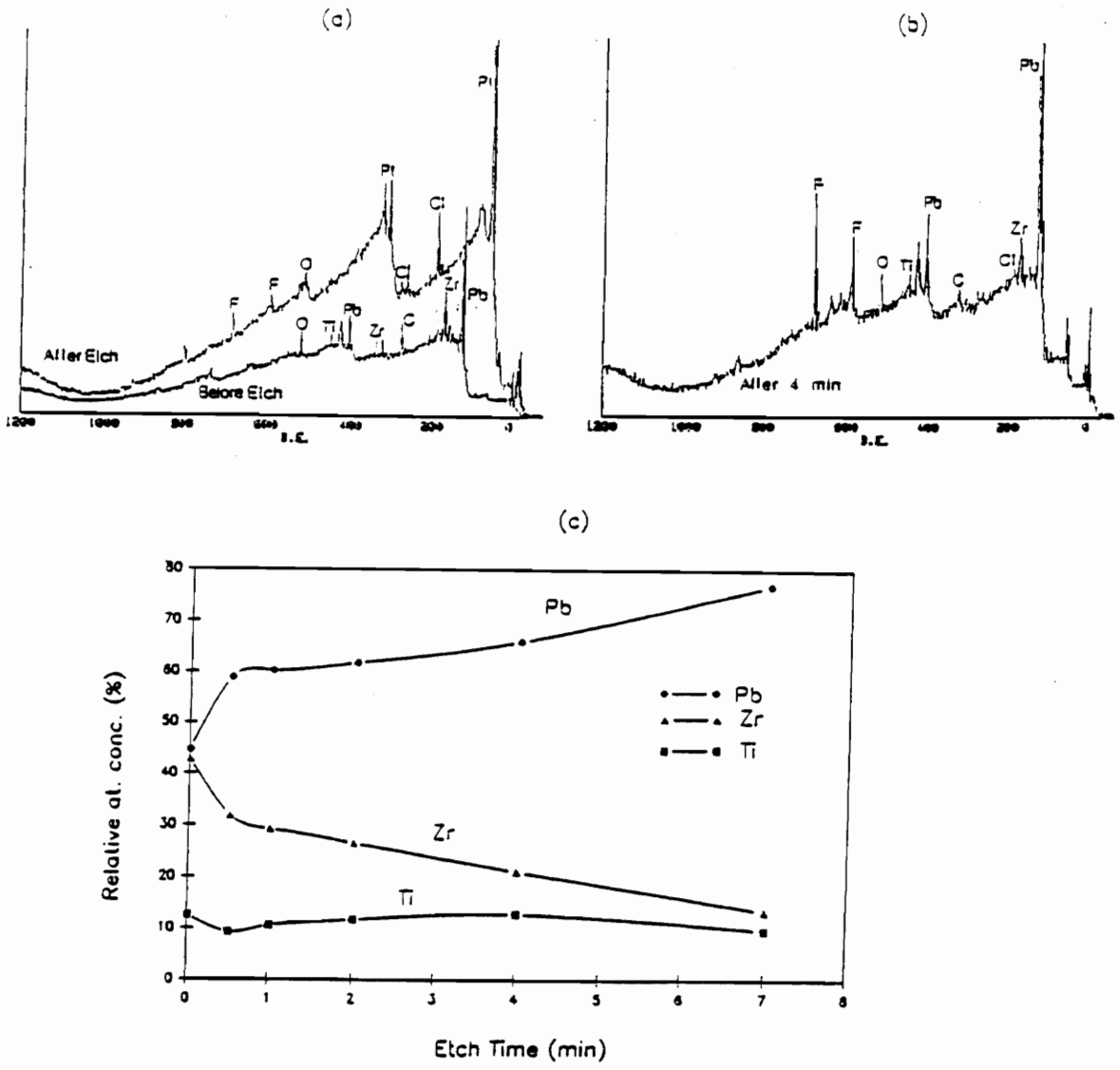

Figure 8.6 (a) The ESCA wide scan of the PZT film surface before and after the etch process (b) the ESCA wide scan of the PZT film surface after partial etching (4 min under the given conditions) and (c) the composition of the PZT film surface as a function of etch time as determined by ESCA.

$TiCl_4$ > $ZrCl_4$ > $PbCl_2$ [9]. However, the actual presence of these compounds in the by-products have not yet been identified experimentally.

It is possible to propose an etch mechanism based on the ESCA results and the vapor pressure data. The plasma generated as a result of the CCl_2F_2 gas can include species such as CCl_xF_x ($x<1$), Cl and F radicals. Although, both the F and Cl radicals react with the elements of the PZT solid solution, the chlorides of these elements are more likely to form the volatile by-products. The Cl etching mechanism is therefore more of an ion-induced phenomena. The ion bombardment possibly increases the reactivity of the surface of PZT films with Cl by causing surface damage. The removal of the chlorides of the constituent elements can also be accelerated by the ion bombardment. Since the chlorides are constantly desorbed from the surface of the films, the wide scan of the ESCA shows only a very small peak during the etching run. The low vapor pressures of the fluorides of Pb, Zr and Ti tend to suggest that the fluorine etch mechanism is likely to be an ion-enhanced phenomena. At low temperatures, in the absence of ion bombardment, the removal of the fluorides from the surface is a very slow process. This is partly evident from the results of Poor et al [4], which indicated etch rates of the order of 10 nm/hr at low temperatures using plasma etching with CF_4 gas. The ion bombardment is the primary cause for etching in this case. This explains the presence of the fluorine peak in the ESCA wide during the etching run. At the end of the etch process, only small amounts of $PbCl_2$ and PbF_2 are possibly present on the sample surface as residues.

The etching of RuO_2 thin films were studied under similar reactor configuration and etching conditions. Thin films (~ 200 nm) of RuO_2 were sputtered reactively on oxidized Si substrates at a gas pressure of 10 mTorr and substrate temperature of 200°C. The films were subsequently annealed at 600°C to form the desired stoichiometry. Data on the vapor pressures of chloride and fluoride derivatives of Ru are scarce in the

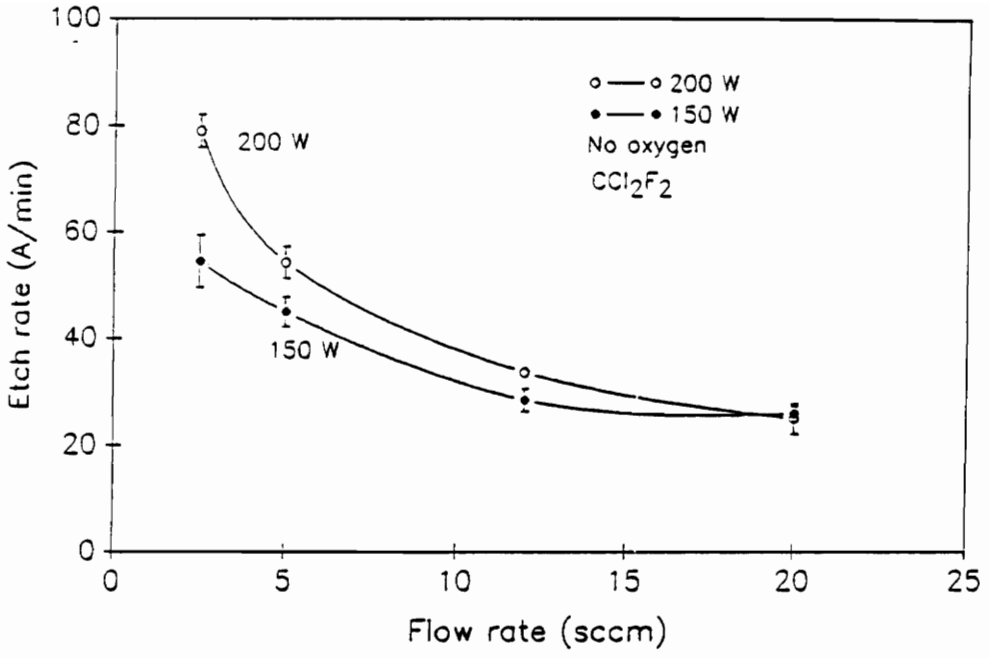

Figure 8.7 **The etch rate of RuO_2 thin films as a function of flow rate of CCl_2F_2 gas (no oxygen added to the etch gas).**

literature. Saito et al. [5] have investigated the reactive ion etching characteristics of sol-gel derived RuO_2 thin films using CF_4/O_2 plasma. They have reported that RuO_3 and RuF_5 are volatile compounds that form as by products during the etching of RuO_2.

Figure 8.7 shows the effect of increasing flow rate/gas pressure on the etch rate of RuO_2 thin films at two different RF power values in pure CCl_2F_2 gas. As in the case of PZT films, the etch rate decreases with increasing gas pressure, indicating that ion-bombardment effects are responsible for the etching of these films. The actual values of the etch rates were however significantly lower than that of the PZT films. Typically, without any O_2 addition in the chamber, etch rates of the order of 7.5-8.0 nm/min were obtained at low gas pressures and high power. With the addition of O_2 (30%) to the etch gas, as shown in Fig. 8.8, there was a considerable amount of increase in the etch rate at lower gas pressures. The effect of O_2 addition at different gas pressures are shown in Fig. 8.9. Once again, the effect of O_2 addition to the etch gas in the etching of RuO_2 films is similar to the etch characteristics of PZT thin films under similar conditions. At very low gas pressures, the etch rate maxima occurs at low O_2 content. With increasing gas pressure, the maxima shifts towards higher $\%O_2$ content values. RuO_2 can react with oxygen ions in the plasma to produce volatile RuO_3/RuO_4 [5]. The ion derivatives of the CCl_2F_2 gas are responsible only for bombardment/sputtering of the reaction products. It is unlikely that fluoride and chloride derivatives of Ru will form as by-products in significant amounts in comparison to RuO_3/RuO_4 because of the relatively higher boiling point of the former. In the absence of any O_2 in the etch gas, the etching process is an ion-induced phenomena as evident from the gas pressure effects. This is also confirmed by the RF power effects on the etch rate, as shown in Fig. 8.10. Increasing the RF power increases the energy of the impacting ions thereby increasing the etch rate. When O_2 is added to the etch gas, the etching mechanism becomes an ion-enhanced phenomena. The

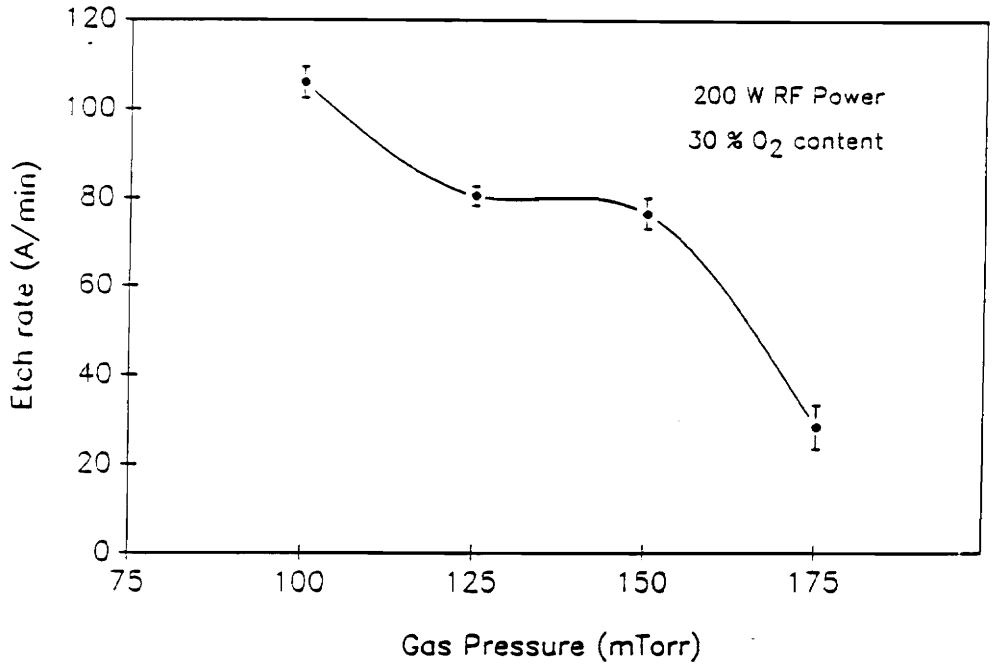

Figure 8.8 **The etch rate of RuO_2 thin films as a function of gas pressure. 30% of the etch gas contained oxygen.**

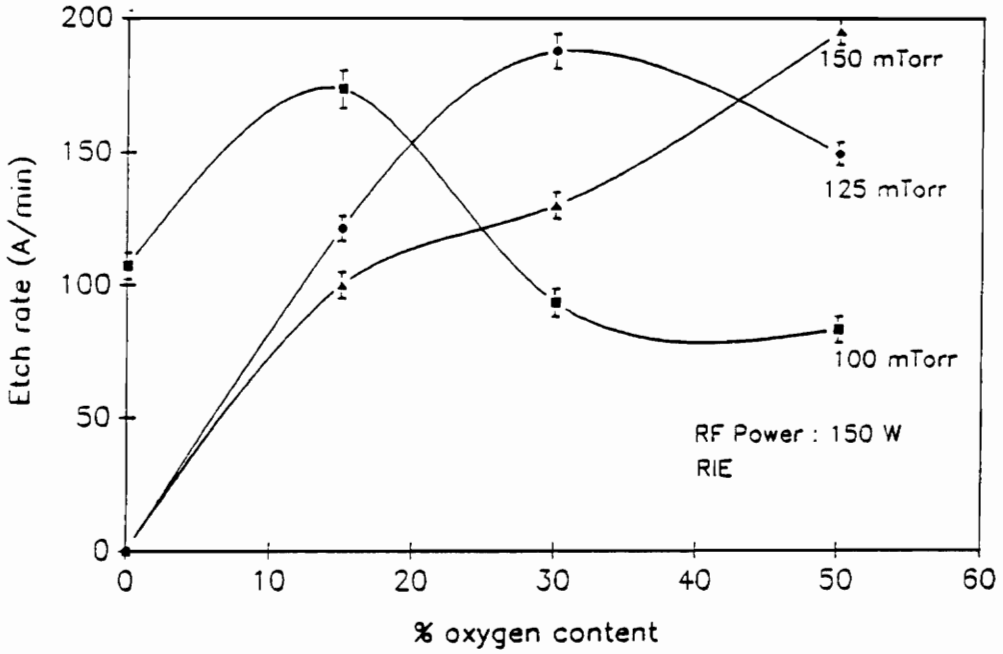

Figure 8.9 **The etch rate of RuO_2 thin films as a function of $\%O_2$ in the etch gas at various gas pressures.**

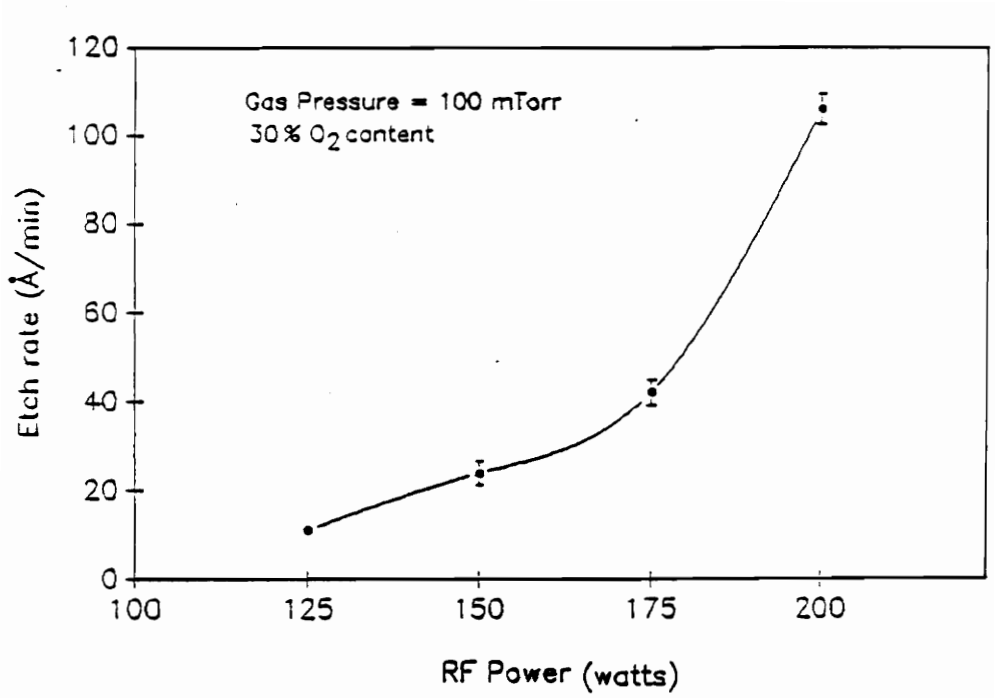

Figure 8.10 The effect of RF power on the etch rate of RuO_2 thin films.

bombarding ions assist in the reaction of O_2 with RuO_2 films and in the removal of the by-products formed thereafter.

The structure of the ferroelectric stack capacitor discussed, consists of Si/SiO_2 as the substrate, RuO_2 as the bottom and top electrode and PZT as the ferroelectric material. If the capacitor is to be etched in a single run, then the only concern regarding the selectivity in the etching process is between the bottom electrode and the substrate. High selectivity can be obtained by etching the RuO_2 bottom electrode in an O_2 enriched plasma. Since, ion bombardment effects are primarily responsible for the etching of PZT and RuO_2 films, it is favorable to use a low gas pressure and high RF power to obtain high rates. However, the RF power needs to be optimized to obtain high anisotropy without any mask damage.

8.5 SUMMARY

Thin films of PZT and RuO_2 have been successfully etched using CCl_2F_2 as the etch gas. The etch parameters, namely, gas pressure, % O_2 content and RF power, have been optimized to obtain high rates (~ 25-30 nm/min) and good anisotropy during etching. It was observed that low gas pressures favor high etch rates of PZT and RuO_2 films indicating that ion bombardment is the primary mechanism of etching in these films. Also, low RF power and low gas pressures favored anisotropic etching. The relative etch rates of the components of PZT films have been determined by studying the surface composition as a function of etch time using ESCA. It has been determined that the etch rate of PbO is the limiting factor in the etching process i.e, ZrO_2 and TiO_2 have relatively higher etch rates than PbO. The ESCA studies also revealed large amounts of fluorine in the initial stages of the etch process that became depleted with increasing etch time. At the

end of the etch process only small amounts of Cl and F residues were present on the surface of the films as residues. Based on these results a possible etching mechanism has been proposed for PZT thin films that includes both ion-induced (fluoride etching) and ion-enhanced (chloride etching) phenomena in the etching process. In the case of RuO_2 thin films, without any O_2 addition to the etch gas, the etching mechanism is possibly an ion-induced phenomena. With O_2 addition, there is an increase in the etch rate, possibly due to the formation of volatile RuO_3/RuO_4 compounds.

8.6 REFERENCES

1. L. Parker and A. Tasch, *IEEE circuit and Device Mag.*, 17, January, 1990.

2. S.M. Sze, *VLSI Electronics*, McGraw-Hill Publishing Company (1988).

3. C.K. Kwok, D.P. Vijay, and S. B. Desu, *Proceedings of the 4th International Symposium on Integrated Ferroelectrics*, Monterey, CA (1992).

4. M.R. Poor, A.M. Hurd, C.B. Fledermann, and A.Y. Wu, *Mat. Res. Soc. Symp. Proc.*, **200**, 211 (1990).

5. S. Saito and K. Kuramasu, *Jpn. J. Appl. Phys.*, **31**, 135 (1992).

6. G. Yi and M. Sayer, *Ceram Bull.*, **70(7)**, 1173 (1991).

7. C.J. Mogab, A.C. Adams, D.L. Flamm, *J. Appl. Phys.*, **49**, 3796 (1978).

8. S.B. Desu and C.K. Kwok, *Mat. Res. Soc. Symp. Proc.*, **200**, 267 (1990).

9. R.C. Weast and M.J. Astle, *CRC Handbook of Chemistry and Physics*, CRC Press Inc. (1980).

Chapter 9 : Conclusions and Recommendations

The main objectives of this study were to overcome the degradation mechanism of fatigue in ferroelectric thin films capacitors and to provide a patterning technology for etching of the capacitors. Based on this study, the following conclusions were made :

1. Fatigue in oxide ferroelectric thin film capacitors with metal electrodes (e.g., Pt/PZT/Pt) was attributed to domain pinning by space charge caused by defect entrapment (mainly oxygen vacancies) at various structural interface sites such as electrode-ferroelectric interface, grain boundaries, domain boundaries etc. Based on this quantitative fatigue model, (a) control of the interface state and (b) control of the defect density were suggested as possible guidelines to minimize the degradation problem.

2. For control of the interface state, conducting oxides electrodes were suggested as possible replacements for the metal electrodes. The feasibility of using several conductive oxide/PZT capacitors, including RuO_2 and indium tin oxide based PZT capacitors were studied on the basis of their diffusion barrier properties, interface nature, perovskite formation temperature of PZT and their ferroelectric properties. It was found that RuO_2 electrodes are good candidates fatigue free nonvolatile memory applications. However, the leakage current of RuO_2/PZT capacitors were far higher than Pt/PZT capacitors. Schottky emission was attributed as the possible mechanism for the higher leakage current density.

3. Multilayer metal/metal oxide electrodes (e.g., Pt/RuO_2 and Pt-Rh/Rh_2O_3) was suggested as a possible solution to minimize both fatigue and leakage current in PZT films. For example, PZT films annealed at 650 ^oC on Pt-Rh/Rh_2O_3 show good hysteresis

behavior ($2P_r \sim 35\ \mu C/cm^2$), no fatigue up to 10^{10} cycles, low leakage currents ($\sim 1 \times 10^{-8}$ A/cm^2) and very good TDDB characteristics (breakdown at 10^4 sec at 100 kV/cm). The thickness of the surface oxide electrode was found to critically determine the properties of the ferroelectric film. The decrease in polarization with decreasing oxide layer thickness has been attributed to the change in orientation of the PZT films from predominantly (111) to (100). The concept of multilayer electrodes was extended to develop a novel electrode system that overcomes the hillock formation problems in the existing Pt films. The commonly used Ti interlayer in the $Si/SiO_2/Ti/Pt$ was replaced by a Pt-Rh-O layer that provided the necessary adhesion between the electrode and the substrate and eliminated the hillock formation problems.

4. For control of defect density, two different approaches were suggested : (a) addition of donor dopants. It has been shown that Nb donor dopant additions to PZT films can reduce both the fatigue and leakage current on Pt and RuO_2 electrodes, respectively. (b) utilizing ferroelectric materials that have a low intrinsic defect concentration. On this basis, several ferroelectric oxides belonging to the pyrochlore, layered structure and tungsten bronze families were considered for possible memory applications. It was found that $SrBi_2(Ta_xNb_{1-x})_2O_9$ family of layered structure compounds are very good candidates for fatigue free ferroelectric thin film applications. The fundamental criterion for the selection of this family of compounds was that fact the lack of any volatile species which could cause the formation of intrinsic defects such as oxygen vacancies in the ferroelectric sublattice that is responsible for the spontaneous polarization. High quality stoichiometric thin films of these compounds with a dense microstructure have been deposited on platinized Si/SiO_2 wafers using laser ablation. The films showed excellent hysteresis characteristics and no fatigue up to 10^9 cycles. For example, SBTN films with

composition of x =0.8 , showed 2Pr values close to 22 $\mu C/cm^2$, a coercive field of 65 kV/cm and a leakage current density of less 10^{-7} A/cm^2 at 3V.

5. The effect of processing temperature on the ferroelectric properties of layered structure $SrBi_2Ta_2O_9$ thin films grown by laser ablation was investigated. Good ferroelectric properties were observed only in films deposited above 700 ^oC. There was an observed transition in ferroelectric properties from poorly saturated hysteresis loops in the films deposited at 650 ^oC to well defined and saturated hysteresis properties in 700 ^oC deposited films. The reason for this transition in ferroelectric properties has been ascribed to grain size effects; the grain size increased from an average value of 80 nm to 160 nm between 650 and 700 ^oC. These results suggest that to obtain good ferroelectric properties at lower processing temperatures, it may suffice to devise processing methods that can provide a grain size above the observed critical value (160 nm) at lower temperatures.

6. For the first time, the ferroelectric properties of $SrBi_2Ta_2O_9$ ferroelectric thin film capacitors were characterized as a function of crystallographic orientation; the remnant polarization, coercivity and dielectric constant were found to decrease with increasing degree of c-axis orientation. It has been shown that the structural flexibility of these materials can now be used for a wide variety of nonvolatile memory applications ranging from high voltage (5V) DRO NvRAMs to low voltage memory applications (single transistor-single capacitor) and nondestructive readout MSFT applications (single transistor). It has also been shown for the first time that highly c-axis oriented or epitaxial layered structure SBT films exhibit very small polarization, coercivity and dielectric constant values and are thereby attractive candidates for NDRO MSFT applications.

7. Thin films of PZT and RuO_2 were successfully etched using CCl_2F_2 as the etch gas. The etch parameters, namely, gas pressure, % O_2 content and RF power, have been optimized to obtain high rates (~ 25-30 nm/min) and good anisotropy during etching. It was observed that low gas pressures favor high etch rates of PZT and RuO_2 films indicating that ion bombardment is the primary mechanism of etching in these films. Also, low RF power and low gas pressures favored anisotropic etching. The relative etch rates of the components of PZT films have been determined by studying the surface composition as a function of etch time using ESCA. It has been determined that the etch rate of PbO is the limiting factor in the etching process i.e, ZrO_2 and TiO_2 have relatively higher etch rates than PbO. The ESCA studies also revealed large amounts of fluorine in the initial stages of the etch process that became depleted with increasing etch time. At the end of the etch process only small amounts of Cl and F residues were present on the surface of the films as residues. Based on these results a possible etching mechanism has been proposed for PZT thin films that includes both ion-induced (fluoride etching) and ion-enhanced (chloride etching) phenomena in the etching process. In the case of RuO_2 thin films, without any O_2 addition to the etch gas, the etching mechanism is possibly an ion-induced phenomena. With O_2 addition, there is an increase in the etch rate, possibly due to the formation of volatile RuO_3/RuO_4 compounds.

Possible future work related to the current research include the following :

1. Dynamic studies on the switching behavior and domain interaction of PZT based ferroelectric capacitors to provide a deeper insight into the fatigue phenomena.

2. Study the feasibility of using other conducting transition metal oxide electrodes such as IrO_2, Rh_2O_3 etc. for PZT based ferroelectric memory applications. Some of these oxides may provide lower leakage current in PZT films.

3. Understand the mechanism of fatigue and leakage current in multilayer metal/metal oxide/PZT capacitors.

4. TEM studies on the Pt/$SrBi_2Ta_2O_9$ based capacitors to understand the nature of the interface.

5. Reduce the final processing temperature of $SrBi_2Ta_2O_9$ thin films on Pt electrodes. One of the ways to achieve this may include increasing the grain size at lower processing temperatures.

6. Using tools such as optical emission spectroscopy for in-situ examination of the RIE process for PZT so as to obtain further understanding of the etching mechanism.

Appendix A

Sol-gel processing of PZT films

The preparation methods for precursors and the thin films are described in separate sections. The procedures for preparing a 50 mL, 0.4M, Zr/Ti =53/47, 10 % excess lead PZT precursor is listed.

A1. Precursor preparation

1. Add a 4.961g of Zr-n-propoxide into a clean 50 mL beaker in an analytical balance.
2. Add 2.672 g of Ti isoporpoxide into the Zr n-propoxide solution and mix the two alkoxides in an ultrasonic cleaner for 5 min.
3. Add 5 mL of acetic acid into the Zr-Ti solution.
4. Add 10 mL of n-propanol to the above solution.
5. Add 8.345 g of Pb-acetate to the above solution.
6. Heat the Pb-Zr-Ti solution in a silicon oil bath to 95 °C, stir the solution with the wooden end of a cotton-swab stick to dissolve the lead acetate.
7. Remove the solution from the oil bath, clean the outside of the beaker and cover the beaker with a plastic film and let the solution cool down close to room temperature.
8. Add 1.188 g of distilled water into the solution and mix them in an ultrasonic cleaner for 2 min.
9. Add appropriate amount (15 mL) of n-propanol to make 50 mL of final precursor solution.
10. Store the precursor solution in a capped test tube and keep them in a dry and cool place.

A2. Film preparation

1. Place a clean substrate on the platform of the spin coater.

2. Heat up the hot plate to 150 ^{o}C.

3. Turn on the mechanical pump.

4. Set the time (autostop) to 30 sec and spin speed to 2000 rpm.

5. Cover the whole substrate with precursor solution, this will minimize the streaking.

6. Start the spin coater by the foot paddle.

7. Transfer the substrate to the hot plate and dry for 5 min.

8. Remove the substrate from the hot plate and wait until it is cooled down to room temperature before the next spinning (if required).

9. Repeat the spin-bake cycle to obtain the required thickness.

10. Anneal the film in a tube furnace in a controlled O_2 atmosphere at the desired temperature.

Appendix B

Ferroelectric property measurements

In this study, a commercially available ferroelectric test system (Radiant Technologies RT66A) was used to measure the hysteresis and fatigue properties of the ferroelectric capacitors. The hysteresis properties were determined by a modified Sawyer-Tower circuit. The block diagram for the RT66A is shown in Fig. A.B.1. The test system was completely automated and controlled by a personal computer. All of the hysteresis measurements were conducted in the virtual ground mode. In this mode, the total charge stored in the ferroelectric sample is measured by integrating the current required to maintain one terminal of the sample at zero volts. The basic operation for hysteresis measurements can be described as follows :

1. The maximum applied voltage and number of data points are selected by the user.
2. Then the number of points is divided by four. This is the number of points for each voltage segment (V_{max}, 0, $-V_{max}$ and 0).
3. The Vmax is divided by the number of points in a segment to generate the voltage steps and an array of drive voltages is generated and stored in the computer.
4. The integrated capacitor and the sample are shorted and then opened.
5. The computer program will step through the hysteresis array, pick up the appropriate voltages and send them to the driver section. After a certain waiting period for the sample to fully charge from the voltage step, the output of the integrator is measured.
6. When the acquisition is complete, the integrator and the sample are left shorted. the data is processed by the software program for analysis and plotting.

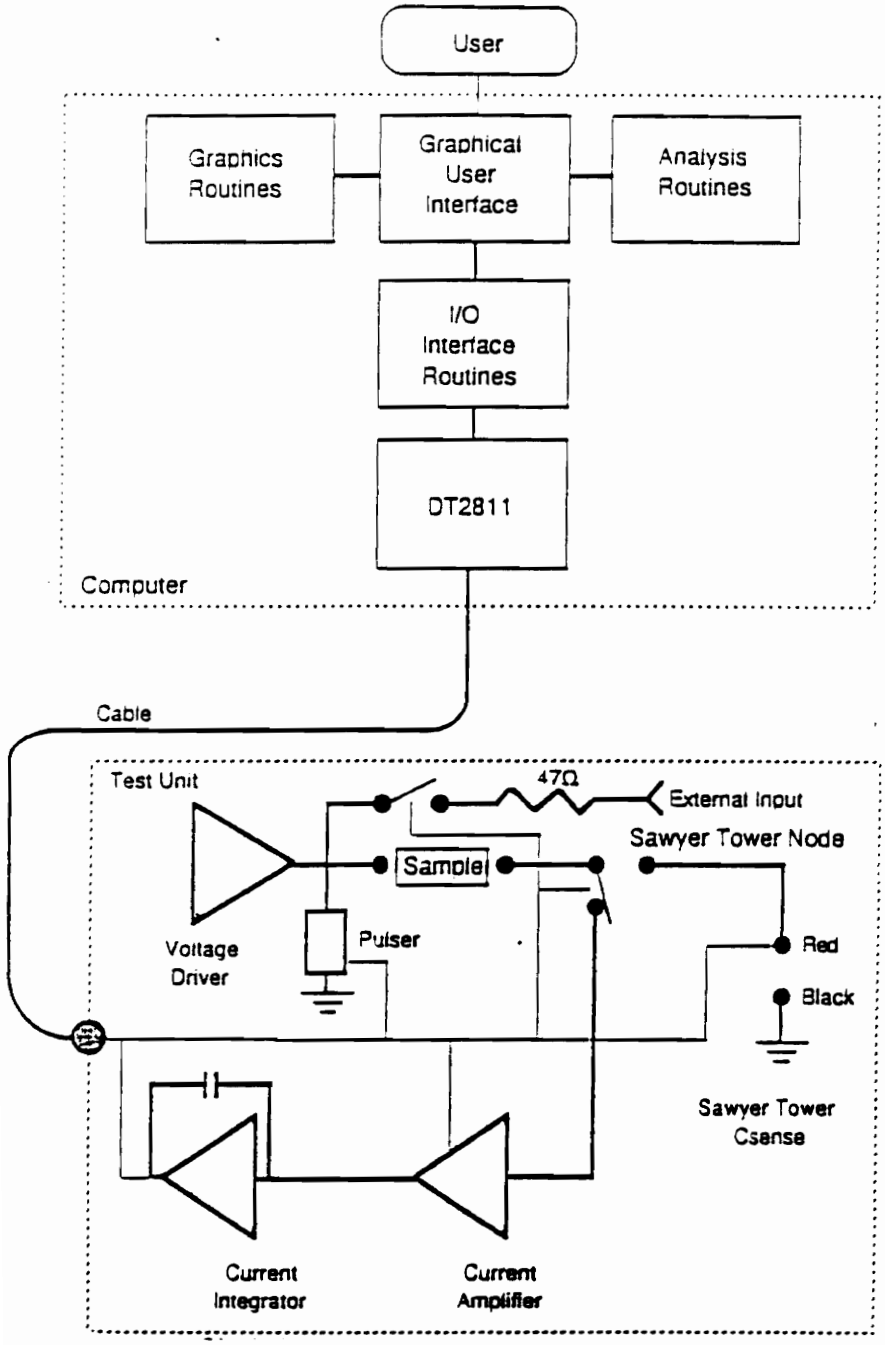

Block diagram of the RT66A ferroelectric tester

VITA

Dilip Vijay was born in Trichur, Kerala State in the south of India. He was raised in Madras, India, where, after receiving his high school degree in 1986, he was admitted to the Indian Institute of Technology-Madras for undergraduate studies. He completed his Bachelor of Technology in Metallurgical Engineering in 1990 from the same institute. During this period he was supported fully for his education through a scholarship awarded by the Govt. of India for undergraduate studies.

In 1990, he joined the Department of Materials Engineering at Virginia Polytechnic Institute and State University. The early part of graduate studies (August 1990-May 1991) was conducted under the supervision of Dr. R.W. Hendricks on Residual Stresses in Hybrid Microelectronic Circuits. He then started his doctoral research in the area of ferroelectric thin films under the guidance of Dr. S.B. Desu. He had 17 journal publications, 6 conference articles, 2 invited presentations, 2 approved patents and 6 patent disclosures in the area of ferroelectric thin films.

He was a recipient of University Distinguished Paul Torgeson award for excellence in graduate research in the year 1995.